Session 2

Concrete Structures

MODELLING OF REINFORCED CONCRETE FRAMES IN FIRE FOLLOWING AN EARTHQUAKE

Ab.Kadir M A[a], A.S Usmani[b], M. Gillie[c]

[a]PhD student, School of Engineering, The University of Edinburgh, Edinburgh EH9 3JF, United Kingdom
[b]Professor, School of Engineering, The University of Edinburgh, Edinburgh EH9 3JF, United Kingdom
[c]Lecturer, School of Engineering, The University of Edinburgh, Edinburgh EH9 3JF, United Kingdom

INTRODUCTION

Earthquakes are natural hazards which occur in seismic areas and can cause devastating damage in urban infrastructure and facilities. Sometimes earthquake events are followed by fires which may cause more damage than the earthquake itself. Essentially, seismic design codes are relevant for designing a structure for an expected level earthquake and do not consider fire safety. In general, these two events are considered to occur separately.

A large number of post-earthquake building fires result in the collapse of the buildings. As a result of earthquake damage the fire resistance of a structure may be significantly impaired. In their study of the 1906 San Francisco earthquake and the 1923 Tokyo earthquake (Scawtorn e.al,2005) have shown that about 80% of the building damage was due to the fires following the earthquake rather than the earthquake itself. This may pose a serious threat to the structural integrity and be detrimental to the life safety of the occupants and rescue workers. Hence, it is prudent to consider such scenarios in the design of buildings constructed in seismic zones (Mousavi et al. 2008). Consequently, understanding the performance and response of structures in a fire following an earthquake is important at the design stage.

The aim of this study is to model a number of experiments being conducted on 2D reinforced concrete frames exposed to fire following simulated cyclic pushover. Increasing cyclic displacements are applied at the slab level in a pushover analysis to simulate the damage to the structure as a result of an earthquake.

1 REINFORCED CONCRETE FRAME MODELLING

A number of preliminary analyses were carried out on a 2D finite element model of the frame to determine its capacity under lateral pushover and its behaviours under cyclic loads. Based on the results, from the preliminary analyses, increasing cyclic displacements was applied to the frame as a second loading step (after applying all gravity loading in the first step). The columns and beam cross-sections were then exposed to temperature distributions obtained from a heat transfer analysis also carried out in the preliminary stage.

The temperature distributions were the result of radiative hear fluxes from a one hour compartment fire applied to the internal surfaced of the frame.

A computational analysis for this study was performed using ABAQUS. The reinforced concrete frame consisted of four columns supporting four beams and a slab on top floor and four beams at plinth level. The frame was modelled as a 2D frame with beam elements assigned for columns, beams and slab. Truss elements were used to model reinforcement bars. The frame model is shown in Figure 1. The total height of the frame is 6.0m with the distance between the plinth and top beams being roughly 3m. The cross section of the columns is 300mm x 300mm and that of the beams is 230mm x 230mm. Slabs thickness is 120mm. In order to reduce computational time the slab was modelled as apart of the overall

beam cross section in 2D. Eight steel bars of 20 mm diameter were used for the columns and six steel bars of 16 mm diameter were used for beam (3 each on he top and bottom). Node and element numbering of the model was as shown in Figure 2 and Figure 3.

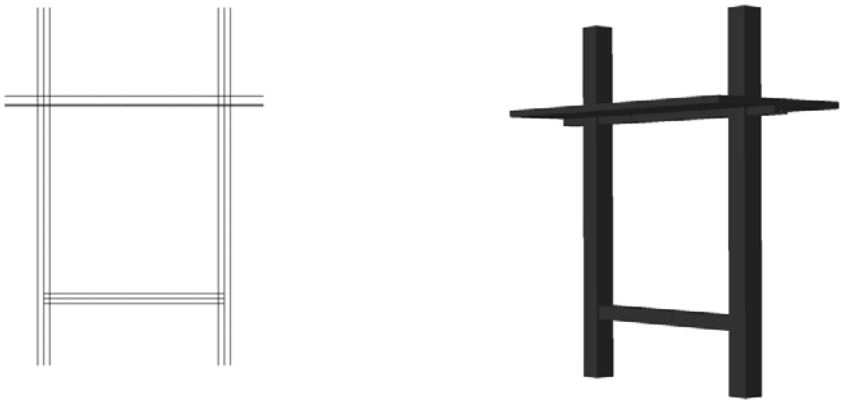

Fig. 1 2D The Analytical model

Temperature dependent material properties for concrete and steel were assigned according to the Euro Code 2. Concrete strength of 34MPa and steel strength 415 MPa was used. Permanent loads of 100kN on each column and 2.3kN/m^2 on the slab are applied. This load was constant throughout the analysis. Due to loading and unloading cycles on the frame, degradation of strength of the concrete and reinforcing bars was considered. Therefore, the concrete damaged plasticity was used in the analysis.

In the thermo-mechanical analysis, temperatures were assigned at the integration points of the elements at node locations. Five temperatures were assigned to the beam and three node temperatures to the column. The temperature exposures were assumed to occur only between the plinth beams and the top beam slab. The compartment temperatures were increased from 20^{o}C to 1000^{o}C in 5 minutes and maintained for another 55 minutes, as in Figure 4.

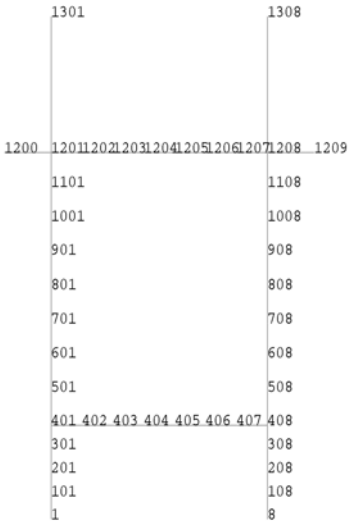

Fig. 2 Node Numbering

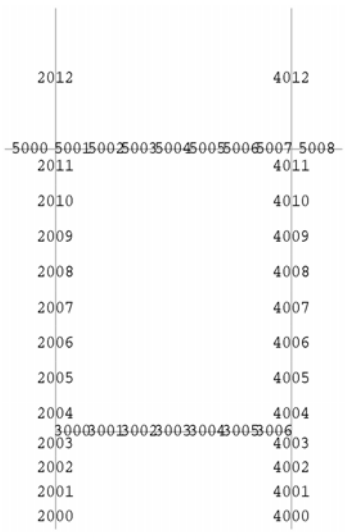

Fig. 3 Element Numbering

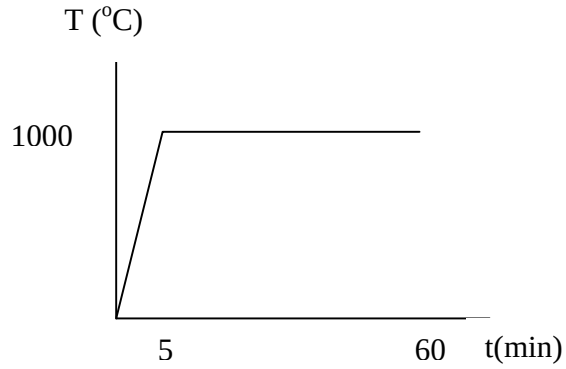

Fig. 4 Temperature Amplitude

2 PERFORMANCE OF RC FRAME

An analysis was performed to get an overview of the capacity of the frame. Figure 5 shows the hysteresis curve after a 7 cycle displacement load was applied at the slab level of the frame. Displacement was also observed at the slab level (node number 1208). The maximum base shear is around 300kN corresponding to a displacement of the frame of approximately 90mm. Three further cases were studied. A maximum displacement of 100mm was applied over 4 cycles for case I, 70% of this for case II and 30% for case III.

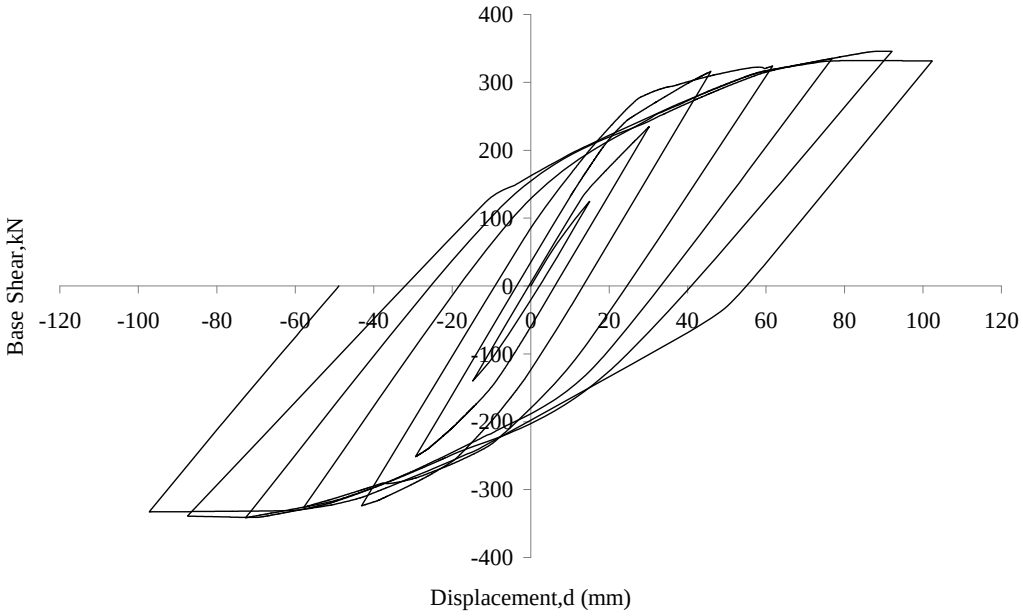

Fig. 5 Hysteresis Curve

Figure 6 illustrates the displacement history for the three cases. The results in this figures show that there are residual displacements after when the base shear is brought to zero at the end of the loading

cycles. The residual displacements are seen to increase with increasing magnitudes of the applied cyclic displacements.

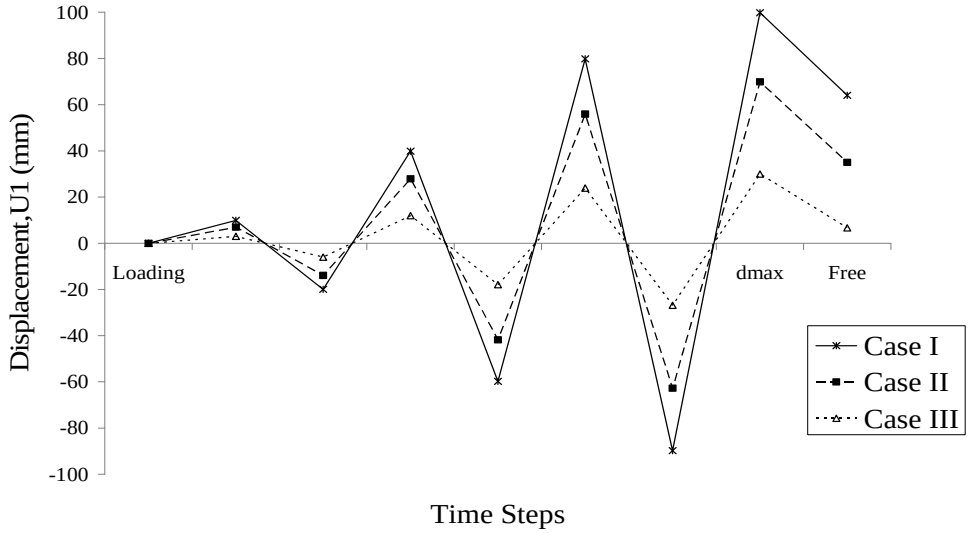

Fig. 6 Displacement history

Figure 7 shows the displacement history when after the frame is subjected to heating for all the three cases. The frame appears to stiffen under the heating and the residual displacements seem to recover. The reaction forced of the frame for the cases was observed in this study as shown in Figure 8.

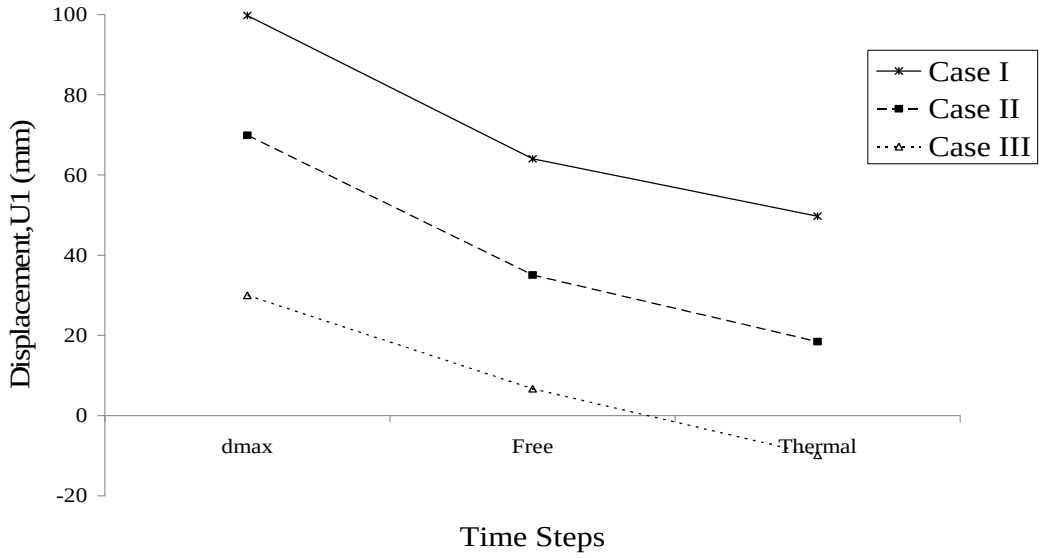

Fig. 7 Displacement of the frame after the temperature applied

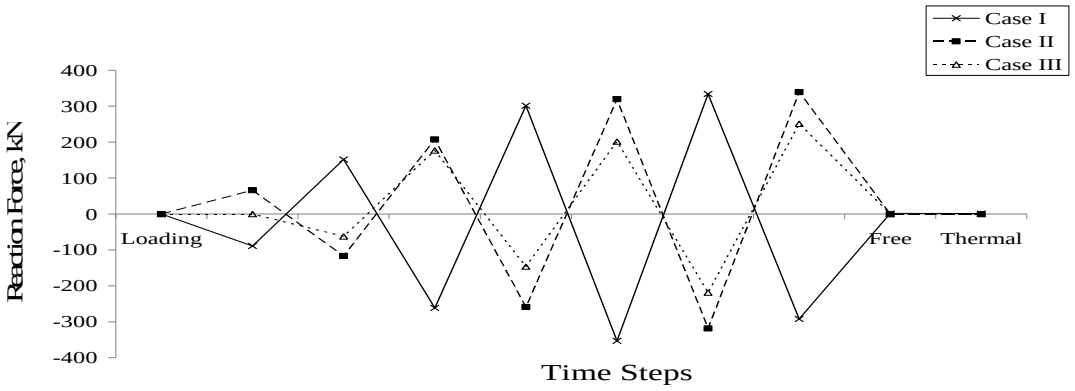

Fig. 8 Reaction force of the frame for the three cases

3 COMPARISONS

The eventual aim of this work is to compare the computational results with the test results on real frame currently being carried out at IIT Roorkee in India.. Both the model development and the tests are currently incomplete and full finding will be reported in future papers.

4 CONCLUSION

This study was carried out to model a number of experiments being conducted on 2D reinforced concrete frame exposed to the fire following simulated cyclic pushover. The computational analysis shows there is a reduction in the residual displacement of the frame after heating. Further studies need to be implemented to compare the computational analysis with the test results.

5 ACKNOWLEDGEMENTS

This study has been funded by Universiti Teknologi Malaysia. We would like to thank all members in the UK-India Education and Research Initiative (UKIERI) project group which has contributed the data.

REFERENCES

Abaqus: Abaqus Analysis User's Manual. Providence, Dassault Systemes Simula Corp,2008

EN1992-1-2. Eurocode 2: Design of concrete Structures-Part 1-2: General Action-Actions on Structures Exposed to Fire, 1999.

Mousavi, S. Bagchi, A. Kodur, V.K.R. Post-Earthquake Fire Hazard to Building structures, Canadian Journal of Civil Engineering, 35: 689-698, 2008

Scawthon, C., Eidinger J.M. and Schiff, A.J., editors, Fire Following Earthquake, ASCE Publications, 2005.

TECHNIQUES FOR THE EVALUATION OF CONCRETE STRUCTURES AFTER FIRE

Emmanuel Annerel[a], Luc Taerwe[b]

[a]Ghent University, Faculty of Engineering and Architecture, Department of Structural Engineering,
[b]Magnel Laboratory for Concrete Research, Ghent, Belgium

INTRODUCTION

During a fire, concrete structures behave in most cases very well (Taerwe, 2008). It could therefore be of economic interest to repair the damaged structures, as costs for demolition and rebuilding can be avoided and the building can be reused faster. Different assessment techniques are possible to detect the internal damage (Annerel, 2009).
This paper studies the application of the Schmidt Rebound Hammer and colorimetry as tool to assess the fire damage of concrete structures. Firstly, experimental data is acquired under laboratory conditions on small specimens. Secondly, this information is used to evaluate the damage of a case study consisting of a girder exposed to a real fire. Both techniques show to be very useful in evaluating the fire damage and can provide the necessary information for a calculation of the residual load bearing capacity.

1 CONCRETE MIX

In this paper a traditional vibrated concrete with siliceous aggregates and ordinary Portland cement (TC) is studied. For 1 m³, it is composed of 640 kg sand, 525 kg gravel 2-8 mm, 700 kg gravel 8-16 mm, 350 kg cement and 165 liter water. Cubes with size 150 mm are cast and cured for 4 weeks in an air-conditioned room (RH >90%, 20±1°C), after which they are stored at 60% RH and 20±1°C for drying until further testing. The mean compressive strength at 28 days is 56.5 N/mm².

2 COLORIMETRY

At an age of 3 months, cores are drilled out of the cubes, sawn in 6 discs, polished and dried till testing time for at least two weeks at 60°C. Since this was repeated for another cube cast at a later time, a total of 24 discs were obtained. Two discs (belonging to different mixes) were heated without mechanical load at a heating rate of 30°C/min to the target temperature (till 1160°C), which was kept constant for 1h. The discs were slowly cooled in the oven, after which they were immediately tested for colour.
The colour is measured with an X-rite SP60 spectrophotometer according to the CIE Lab-colour space. In this colour system ‘L*’ is the lightness with values between 0 (black) and 100 (white), while ‘a*’ is spread between magenta (positive values) and green (negative values) and ‘b*’ is positioned between yellow (positive values) and blue (negative values). The coarse aggregates were masked with black ink to minimize the effect of the colourful aggregates. During heating the colour describes a path in the a*b*-colour space (Fig. 1), changing from grey at 20°C to red-pink at 300-600°C, to whitish grey at 600-900°C and buff at 900-1000°C.

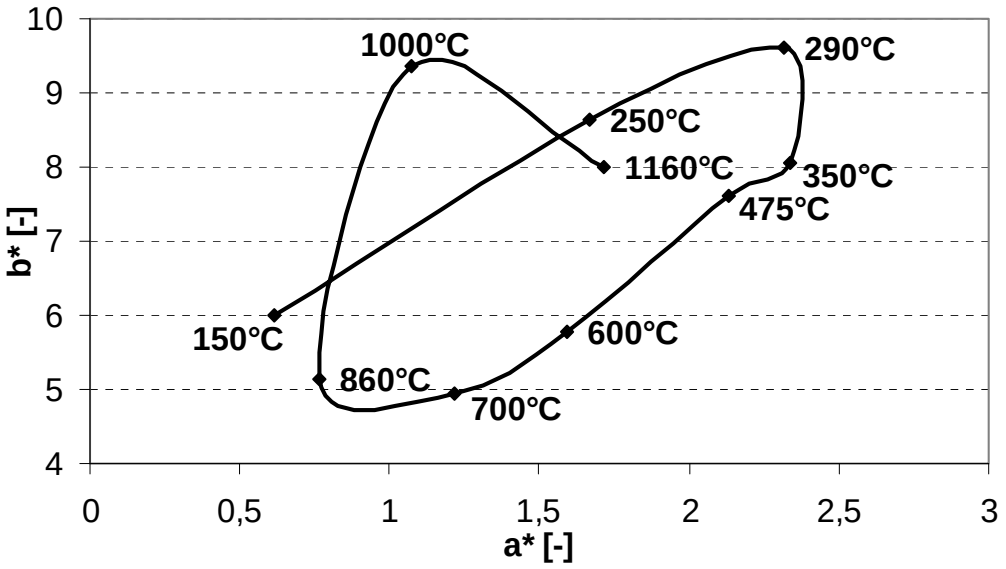

Fig. 1: Colour evolution of traditional concrete with masked aggregates

Similar colour paths can be found from cores drilled out of a heavily heated structure and cut in discs parallel to the fire exposed surface. Comparing the shape of these paths with Fig. 1 results in the detection of different isotherms, such as ~300°C, ~600°C, ~800°C, ~1000°C. On the other hand, the core can also be sawn in halves along its longitudinal axis. Study of the colour changes along this longitudinal axis would only result in the detection of the 300°C isotherm, since the temperature gradient is steep at the surface layers. Based on the found isotherms, the residual load bearing capacity can be calculated with the methods given in EN 1992-1-2:2004.

3 SCHMIDT REBOUND HAMMER

The influence of the temperature and storage conditions after fire are tested on half TC cubes heated till uniform temperatures of up to 600°C. The specimens are allowed to cool slowly in the furnace, after which they were stored for 28 days in water or in air (60% R.H., 20±1°C). Fig. 2 depicts the relative rebound index (RRI) tested immediately after cooling (0d) and after 28 days of storage, as well as the compressive strength loss measured on an additional series of heated cubes. RRI is calculated as the percentage of the rebound belonging to a target temperature after a storage period (RI_T) divided by the rebound of an unheated reference sample at the beginning of the storage period ($RI_{20°C}$).

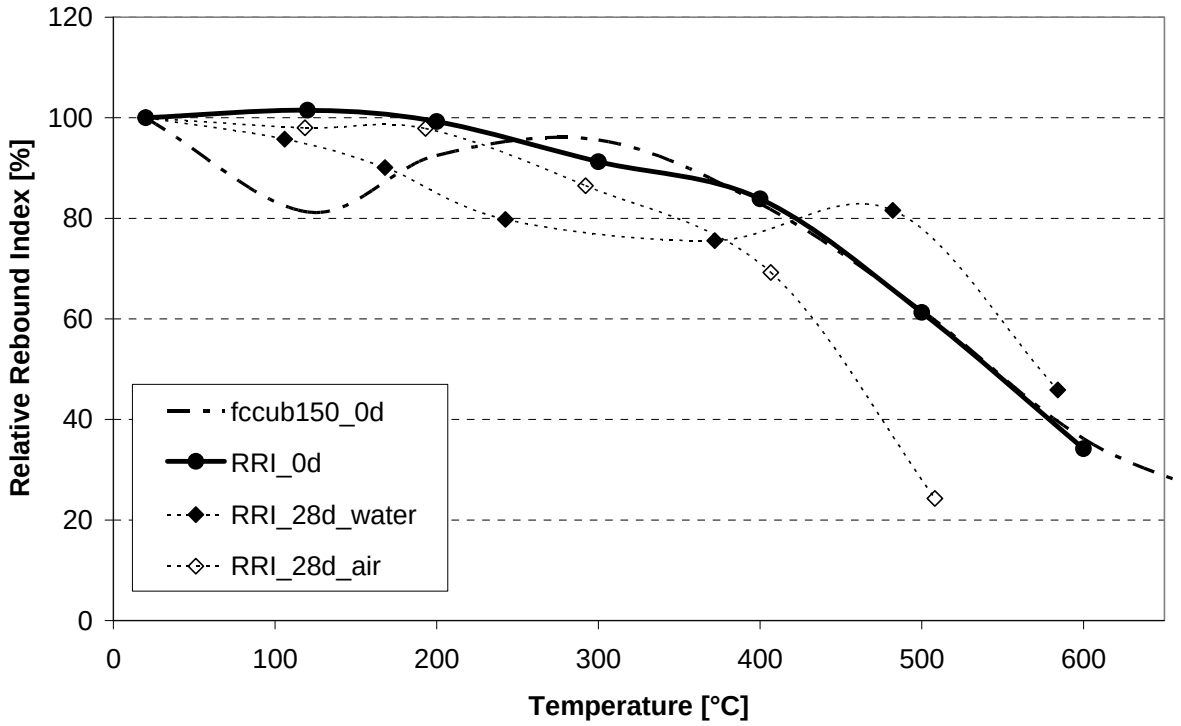

Fig. 2: Decrease of Rebound Index as function of temperature and storage conditions for traditional siliceous concrete

It appears that the results at 0 days after heating are close to EN 1992-1-2:2004 and the compressive strength decay of TC cubes (except for the strength drop at about 100°C). Differences in the evolution of the surface hardness between storage in water and in air are clearly visible. Below 400°C, a higher loss of Rebound Index is noticed for storage in water than in air. On the other hand, beyond 400°C, the surface hardness recovers strongly for specimens stored in water and a further decay is found for air storage. Due to atmospheric effects such as rain and sun, measurements on in-situ structures will be between the extremes as given on the graph.
Based on these results, the following criteria are formulated for the interpretation of the relative rebound index ($RI_T/RI_{20°C}$):

$RI_T/RI_{20°C} \geq 0.85$: concrete element is superficially damaged only
$0.85 \geq RI_T/RI_{20°C}$: concrete element should be further investigated

The Schmidt Rebound Hammer can be used as a valuable tool to have a first attempt of the fire damage of concrete elements. Due to its penetration depth of about 30 mm, the degradation of the concrete cover is tested. This degradation is strongly related to the remaining load bearing capacity, since it protects the reinforcement from heating.

4 CASE STUDY: FIRE DAMAGE OF A GIRDER FROM AN INDUSTRIAL HALL

4.1 Description

In 2010 an industrial hall in Belgium consisting of pretensioned roof girders with a span length of 21 meters has burnt out. The fire started in the archive located at a mezzanine, just beneath the girders.
Fig. 3 shows the damage to one of the roof girders. Considering the colour change of the concrete surface, the surface temperature must have been around 900-1000°C. The roof consists of a composite concrete-steel slab, which has bent towards the fire. The concrete of the girder has spalled over a few centimetres. However, the strands are still covered with concrete and were not directly exposed to the fire. Therefore, it is investigated to which extent the fire damaged has

reached the reinforcement. This information is necessary for a calculation of the residual load bearing capacity of the girder.
The concrete cover of a reference girder is 36-40 mm for the stirrups and 45-50 mm for the strands when measured from the side faces. From the bottom, the cover is 39-40 mm for the strands.

Fig. 3 Fire damage of roof girder

4.2 Results Schmidt Rebound Hammer

Surface hardness readings are performed along the length of the girder, as presented in Tab. 1. Locations 1 and 2 are situated at half span length and in the zone with severe fire damage, while location 3 is at 2.5 m of the supports and approximately 4 m from the fire. The relative rebound index is calculated by means of the measurement of a reference girder found in the neighbouring construction with similar properties. It is clear that the fire has influenced the surface hardness ($RI_T/RI_{20°C} < 0.85$) at locations 1 and 2, while location 3 is not affected.

Tab. 1 Schmidt Rebound Hammer measurements

Test location		Direction of measurement	Average	Standard deviation	$RI_T/RI_{20°C}$ [-]
Reference girder	web	side	45.6	2.0	1.00
	flange	side	44.3	2.5	1.00
	flange	bottom	50.9	1.0	1.00
Location 1	web	side 1	36.8	1.8	0.81
	web	side 2	41.2	1.1	0.90
	flange	side 1	30.8	2.3	0.70
	flange	bottom	44.8	1.1	0.88
Location 2	web	side 2	38.0	1.4	0.83
	flange	side 2	30.0	5.7	0.59
	flange	bottom	39.6	1.7	0.78
Location 3	web	side 1	41.0	2.4	0.90
	flange	side 2	44.6	1.3	0.98
	flange	bottom	47.8	4.1	0.94

4.3 Results colorimetry

To know the depth of the fire damage inside the concrete, a core is drilled through the web of the exposed girder in the heavily damaged zone. The core has been exposed to fire from both sides. Damage is observed with the naked eye till a depth of 12 mm from one side and 10 mm from the other side. Based on these findings, the zone between 50 and 70 mm is assumed to be not affected by the heat and is taken as reference. From recordings with the spectrophotometer, a fire damaged zone of 25 mm from the first side and 13 mm from the other side can be detected (Fig. 4). The

values near to the surface can be related to temperatures of about 300-600°C (based on Fig. 1). These depths of fire damage are below the measured concrete cover thicknesses. Therefore, the reinforcement has not been heated to critical temperatures and the load bearing capacity of the girder should be adequate.

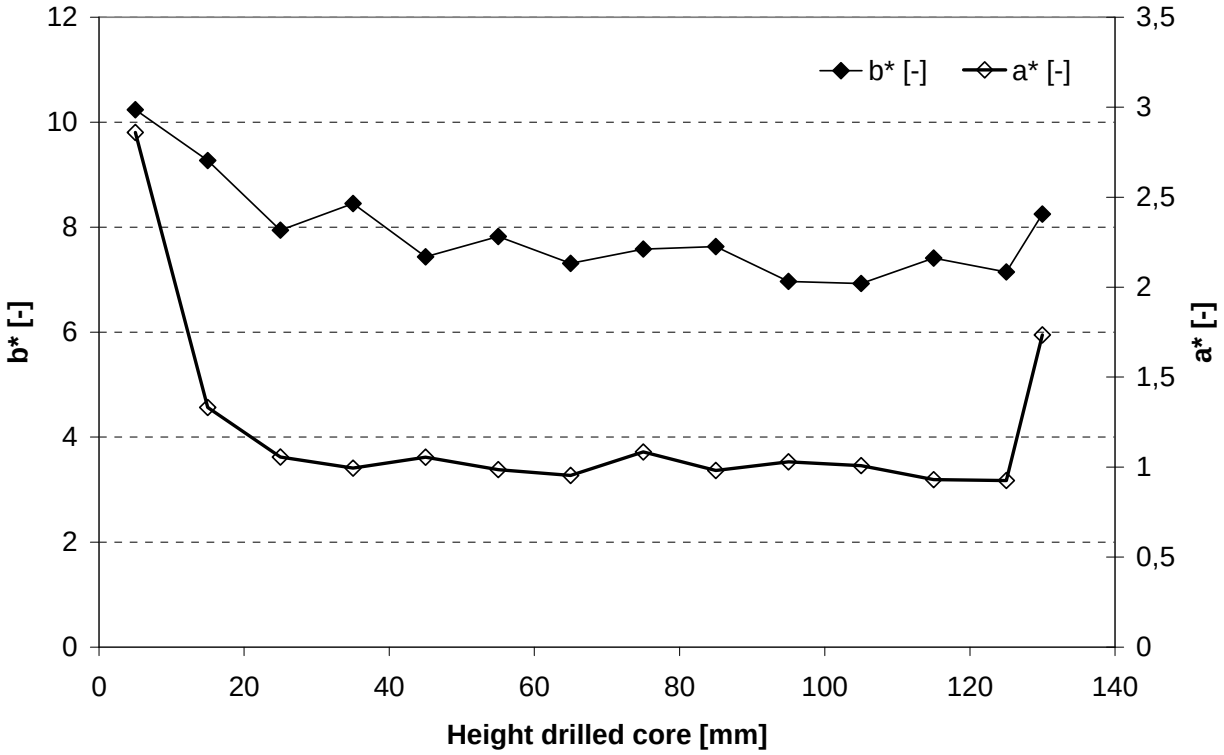

Fig. 4: Development of a* and b* over the body of the girder

5 CONCLUSIONS

- With increasing temperature, the concrete colour describes a colour path in the a*b* colour space.
- Experimental laboratory work results in a critical relative rebound index of 0.85 for siliceous concrete.
- Both techniques proved to be useful to detect the extent of fire damage of a concrete girder exposed to a natural fire.
- Although a pretensioned girder was exposed to high temperatures, the remaining bearing capacity is assumed to be sufficient since the strands are not heated.

6 ACKNOWLEDGEMENT

The authors would like to thank the Fund for Scientific Research in Flanders (FWO) for the financial support through the research grant “Damage assessment and estimation of the residual strength of concrete members after exposure to fire”.

REFERENCES

Taerwe L., Annerel E., Loading test on a retrofitted pretensioned concrete girder after fire, Proceedings of the 2nd International Conference on Concrete Repair, Rehabilitation, and Retrofitting (ICCRRR), Alexander, M. et al. (Eds.), CRC Press, Cape Town, 2008.

Annerel E., Taerwe L., Revealing the temperature history in concrete after fire exposure by microscopic analysis, Cement and Concrete Research, vol. 39, Issue 12, 2009.

THERMAL DIFFUSIVITY OF TENSILE CRACKED CONCRETE

Adam Ervine [a], Dr. M. Gillie [a], Dr. T.J. Stratford [a], Dr. P. Pankaj [a]

[a] University of Edinburgh, School of Civil, Edinburgh, UK

1 INTRODUCTION

Safety and economic considerations dictate that structures are built to resist extreme events, such as a major earthquake or fire, without collapse but some structural damage may be allowed. However, in seismic regions, a fire following an earthquake is considered to be a major threat due to the risk of ignition of damaged gas and/or fuel services. The fire resistance such as the concrete cover of the structure may be compromised during the earthquake period; hence the effect of a subsequent fire will be amplified and may lead to collapse of the structure.

This study examines the effect of tensile cracking on the thermal properties of reinforced concrete. Concrete beams in four-point bending are heated on their tensile faces. A comparison is made between the thermal response when the beam is undamaged, and subject to minor or major damage. Whilst the thermal conductivity of concrete is well documented, most available data relates to concrete that is undamaged. There are many scenarios (e.g. analysis of structures subject to fire following earthquake) in which knowledge of the conductivity of damaged concrete may be important. This is because the conductivity of damaged concrete may be significantly different to that of undamaged concrete and could lead to earlier structural failure in fire. The experiments detailed in this paper were designed to establish if tensile cracking resulting from damage alters the effective thermal diffusivity ($k/\rho c$) of concrete to a degree that can not be neglected in analyses of fire affected structures. Three hypotheses are considered,

1.1 Hypothesis I

Tensile cracking affects the thermal diffusivity of concrete so that heat transfer is more rapid, hence the reinforcement layers will experience high temperatures more quickly than in an intact section. This would cause the steel to be subjected to localised heating and elongation which could lead to failure of a member or structure more quickly than an undamaged structure.

1.1 Hypothesis II

Tensile cracking affects the thermal diffusivity of concrete so that heat transfer is less rapid, hence the reinforcement layers will experience high temperatures later in a _re than an intact section. This could cause structures to perform better than an undamaged structure..

1.1 Hypothesis III

Tensile cracking does not significantly affect the thermal diffusivity of concrete. The reinforcement layers will experience similar temperatures in a similar time to those experienced by an intact section. This would mean that the effects of tensile cracking on thermal diffusivity are negligible and do not need to be accounted for in analyses or design.

2 PREVIOUS WORK

There has been research into the thermal properties of concrete and how they vary with temperature. Similarly, there has been work on the cracking of concrete and reinforced concrete in tension. However, these research themes have yet to be fully combined to determine the thermal properties of cracked reinforced concrete.

Kong *et* al (2007), and Beeby and Scott (2005) studied the behaviour of average tensile crack width with respect to the tensile stress within reinforcement. However the stresses and strains considered all fell into the elastic region of the reinforcement which corresponds to very small crack widths (of the order of $1x10^{-1}$mm). It would be inappropriate to extrapolate this information to situations where concrete members are damaged because in such cases the reinforcement steel may have yielded and cracks reached widths in the order of $1e^{1}$mm or greater.

Vejmelková *et al* (2009) studied the effects of cracks on the hygric and thermal characteristics of concrete and obtained data suggesting the conductivity of cracked concrete decreases due to the increased porosity of the material and only increases with an increase in moisture content. They suggested that the air within cracks acts as an insulator and hence hinders the propagation of heat through the structure. A significant limitation of this work is the fact that the crack dimensions were not reported so the results cannot be combined with Kong et al's work to find a relationship between crack width and conductivity. Furthermore, plain, not reinforced concrete was used so application of the results to real structures would be difficult in any case.

Thus, work aimed at determining the thermal properties of crack damaged reinforced concrete is very limited. The work that has been undertaken has either been with un-reinforced concrete or within the elastic range of the reinforcement. The inclusion of reinforcement in the concrete during an experiment that considers cracking is vital because the reinforcement drastically alters the cracking pattern and crack propagation though a section. During extreme events such as earthquakes and blast it is unreasonable to assume that the reinforcement remains within its elastic range as these extreme events will cause larger cracks to form in the concrete. The larger the cracks within the concrete cover the more influential the buoyancy effects within these cracks become. The air within the cracks may no longer act as an insulator as Vejmelková et al suggest but may effectively allow the heat to instantaneously penetrate the concrete to the reinforcement level.

3 EXPERIMENTAL DESCRIPTION

An experimental programme was undertaken to establish which of the three hypotheses detailed in the introduction is most representative of reality. To do this beams in four point bending were heated on their tensile faces and rate of heat transfer measured for different crack widths. The beams used were doubly reinforced 35MPa (nominal) concrete with dimensions of 90×160×870mm. The reinforcement was 10Φ mm 460MPa steel. Concrete cover was 20mm on all sides with the exception of the tensile face which had a cover of 40mm. Increased cover on the tensile face was designed to induce larger tensile cracks which would be representative of beams of larger, more realistic dimensions. The beams were then loaded vertically upwards as shown in Fig. 1, either to failure or to the required deflection depending on the stage of the experiment (see Tab. 1). Heating was applied from above via a radiant gas panel.

Loads were recorded from load cells that sat under the loading jacks and deflections from gauges at mid-span and other key locations. Load and deflection data was recorded at 2s intervals. Strain fields within the area of zero shear were recorded using image correlation by taking photographs of both sides of the beam at 5s intervals and processing these with a program developed by Bisby, Take and Caspary. Temperatures in the beam during both the heating and cooling phases were recorded using a large number of thermocouples within the heated section of the beam, with the highest density being in the tensile concrete cover. Full details of the apparatus are shown in Fig. 1 to Fig. 3.

Beams were tested with various heating and loading arrangements as detailed in Table 1. Critical to the test programme was comparing the heat-transfer in the beams when they were damaged to different degrees. The behaviour of beams with "minor" and "major" damage was compared. To allow damage levels to be defined, two beams were loaded without heating and their load-deflection behaviour recorded. Minor damage was defined as the crack width that occurred when an unheated beam was loaded to point at which it ceased to behave linearly. Major damage was defined as the crack width that occurred when an unheated beam was loaded to its ultimate load. Crack widths of these magnitudes were maintained during the thermal tests by controlling the deflections of the beams.

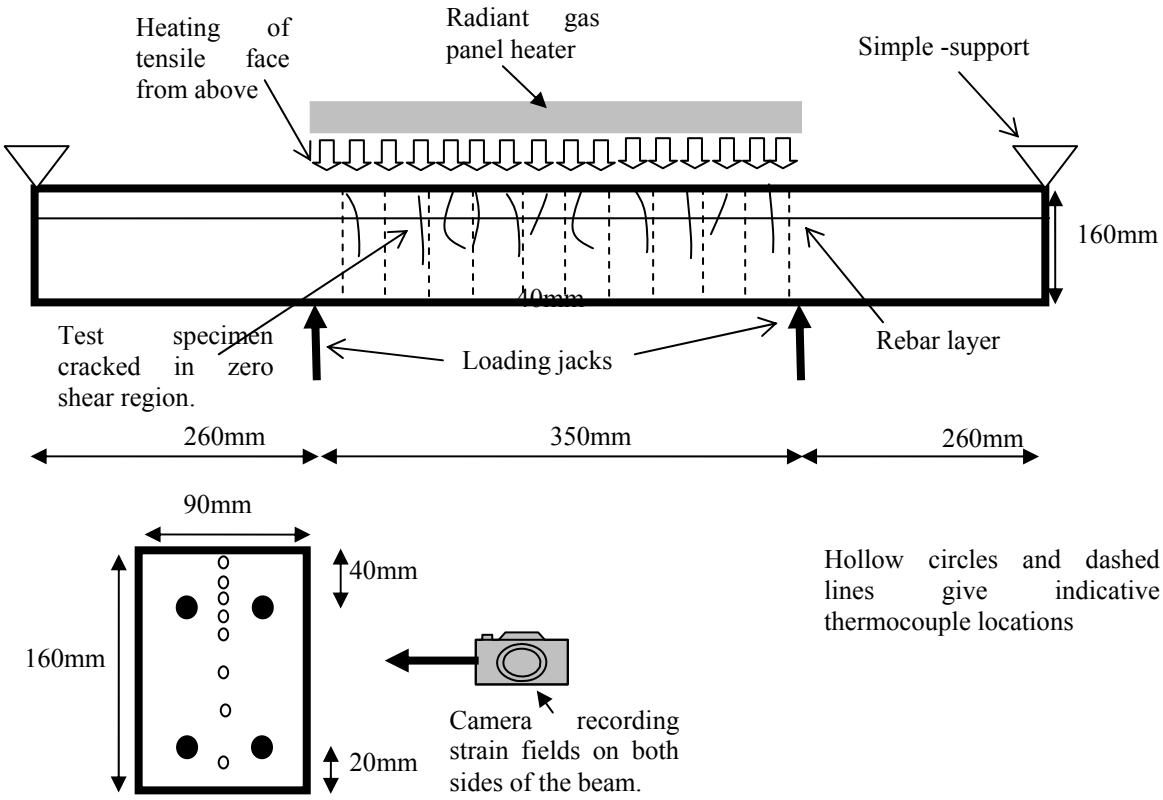

Fig. 1 Experimental setup showing side view of loaded beam and a typical cross-section.

Fig. 2 Loading set-up

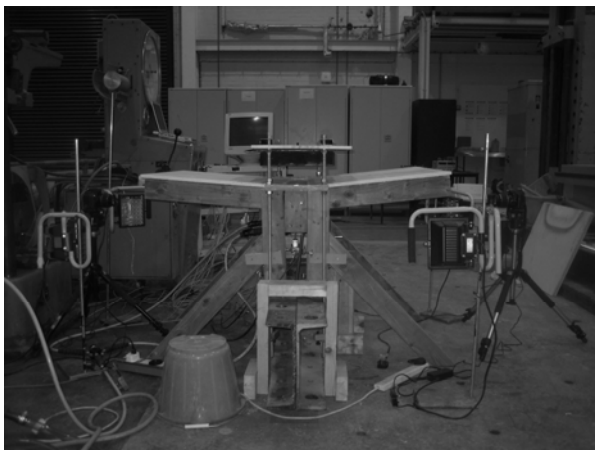

Fig. 3 General thermo-mechanical set-up

Table. 1 Loading permutations examined during the test programme.

Permutation	Thermo-couples	Loading Phase	Heating Phase	Aim
1	-	√	-	Load incrementally to failure to determine crack widths and distribution as function of load
2	-	√	-	Repeat of permutation 1
3	√	√	√	To determine effect of minor damage on thermal behaviour.
4	√	√	√	To determine effect of minor damage on thermal behaviour.

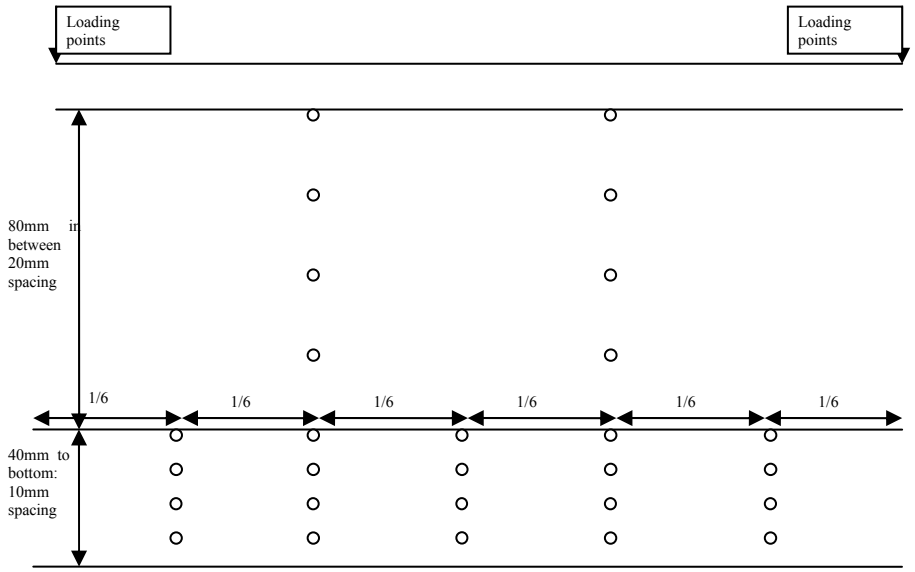

Fig. 4 Placement of thermo-couples

As the investigation is to determine if tensile cracking has any effect on the thermal diffusivity the majority of the thermo-couples were placed within the concrete cover on the tensile side of the beam. This can be seen in Fig. 4.

3 EXPERIMENTAL RESULTS

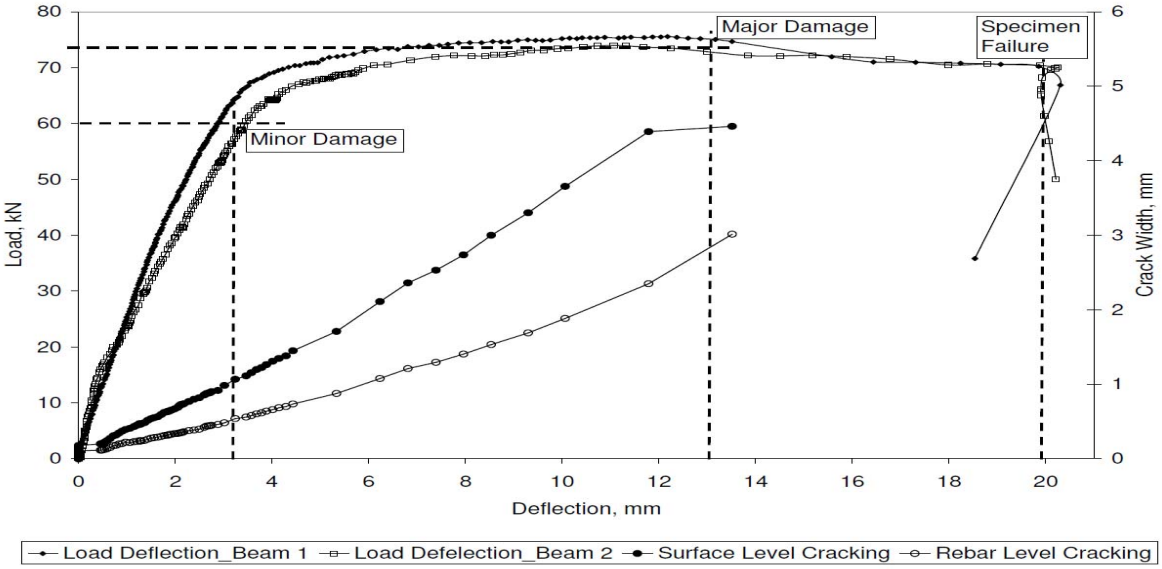

Fig. 5 Load versus deflection (left axis); Crack width versus Deflection (right axis)

3.1 Definition of Damage

From Fig. 5 it can be seen that the beams subject to purely mechanical load behaved similarly. Transition from elastic to plastic behaviour occurred at approximately 60kN with a mid-span deflection of 3.5mm and the ultimate load was approximately 75kN (approximately 1.3 times the design load). These results therefore can be used as measures of minor and major damage states in terms of crack widths. The label "minor damage" will be defined as a state that occurs under reasonable serviceability loads; whilst "major damage" will be defined to occur some way into the plastic region. Therefore, the minor damage state will be set to experience loads in the region of 60kN and a mid-span deflections of 3mm; whereas the major damage state will be set to experience loads in the region of 74kN and a mid-span deflection of 12.5mm. Images of these states can be seen in Figs 6 and 7.

Table. 2 – Damage State Summary

	Minor Damage	Major Damage
Load, kN	60	74
Mid-span Deflection, mm	3	12.5
Average Surface Crack Width, mm	0.75	3
Average Rebar Level Crack Width, mm	0.4	1.5

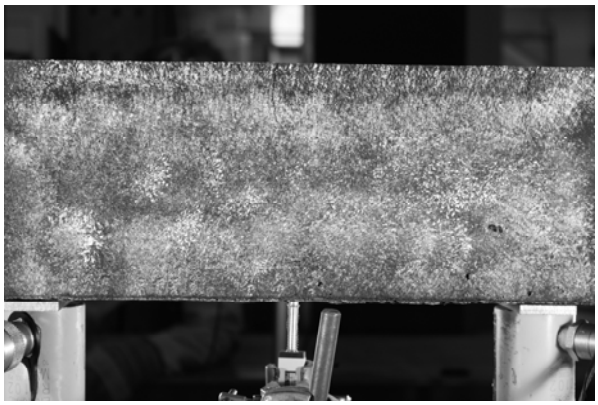

Fig. 6 Minor damage image

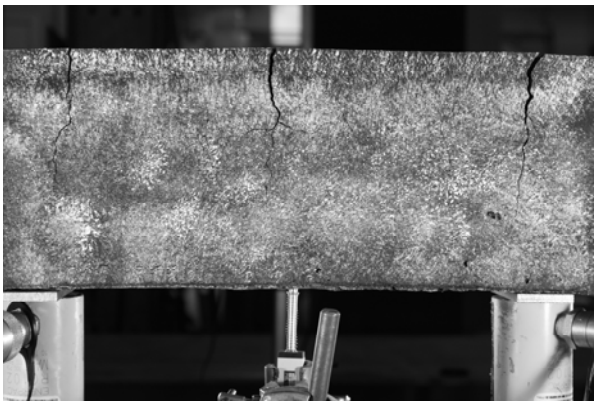

Fig. 7 Major damage image

3.2 Thermal Results

Figs. 8 and 9 show the curves from averaged thermocouple temperatures at depths of 10mm to 40mm (i.e. level of tensile reinforcement). In both figures there is a clear change in gradient at about 100°C for all curves. This is caused by the latent heat required to evaporate the moisture from the concrete during heating. Throughout the heating phase differences are seen between the damaged and undamaged cases whilst during cooling the differences are no longer present. The differences are largest for the case of major damage (Fig. 9) and also at greater depths. The recorded differences in temperatures between the damaged and undamaged cases remain small at all times (a peak difference of about 10% occurs for major damage at around 2000s and 40mm depth).

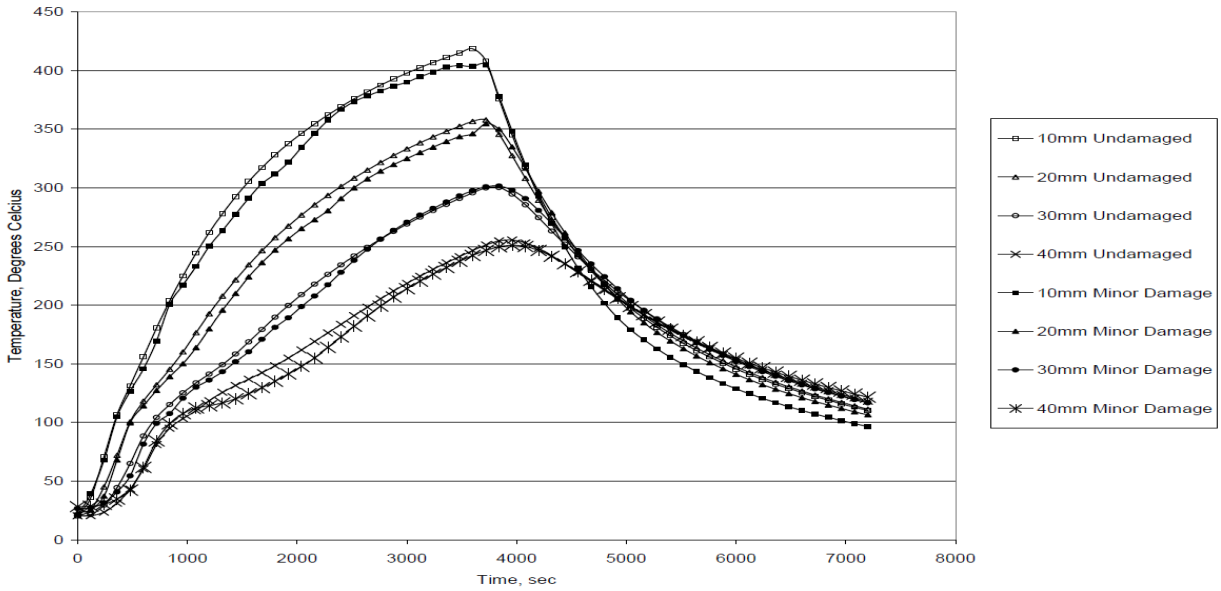

Fig. 8 Comparison of thermal profiles for minor and major damaged sections

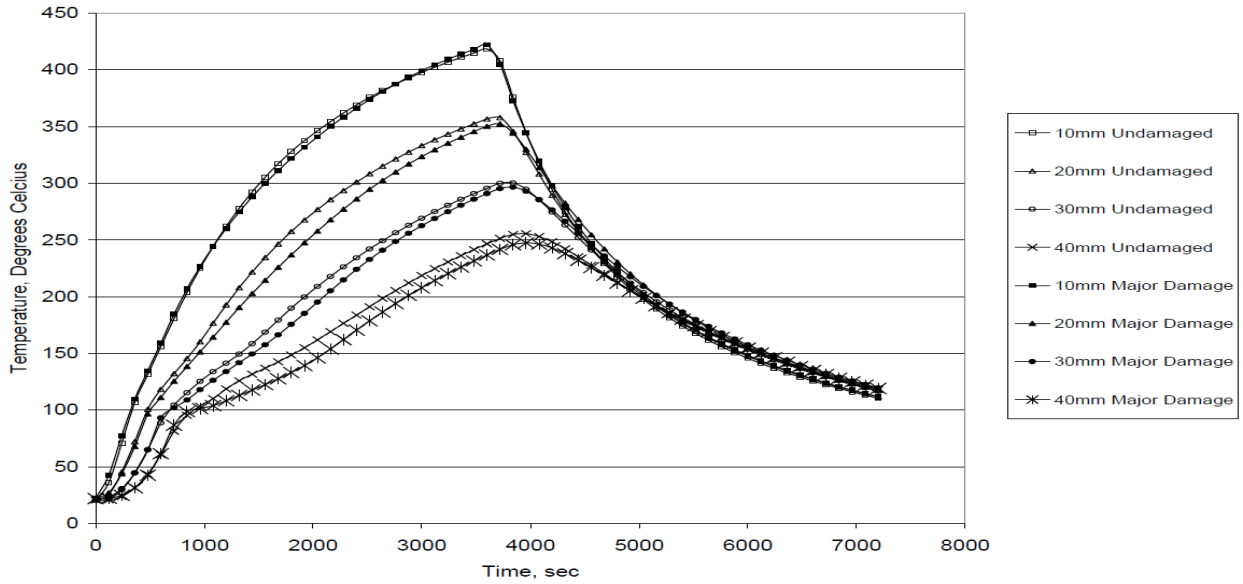

Fig. 9 Comparison of thermal profiles for minor and major damaged sections

4 CONCLUSIONS

The main conclusion of this work is that that there is no significant increase or decrease in the thermal diffusivity of concrete with tensile cracking where the cracks are up to the order of $1e^{1}$mm at the heated surface. Therefore hypothesis III, as defined in the introduction, can be broadly accepted whilst hypotheses I and II are rejected. This conclusion is significant because it implies that in calculations, thermal material properties do not need to be made a function of strain or crack width for the conditions covered within this investigation. This information is particularly relevant for numerical simulations. Performing thermal then mechanical analyses of heated structures sequentially, as is typically undertaken currently, remains a valid approach. It remains the case that fully coupled thermal-mechanical analyses, which involve substantially more complex numerical solutions, are not necessary for structural calculations even when significant tensile damage is induced in the structure.

REFERENCES

Vejmelková, E., Padevět, P. and Černý, R., Effects of cracks on hygric and thermal characteristics of concrete, Ernst & Sohn (2009)

Beeby, A.W. and Scott R.H., Cracking and deformations of axially reinforced members subjected to pure tension, Magazine of Concrete Research, (2005), 57, No.10, December 611-621

Kong, K.L., Beeby, A.W., Forth, J.P. and Scott R.H., Cracking and tension zone behaviour of RC flexural members, Structures and Buildings 160 Issue SB3 (22/03/2007), 165-172

Bisby, L., Take, A.W. and Caspary, A., Quantifying Strain Variation in FRP Confined Concrete using Digital Image Correlation: Proof-of-Concept and Initial results, Department Civil Engineering, Queen's University, Canada

COLOUR CHANGE OF HEATED CONCRETE

RGB colour histogram analysis as a method for fire damage assessment of concrete

Izabela Hager [a]

[a] Cracow University of Technology, Faculty of Civil Engineering, Cracow, Poland

INTRODUCTION

The assessment of fire damage to concrete structures usually starts with a visual evaluation, which consists of observing the presence of changes caused by heat exposure. In order to simplify this task, a four-degree classification of damage to beams, columns and slabs (LCPC, 2005, The Concrete Society, 2008) has been developed, which includes the usual repair methods for each class of damage. The condition of members is classified through the assessment of the following parameters: the presence of soot and smoke deposits; the colour change of concrete; concrete flaking or spalling; the presence of cracks and microcracks; the degree to which reinforcing steel is exposed; and possible visible deformation to the structure (excessive deflection of beams and lateral distortion of columns). Most of the in situ techniques used to assess the condition of concrete after being exposed to fire are well-known methods, widely used to check the properties of concrete in structures. In case of fire damage, laboratory techniques are also frequently used to assess concrete integrity. These tests require the sampling of material and laboratory testing. The tests carried out on concrete core samples are designed to determine the residual mechanical properties of the damaged concrete (direct method) or else to estimate the temperature to which the concrete was exposed during the fire (indirect methods). Such tests include resonance frequency method, ultrasound method, DTA, TGA, X-ray diffraction, scanning microscopy, thermoluminescence, chemical or petrographic analyses or colourimetry.

1 COLOURIMETRY APPLICATION

Colourimetry is an indirect method that uses the fact that when concrete is heated, its colour changes. Colour changes caused by temperature within construction concrete are easy to identify by means of visual comparison with concrete unaffected by high temperature. However colour change is not directly related to changes in the mechanical and physical properties of concrete, but provides an indicator of the temperature achieved by the concrete during fire. Temperature data can be used for a quantitative estimation of properties such as the compressive strength or modulus of elasticity when the fc(T), and E(T) relationship are identified.

The existing technique of a rough estimation of the temperature to which concrete was subjected involves an inherently subjective visual colour analysis. It is generally agreed (Short et al, 2001) that when heated up to between 300 °C and 600 °C concrete will turn red, between 600 °C and 900 °C it will turn whitish-grey, and heating to between 900 °C and 1000 °C gives the concrete a buff colour. The most pronounced changes in colour occur in concretes made from silicate aggregates which become red or pink when heated to between 300 °C and 600 °C The red colouration in the temperature range is caused by the oxidation of mineral components with iron compounds (oxides or hydroxides, etc.).

In order to describe concrete colour changes in a precise manner, a variety of colour description techniques are used (Short et al., 2001, Luo, Lin, 2007, Annerel, Taerwe, 2009, Felicetti, 2004).

In the tests conducted by Faure and Hemond described in (LCPC n°62, 2005), a spectrophotometer was used directly on the surface of concrete samples. The method used by Short (Short et al., 2001) consisted of observing samples through a polarising microscope equipped with a colour analysing software package. The technique proposed by Felicetti (Felicetti, 2004) employs a general purpose digital camera for taking pictures and analysing the colour changes of the concrete depending on the temperature reached. The latter method, however, requires consistent lighting, which is not easy to

achieve. A light tent is required, and the white balance of the camera has to be adjusted. Recently, the author proposed a technique in which a flatbed scanner (Hager, 2010) is used to obtain constant lighting conditions while pictures of concrete samples are taken. No expensive measurement equipment and/or colour analysis computer software is necessary to perform these measurements. In this method, pictures taken with a general-purpose scanner (HP Scanjet G2410) are analysed using an image analysis software package, in this case Scion Image (version 4.0.3, Scion Corporation ©, USA). The Scion package is a freeware tool created to facilitate digital image analysis within the medical sector. In terms of the method proposed for concrete analysis, a digital image is split into three RGB (Red Green Blue) colour components – red, green and blue – then presented as a histogram using counts of pixel intensity. The results of the histogram show colour distribution in unheated concrete and in concrete heated across a temperature range from 100 °C to 1000 °C. Histograms from laboratory-heated concrete provide a scale which is then used to determine the temperature actually reached by concrete in a structure. This is done by comparing the scale images with the images of cored samples taken from the structure. The method offers a simple and inexpensive way of identifying the areas or depth of the concrete affected by fire temperature.

In general, two different approaches can be used when using colour analysis to assess the condition of concrete after a fire. First, the external surface of the element can be examined; this involves the observation of an element's outer walls – in particular, the cement paste. By examining the extent of change of the element's surface colour, the impact of the temperature can be assessed. However this method is not feasible if the surface has been affected by smoke or covered with soot. The other option is to observe the surface with visible aggregates. This is the engaged, cored, or spalled surface of the element. The observation consists of examining the surface with exposed aggregate grains or a cut surface produced as a result of coring or sawing. These processes reveal aggregate grains that, during heating, often significantly change into more intense red or pink colours. This change is more pronounced and easier to distinguish than the change of the cement paste.

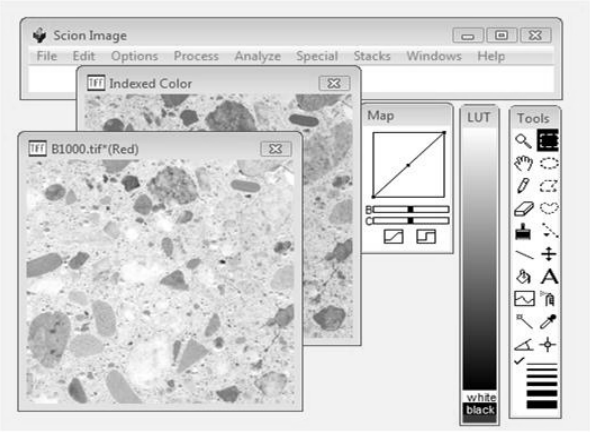

Fig. 1 Scion Image environment.

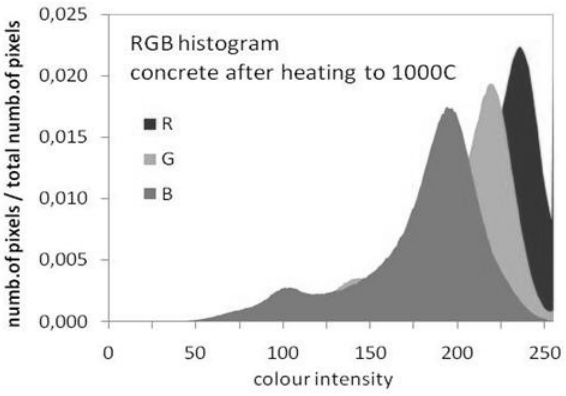

Fig. 2 RGB normalized histogram.

2 SOFTWARE DESCRIPTION

The Scion Image package v. 4.0.3, (Scion Corporation ©, USA) is an image processing and analysis program. It can acquire, display, edit, enhance, analyze and animate images. It reads and writes TIFF and BMP files, providing compatibility with many other applications, including programs for scanning, processing, editing, publishing and analyzing images. It supports many standard image-processing functions, including contrast enhancement, density profiling, smoothing, sharpening, edge detection, median filtering, etc. Scion Image for Windows can be used to measure user-defined regions of interest for an element including its area, centroid, perimeter, etc. It also performs automated particle analysis and provides tools for measuring path lengths and angles. Results can be printed, exported to text files, or copied to the program's clipboard. It supports multiple windows and eight levels of magnification.

All editing, filtering, and measurement functions operate at any level of magnification and can be undone. Scion Image manipulates, displays and analyses images. Images are two-dimensional arrays of pixels (picture elements). All pixels are represented by Red Green Blue values ranging from 0 to 255. The software environment is presented on Fig. 1.

3 MATERIALS AND TESTING PROCEDURE

The tested materials were on ordinary (OC) and high performance (HPC) concretes, mortars and cement pastes. Both concretes consisted of the cement type CEM II/A-V 42.5R, water and natural riverbed aggregates: sand 0-2 mm; gravel 2-8 mm and 8-16 mm. The mix composition of concretes is given in Table 1. The mortars and cement pastes were confectioned with the same cement and w/c (water/cement) ratio than concretes.

Tab. 1 Concretes mix proportions

	Unit	OC	HPC
cement CEM II/A - V 42,5 R	kg/m^3	322	478
water	dm^3/m^3	193	129
w/c	-	0,6	0,27
sand 0 - 2 mm	kg/m^3	623	
gravel 2 - 8 mm	kg/m^3	660	
gravel 8 - 16 mm	kg/m^3	550	

The colour change observation was performed on the surfaces of the sample concretes, mortars and cement pastes. The samples were heated in an electric furnace with a constant heating rate of 1°C/min to reach subsequent temperatures of T =100, 200, 300, 400, 500, 600, 700, 800, 900 and 1000 °C. After cooling digital images were taken from the sample surfaces with scanner.

A general-purpose flatbed scanner (HP Scanjet G2410) was used. The pictures were taken with a pixel density resolution of 600 ppi. The images were then exported as TIFF raster files into the Scion Image software described above. It features an option to export the results in a text file for further processing. The testing was based on the RGB colour model because of its widespread use in digital equipment (scanners and computer screens). The RGB model is of the additive type, where adding the RGB components produces colours.

The digital images of samples surfaces were decomposed into RGB components using Scion Image. The frequencies of occurrence of red, green and blue pixel components were presented as frequency histograms. The RGB model assumes intensity levels ranging from 0 to 255 that are shown on the horizontal axis where black equals 0, and white 255. On the vertical axis the numbers of pixels of a certain intensity in an image are presented.

The testing involved a normalisation process where the values corresponding to the number of pixels with a specified intensity were divided by the total number of pixels in a given image (Fig.2). Histogram normalisation makes comparison of images with different pixel counts possible. Additionally, the process produces functions that have properties of the probability density function (Hager, 2010). Histograms can be used to generate a number of parameters defining the properties of this function, including the maximum and standard deviation values, curtosis, etc. Differences between these parameters reflect different properties of the image histogram and allow for comparisons.

4 RESULTS

The results of the testing of the impact of heating temperature on the colour change of ordinary and high performance concretes, mortars and cement pastes are presented in Fig.3.

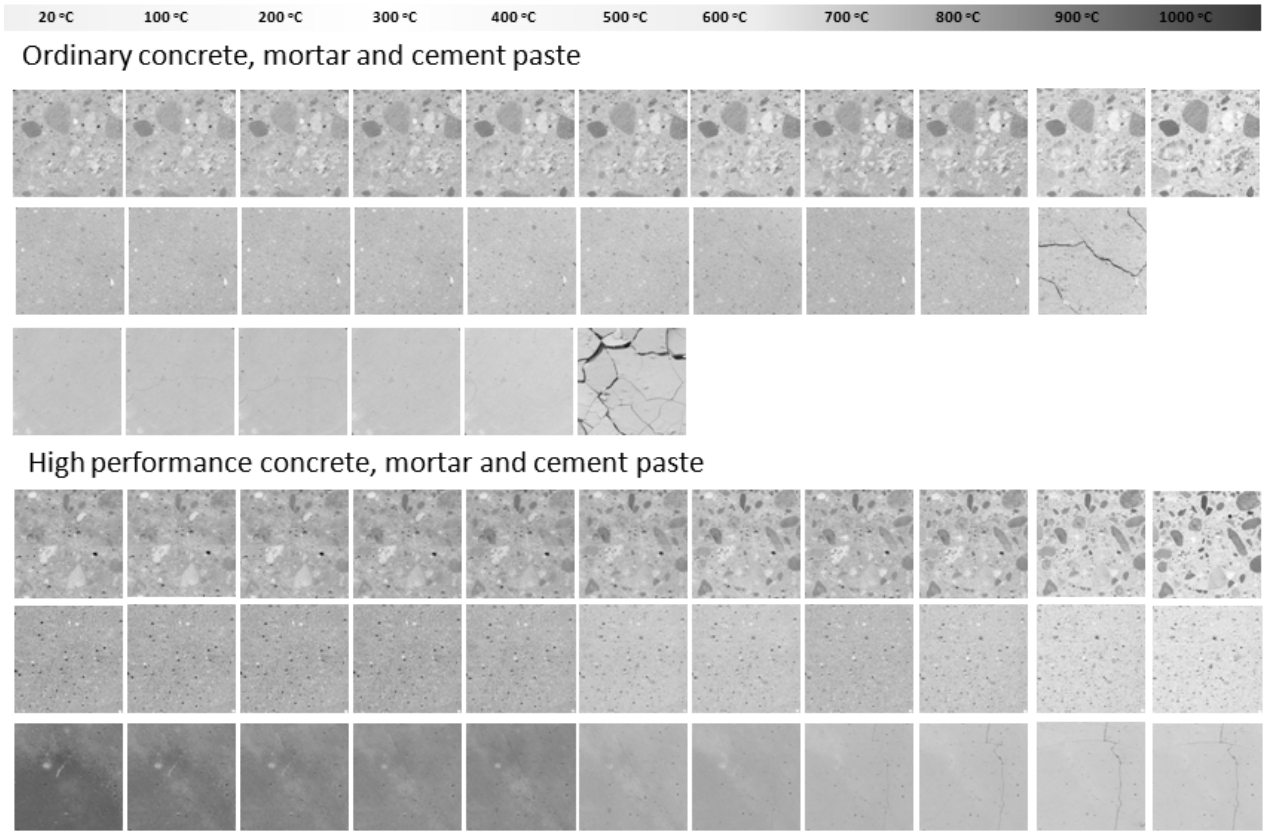

Fig. 3 Colour change of ordinary and high performance concretes, mortars and cement pastes heated to temperature ranging from 100 to 1000 °C.

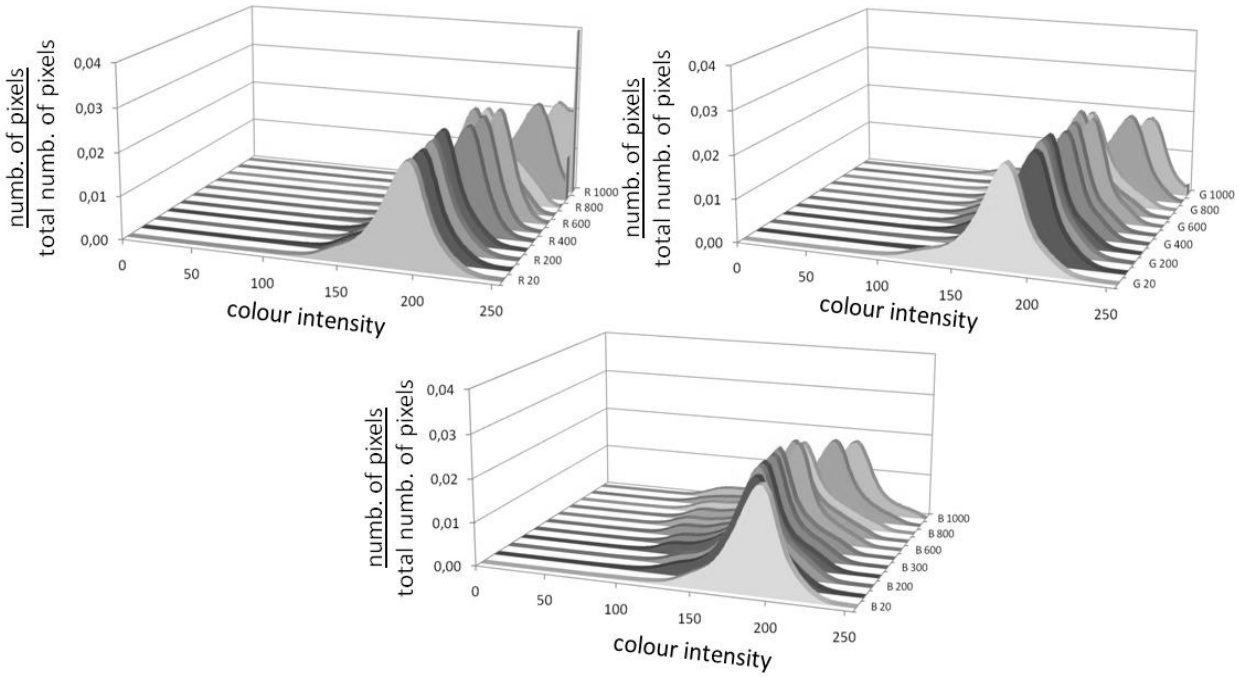

Fig. 4 A comparison of normalised histograms of the red, green and blue component intensity values obtained for an ordinary concrete samples in the range of temperatures from 20 to 1000 °C.

As an example, for ordinary concrete the normalised histograms of the red, green and blue components (Fig. 4) are presented as a function of heating temperature.

Colour changes observed as a result of heating were mainly caused by water evaporation and dehydration of cement paste and chemical reactions in the mineral components of the aggregate. The most intense colour change was observed in components containing minerals including iron (jarosyte, goethite). As temperature rises, aggregates and components containing calcium carbonate $CaCO_3$ go through the process of calcination and their colour is dominated by pale shades of white and grey.
The samples of concretes used in this study were also tested in compression in order to determine a relationship between the strength parameters of the material concerned and the temperature of exposition. To this end samples in the form of a 15 cm cube were heated at a rate of 0,5°C/min. to reach the target temperatures of 200, 400, 600 and 800 °C. Once the temperature was reached the samples were heated for five more hours to stabilise the temperature across the section. The samples were then cooled down to 20 °C and tested in compression. The chart on Fig. 5. shows the residual compressive strength of tested HPC and OC concretes.

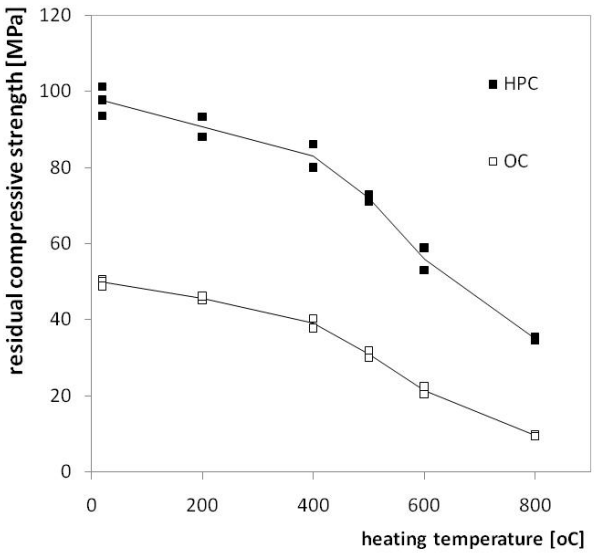

Fig. 5 Residual compressive strength of a) ordinary concrete, b) high performance concrete as a function of temperature.

5 SUMMARY AND ACKNOWLEDGMENT

During a real fire, temperatures within a concrete section do not generally reach equilibrium values. A thermal gradient is established where the temperature of the outside layers is drastically increased, while the temperatures of the inner concrete may be relatively low. The method described in the paper is the useful technique for estimating the maximal exposition temperature of concrete subjected to fire by using an analysis of the colour image. A scanner seems to be a useful and simple tool for making digital images of samples/cores resulting in guaranteed consistent lighting conditions. The scanner requires no special preparation of the samples. A similar degree of usefulness and simplicity was established with regard to the colour analysis using the RGB model and the readily available software package Scion Image. A calibration scale was produced by taking images of concrete samples heated to temperatures across the 100 - 1000 °C range. The scale can be used to estimate the exposition temperature of concrete in structures subjected to a real fire. In practice, several techniques should be combined in order to obtain a sufficiently complete and accurate picture of the damage to the concrete member in question.
The study was supported in part by the Polish Ministry of Higher Education Grant N N506 045040.

REFERENCES

LCPC n°62, Présentation des techniques de diagnostic de l'état d'un béton soumis à un incendie, Laboratoire Central des Ponts et Chaussées, Paris, France, 2005, p. 114.

Assessment, Design and Repair of Fire-Damaged Concrete Structures, Technical Report No.68, The Concrete Society, London, United Kingdom, 2008, p.80.

Hager I., The Application of RGB Histogram Analysis of Colour Images as a Method of Assessing the Condition of Concrete in Structures After Fire, Proceedings 6th International Conference on Structures in Fire SiF'10, Michigan State University, East Lansing, United States of America, 2-4 of June of 2010, ed.: Venkatesh Kodur, Jean-Marc Franssen

Hager, I., Methods for assessing the state of concrete in fire damaged structures, Cement Lime Concrete, July / August 2009, nr 4, p. 167-178.

Annerel E., Taerwe L., Reveling the temperature history in concrete after fire exposure by microscopic analysis, Cement and Concrete Research 39 (2009)

Felicetti, R. Digital camera colorimetry for the assessment of fire-damaged concrete, in: P.G. Gambarova, R. Felicetti, A. Meda, P. Riva, Proceedings of the Workshop: Fire Design of Concrete Structures: What now? What next? fib Task Group 4.3 'Fire Design of Concrete Structures', Milan, 2004, pp. 211–220.

Luo H. L., Lin D.F. Study the surface color sewage sludge mortar at high temperature, Construction and Building Materials 21 (2007), p 90-97

Short N. R., Purkiss J. A., Guise S. E., Assessment of fire damaged concrete using colour image analysis, Construction and Building Materials, Vol. 15 (2001) p. 9-15.

INFLUENCE OF TRANSIENT STRAIN ON FIRE RESISTANCE OF CONCRETE ELEMENTS

Limin Lu [a], Emmanuel Annerel [a], Luc Taerwe [a], Yong Yuan [b]

[a] Ghent University, Faculty of Engineering and Architecture, Department of Structural Engineering, Ghent, Belgium
[b] Tongji University, Department of Civil Engineering, Shanghai, China

INTRODUCTION

Reinforced concrete (RC) elements generally have good fire-resistance ability. Knowledge of the temperature dependant material properties of concrete and steel bars is important for understanding of the fire-response of a RC structure. At high temperatures, the total strain of concrete is for a large extent influenced by load dependent strains, the so called transient strain and creep strain. Although these types of strain are not considered in simplified calculation procedures of concrete elements exposed to fire as provided in EN 1992-1-2, they may be of major importance for the development of deformation during heating (Sebastjan Bratina, 2006; Paolo Riva, 2002).
Based on the mechanical properties of concrete and steel bars at elevated temperatures as given in literature (EN 1992-1-2, Jin, Tao 2009), a numerical model which includes transient strain and creep strain is proposed. The computational procedure consists of a coupled thermo-mechanical analysis, including the development of the temperature, the deflection and ultimate bending moment. The proposed approach is validated by experimental data from fire tests executed on simply supported slabs exposed to an ISO 834 fire load. The influence of transient strain is analyzed by comparing the calculating results.

1 NUMERICAL MODEL

1.1 General

The proposed method is based on an average stiffness method to analyze reinforced concrete elements subject to bending. The numerical process is performed in three steps: 1) thermal calculation; 2) mechanical properties of the cross section and 3) structural analysis.
The RC element is divided into a number of small segments along its length (Fig.1). The mid-section of each segment represents the behavior of the whole segment. Firstly, the thermal field of the cross sections is analyzed at each time step and then material properties are adjusted according to the obtained temperatures. Secondly, the stiffness of each segment is generated by sectional stress strain analysis using the changing properties of concrete and steel bars. The ultimate bearing moment can also be generated during this process. Thirdly, average stiffness of the element will be induced based on the conclusions of sectional analysis, and the deflections can be calculated by structural analysis.

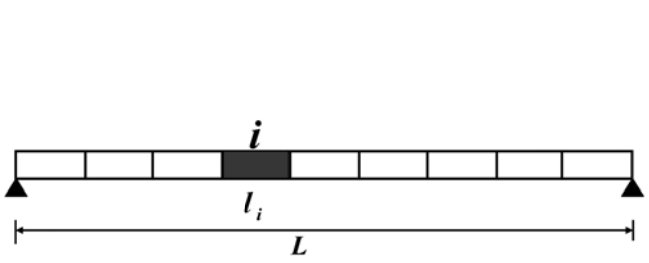

Fig.1. RC element and layout of segments

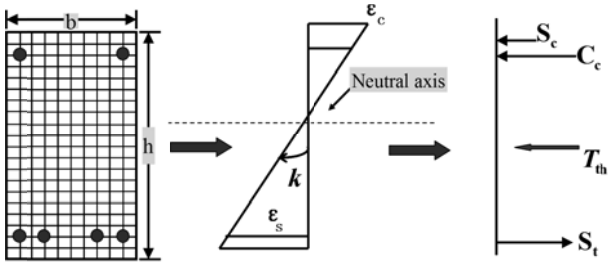

Fig.2. Section and strain relationship

1.2 High temperature properties of concrete and steel bars

The temperature field at each time step within the element is calculated by finite element method. As the heating conditions along the element are assumed to be identical, the temperature field of the

element can be simplified into a 2D problem. Steel bars are neglected as they don't significantly influence the temperature distribution in the cross section. The thermal conduction coefficient and the specific heat of concrete are taken according to EN 1992-1-2 (EC2). Generally, beams are assumed to be heated from three sides and slabs only from the bottom. The temperature calculation is carried out by means of the finite element package DIANA.

(1) High temperature properties of concrete

According to EC2, the total strain of concrete ε_{mc} at a higher temperature T is a sum of four parts: mechanical strain ε_{σ}, thermal strain ε_{th}, transient strain ε_{tr} and creep strain ε_{cr}, as shown by equation (1).

$$\varepsilon_{mc} = \varepsilon_{\sigma}(\sigma,T) + \varepsilon_{th}(T) + \varepsilon_{tr}(\sigma_0,T) + \varepsilon_{cr}(\sigma_0,T,t) \tag{1}$$

Thermal strain is a function of temperature only, mechanical and transient strain are determined by both the temperature and initial stress and the creep depends on all three basic. These properties can be well approximated by the equations (2), (3) and (4) (Jin Tao, 2009). The stress-stain relationship of concrete at high temperature is given by equation (5).

$$\varepsilon_{th} = \begin{cases} -1.8\times10^{-4} + 9\times10^{-6}T + 2.3\times10^{-11}T^3 & \text{for } 20°\text{C} \le \text{T} \le 700°\text{C} \\ 14\times10^{-3} & \text{for } 700°\text{C} \le \text{T} \le 1200°\text{C} \end{cases} \tag{2}$$

$$\varepsilon_{tr}(\theta,\sigma) = \frac{\sigma}{f_c}(-2.64\times10^{-13}T^4 + 2.93\times10^{-10}T^3 - 9.46\times10^{-8}T^2 - 5.79\times10^{-6}T + 0.00027) \tag{3}$$

$$\varepsilon_{cr} = \frac{\sigma}{f_c}\times\left(43.11e^{-0.00477T} + 123.21\right)\left(\frac{t}{10800}\right)^{0.3}\times10^{-6} \tag{4}$$

$$\sigma_c = \begin{cases} f_c^T\left[a\left(\dfrac{\varepsilon_\sigma}{\varepsilon_p^T}\right) + (3-2a)\left(\dfrac{\varepsilon_\sigma}{\varepsilon_p^T}\right)^2 + (a-2)\left(\dfrac{\varepsilon_\sigma}{\varepsilon_p^T}\right)^3\right] & 0 \le \varepsilon_\sigma \le \varepsilon_p^T \\ \dfrac{f_c^T\left(\varepsilon_\sigma/\varepsilon_p^T\right)}{b(\varepsilon_\sigma/\varepsilon_p^T - 1)^2 + \varepsilon_\sigma/\varepsilon_p^T} & \varepsilon_\sigma \le \varepsilon_p^T \end{cases} \tag{5}$$

where σ initial stress of concrete ;

a, b coefficients;

ε_p^T elastic limit strain at high temperature;

f_c, f_c^T compressive strength of concrete at ambient and high temperature;

t, T time and temperature.

(2) High Temperature properties of steel

Similar to concrete, the total strain of steel bars contains three parts: mechanical strain $\varepsilon_{s,\sigma}$, thermal strain $\varepsilon_{s,th}$ and creep strain $\varepsilon_{s,cr}$ .as shown by expression (6). Thermal strain of steel can be calculated with reference to the length at 20˚C, by equation (7). Compared to the thermal and mechanical strain, creep strain of steel is quite small, and is neglected in the calculation. The stress-strain relationship of steel bars can be expressed by equation (8).

$$\varepsilon_{ms} = \varepsilon_{s,\sigma}(\sigma,T) + \varepsilon_{s,th}(T) + \varepsilon_{s,cr}(\sigma,T,t) \tag{6}$$

$$\varepsilon_{s,th} = \begin{cases} -2.416\times10^{-4} + 1.2\times10^{-5}T + 0.4\times10^{-8}T^2 & for\ 20°C \le T \le 750°C \\ 11\times10^{-3} & for\ 750°C < T \le 860°C \\ -6.2\times10^{-3} + 2\times10^{-5}T & for\ 860°C < T \le 1200°C \end{cases} \tag{7}$$

$$\sigma_s = \begin{cases} \varepsilon \mathrm{E}_\mathrm{s}^T & 0 \le \varepsilon \le \varepsilon_{sp}^T \\ f_{sp}^T - c + (b/a)[a^2 - \left(\varepsilon_{sy}^T - \varepsilon\right)^2]^{0.5} & \varepsilon_{sp}^T \le \varepsilon \le \varepsilon_{sy}^T \\ f_{sy}^T & \varepsilon_{sy}^T \le \varepsilon \le \varepsilon_{st}^T \\ f_{sy}^T[1-(\varepsilon - \varepsilon_{st}^T)/(\varepsilon_{su}^T - \varepsilon_{st}^T)] & \varepsilon_{st}^T \le \varepsilon \le \varepsilon_{su}^T \end{cases} \tag{8}$$

where

$e_{sp}^T = f_{sp}^T / E_s^T; e_{sy}^T = 0.02; e_{st}^T = 0.15;\ e_{su}^T = 0.20;$

$a = (e_{sy}^T - e_{sp}^T)(e_{sy}^T - e_{sp}^T + c / E_s^T); b = c(e_{sy}^T - e_{sp}^T)E_s^T + c^2;$

$c = (f_{sy}^T - f_{sp}^T)^2 / [(e_{sy}^T - e_{sp}^T)E_s^T - 2(f_{sy}^T - f_{sp}^T)];$

E_s^T is young's modulas of steel at T;

f_{sp}^T is yield strength of steel at T;

f_{sy}^T is ultimate strength of steel at T;

1.2 Mechanical properties of the cross-section

At each time step, a moment-curvature relationship (M-k) can be generated by sectional analysis (Fig.2). The mechanical analysis is based on the following assumptions mentioned in (Kodur, V.K.R, 2008):

(1) Plane sections remain plane after bending;

(2) Bond slip between steel bars and concrete is neglected;

(3) Spalling of concrete is neglected;

(4) For bending elements, shear deformations are not considered.

Firstly, the rectangular section with dimension $b \times h$ is set into a coordination system, with the bottom line of the section coinciding with the X-coordinate and left line of the section coinciding with the Y-coordinate. Then the section is divided into $m \times n$ small units (Fig.2), the area of each unit being $\frac{b}{m} \times \frac{h}{n}$. The location of each unit in this system can be expressed as (x_i, y_i).

According to the plane section assumption, a linear relationship exists for the concrete strains and steel bar strains. The total strain of the upper most units is remarked as ε_{mc0}, and then the total strain of other concrete units and the total strain of the steel units can be computed by the following expressions:

$$\varepsilon_{mc} = \varepsilon_{mc0} - k(h - y_i) \tag{9}$$

$$\varepsilon_{ms} = k(h - \alpha_s) - \varepsilon_{mc0} \tag{10}$$

where $\varepsilon_{mc}, \varepsilon_{ms}$ the total strain of concrete units and steel bars;

y_i Y-coordinate location of unit i $(i = 1, 2, 3.....)$;

k curvature;

α_s thickness of the concrete cover of steel bars.

The mechanical strain of concrete and steel units can be generated by substituting $\varepsilon_{mc}, \varepsilon_{ms}$ expressed by (9) and (10) into equation (1) and (2). With the mechanical strain of concrete units and steel units, stress of each unit is determined by solving equations (5) and (8). Once the stresses of concrete units and steel units are known, the force of them in high temperature can be computed by equation (11) and (12).

$$S_R = \sum_{i=1}^{n_s} A_{si}\sigma_s \tag{11}$$

$$C = \int \sigma_c \mathrm{dA} = \sum_{i=1}^{m} \sum_{j=1}^{n} \sigma_c (T_{i,j}, \varepsilon_\sigma) \tag{12}$$

where $C,\ S_R$ the resulting force of concrete and steel stresses;

A_{si} the area of one steel bar;

Based on the compatibility criterion and a convergence criterion, an iterative process of curvature k is carried out to make a balance between C and S_R. The iterative process will end at a balanced state and the moment of this state can be expressed by equation (13) where y_c is the effective center of concrete. Through this process, moment-curvature curves at each time step will be generated, and the average stiffness of each segment can be computed by equation (14).

$$M = C(y_c - \alpha_s) = S_R(y_c - \alpha_s) \tag{13}$$

$$EI(t, l_i) = M(t, l_i) / k(t, l_i) \tag{14}$$

1.3 Structural analysis

The next step is nonlinear structural analysis using the calculation results of the cross section. To obtain the deflection of the bending element at any time step under a given load, the global stiffness matrix and related nodal loads should first be analyzed. The deflection of the structure can be determined by equation (15).

$$\left[K_g\right][u] = [P] \tag{15}$$

where $\left[K_g\right]$ the global stiffness matrix of the elements;

$[u]$ the deformation matrix of all the segments nodes;

$[P]$ the relative nodal load matrix.

Thus, for each time step, after thermal computing, sectional analysis and structural analysis, the ultimate bearing moment and the deflection of the RC element under a given fire curve will be generated.

2 TEST VALIDATION

The proposed numerical model is validated by the fire test results reported by Minne R et al, (1979).

2.1 Slab tests

Simply supported slabs, measuring $1900 \times 150 \times 4900$ mm, were positioned in a steel frame and loaded by means of two hydraulic jacks situated at ¼th of the effective span which measured 4.5 m. The slabs are one-way spanning, designed for a service live load of $3kN/m^2$ and an admissible steel stress of $240N/mm^2$. Table 1 presents the total applied load during heating and the properties of siliceous aggregates concrete before heating. Table 2 shows the reinforcement properties. For each group of slabs, differences can be found in the number of reinforcing bars and the concrete cover on the main reinforcement. During the fire tests, the temperature at the main reinforcement depth and the deflection at mid-span were measured.

Tab.1. Applied load and concrete material properties

	Applied force [kN]	f_c *[N/mm²]*	f_{ct} *[N/mm²]*	E_c *[N/mm²]*	ρ *[kg/m³]*
G1	14.5	53.4	4.62	45200	2420
G2	15.7	54.6	4.63	38100	2400
G3	14.6	53.8	5.45	39800	2393

Tab.2. Reinforcement properties before heating.

	Longitudinal reinforcement			*Transversal reinforcement*	*Concrete cover [mm]*
	f_s N/mm²]	*εfailure [%]*			
G1	504	17.7	15 x Ø10	26 x Ø 6	15
G2	504	17.7	17 x Ø10	26 x Ø 6	25
G3	504	17.7	18 x Ø10	26 x Ø 6	35

2.2 Results and conclusions

The obtained deformation of slab G1, G2 and G3 measured during test as well as the calculation results without transient creep strain considered are shown in figure 3. The mid-span deflection curves calculated with and without transient strain are compared in figure4.

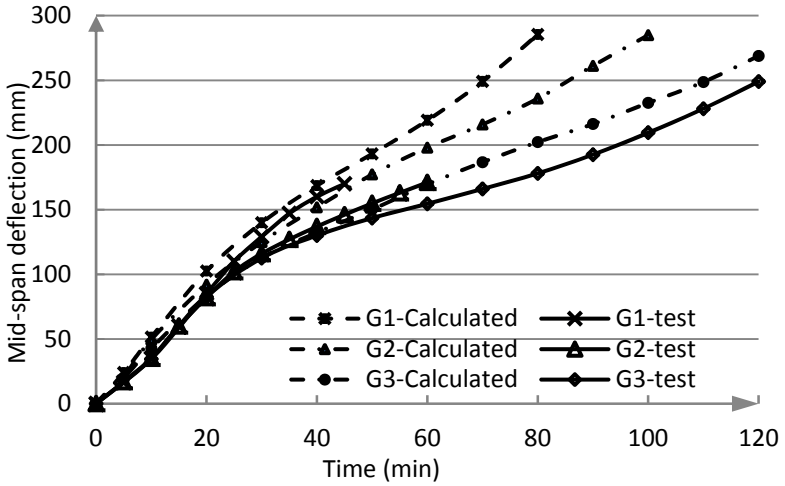

Fig.3 Mid-span deflections of G1, G2 and G3 (transient strain not considered)

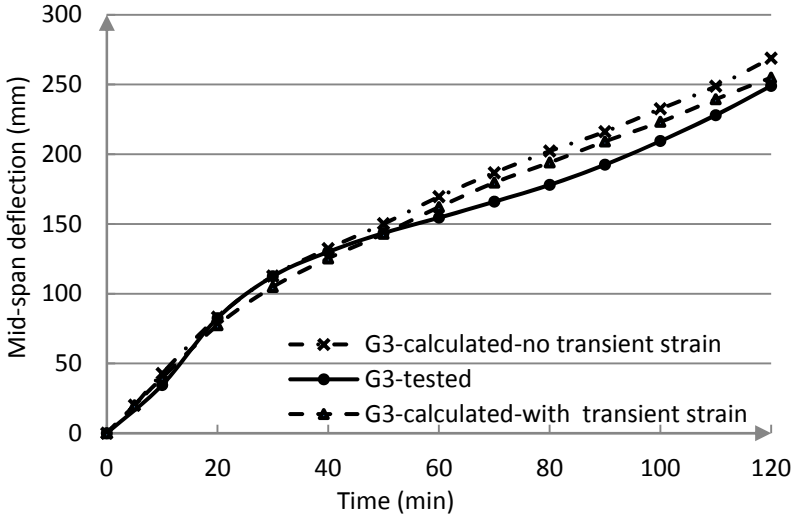

Fig.4 Mid-span deflections of G3 with and without transient strain

From Fig.3 and Fig.4, the following conclusions can be derived:

(1) G1 and G2 failed after 60 min heating in the test, and G3 last until 2hrs. As the slabs are heated from the tensile side, the ultimate bearing capacity of the elements is decided by steel bars, so the thickness of the concrete cover is essential for the fire-resistance of the structures.

(2) The numerical results and the test results are very close and have similar trend. After 30 min, the numerical results are higher than the tested ones, but the differences are acceptable.

(3) Fig.4 indicates that the calculation became more accurate when transient strain is considered. Without it, the deflections will be overestimated. However, for slabs this influence is small and can be neglect in the future design.

3 ACKNOWLEDGMENT

The author would like to thank the China Scholarship Council for the financial support through her PhD study.

REFERENCES

Eurocode 2: Design of concrete structures-Part 1.2: General rules-Structural fire design, EN1992-1-2, 2004.

Fib Bulletin 38: Fire Design of Concrete Structures—Materials, Structures, and Modeling, 2007.

Kodur, V.K.R., Dwaikat, M.B, Flexural Response of Reinforced Concrete Beams Exposed to Fire. Structural Concrete, 2008, 1(9):45-54.

Minne R, Vandamme M., Fire Resistance of Reinforced Concrete Slabs, Laboratory for Fuel Technology and Heat Transfer, Ghent University, 1979.

Paolo Riva. Parametric Study on the Behavior of RC Beams and Frames under Fire Conditions. fib Guidelines for the Structural Design of Concrete Buildings Exposed to Fire. 2002.

Sebastjan Bratina, Saje M., Igor Planinc, The effects of Different Strain Contributions on the Response of RC Beams in Fire. Engineering Structures, 2006, 29: 418–430.

Tao Jin. Experimental Investigation on Strength and Deformation of Self-compacting Concrete at Elevated Temperature. PhD Thesis, Tongji University and Ghent University, China and Belgium, 2009.

A RATIONAL APPROACH TO FIRE RESISTANCE ANALYSIS OF RC COLUMNS SUBJECTED TO UNIAXIAL/BIAXIAL BENDING AND AXIAL RESTRAINT

Truong Thang Nguyen [a], Kang Hai Tan [a]

[a] Nanyang Technological University, School of Civil and Environmental Engineering, Singapore

INTRODUCTION

Although great efforts have been made in studying the behaviour of reinforced concrete (RC) columns under fire conditions (Lie et al, 1991, 1993; Dotreppe et al, 1999; Tang, 2001; Kodur et al, 2004; Bratina et al, 2005), there is still a need of more sophisticated analytical models for fire resistance analysis of those subjected to practical conditions such as uniaxial and biaxial bending as well as presence of adjacent unheated structural elements. So far, the issue has been discussed by Tan and Yao (2003, 2004) who proposed an indirect approach using separate analyses conducted on two principal cross-sectional bending planes of rectangular columns. Raut et al (2010) proposed an approach for modelling fire response of RC columns under biaxial bending. Fire resistance predictions obtained from the proposed numerical model were compared with those in code provisions. These comparisons indicated that current codes and standards neglect the effect of either uniaxial or biaxial bending and may not yield reliable fire resistance predictions. However, there was no published paper on validation of columns under biaxial bending, since the reported fire tests reported were confined to uniaxially-loaded specimens.

This paper introduces an approach of direct sectional analysis for RC columns subjected to either uniaxial or biaxial bending combined with axial restraint under fire conditions. By incorporating the results of thermal and structural analyses obtained from SAFIR software (Franssen, 2005), in which Eurocode nonlinear material models at elevated temperatures were adopted, temperature-dependent load resistance of columns can be determined at incremental time steps with an arbitrary position of the inclined neutral axis. The failure time can be captured with the most possible failure criterion, i.e. when the applied load reaches either buckling or ultimate capacity of the column at that temperature. Effects of axial restraint and non-standard fires are also considered in the model. A computer program was developed so that experimental data of thirty-nine fire tests conducted at universities of Braunschweig (Hass, 1986) and Nanyang Technological University in 2010 were used to validate the accuracy of the proposed approach.

1 BEHAVIOUR OF RC COLUMNS AT ELEVATED TEMPERATURES

Some aspects of behaviour of axially-restrained RC columns at elevated temperatures are briefly demonstrated in Fig. 1. They include regression of interaction diagram due to deterioration of material strength and stiffness (Fig. 1(a)), non-uniform distribution of strain/stress/strength on the column cross section (Fig. 1(b)), and occurrence of thermal-induced axial force (Fig. 1(c)).

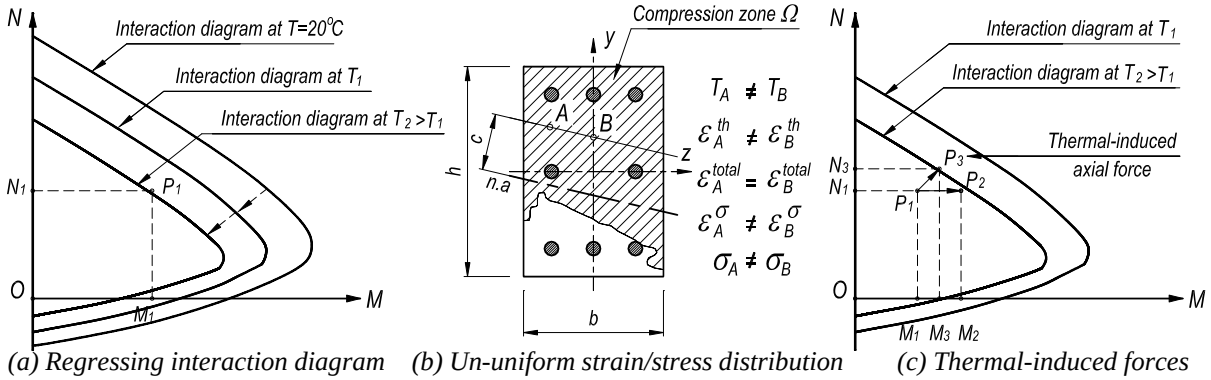

(a) Regressing interaction diagram *(b) Un-uniform strain/stress distribution* *(c) Thermal-induced forces*

Fig. 1 RC Column behaviour at elevated temperatures

2 SECTIONAL ANALYSIS AT ELEVATED TEMPERATURES

2.1 Assumptions

These assumptions are adopted in the analysis: (1) Cross-section remains plane after bending and normal to the centroidal axis; (2) Total strains in concrete and reinforcing steel at the same level are equal; (3) Stresses in concrete and reinforcing steel can be computed from strains based on corresponding elevated-temperature stress-strain curves for these materials; (4) Tensile strength of concrete in fire conditions is neglected in the calculations; (5) At a certain temperature, concrete is assumed to have failed when the maximum stress-induced compressive strain reaches the maximum limit; (6) Lateral-torsional buckling of columns is neglected in the analysis; (7) Effect of shear deformations is very small and negligible, and (8) Only rectangular columns are addressed.

2.2 Principles of Analysis

Consider a uniaxially-loaded column designed at room temperature to sustain a set of ultimate loads (N_1, M_1). As shown in Fig. 2(a), point P_1 (N_1, M_1) is located on the column interaction diagram at ambient condition. Since fires are considered as accidental events, it is regulated that at fire limit state, only the effect of service loads are considered. Hence, at the beginning of the fire, the column is subjected to an axial load N_2 determined by multiplying the ultimate load N_1 by a reduction factor η_{fi}. Point I represents axial load N_2 and the corresponding moment M_2.

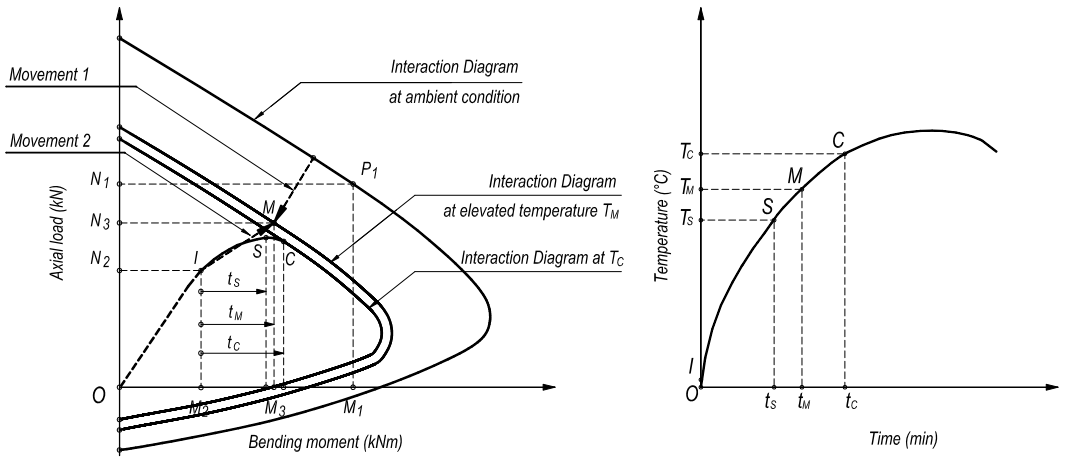

(a) Interaction diagram at failure *(b) Time-temperature curve*

Fig. 2 Principles of analysis

In fire conditions, there are two movements acting in opposite directions in Fig. 2(a). The first inward movement is the regression of interaction diagram as temperature rises. Due to axial restraint, axial force in the column increases resulting in the second outward movement. For

biaxially-loaded columns with temperature-dependent interaction surfaces, these two movements occur in three-dimensional space. If the column is stocky or the load eccentricity is small, material failure occurs after a period of time t_M when the load path and ultimate load capacity at temperature T_M coincide at point M (N_3, M_3). As shown in Fig. 2(b), t_M is the period of time to reach temperature T_M. The terms t_M and T_M can be referred to as the material failure time and failure temperature, respectively. If the column is of either high slenderness or high load eccentricity, due to deterioration of material stiffness as temperature rises, the column may lose its stability at point S where the derivation $\partial M/\partial N$ approaches infinity before becoming negative and a run-away trend occurs in the column mid-height lateral deflection. Then this column is deemed to have failed in stability mode before ultimate load capacity is reached. The terms t_S and T_S respectively represent the buckling time and buckling temperature. Combined failure mode is identified if after the column buckles, the load path and regressing interaction diagram coincide at point C. The terms t_C and T_C respectively represent the critical time and critical temperature.

2.3 Proposed Approach of Sectional Analysis

Consider a rectangular column subjected to an axial load N with eccentricities e_y and e_z corresponding to the respective bending moments $M_z=Ne_y$ and $M_y=Ne_z$. As shown in Fig. 3(c), the maximum compressive stress occurs at point B at the North-East corner of the cross-section. The position of a general neutral axis can be identified by two key parameters, namely, inclined angle β and distance from point B represented by the length c_n of line BG perpendicular to the neutral axis. Based on the neutral axis position, distributions of strain components can be further analyzed.

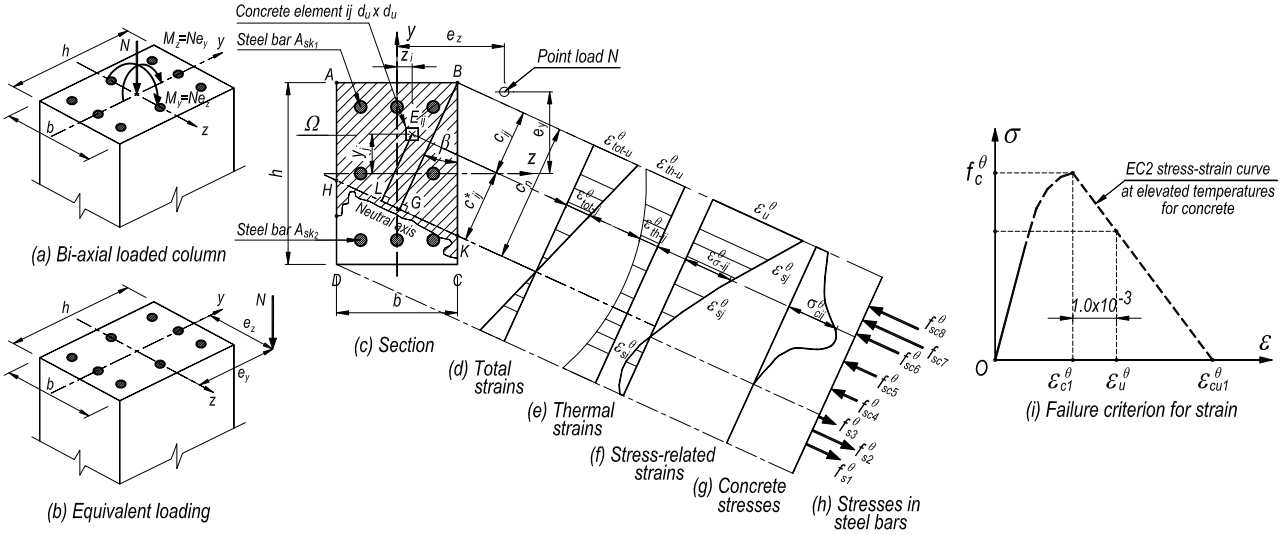

Fig. 3 Direct sectional analysis at elevated temperatures

Sectional analysis at elevated-temperature is more complicated than that at ambient condition due to: (1) The ABHK zone of total softening-strains limited by the neutral axis is no longer rectangular. It can be triangular, trapezoidal, or pentagonal; (2) Compression zone Ω is different from ABHK zone due to the presence of thermal and transient strains, and (3) Distribution of compressive stresses in compression zone is non-uniform due to different temperature distribution profiles across the column cross-section. Therefore, the method of equivalent rectangular stress block cannot be used in this analysis. An approach is proposed in this paper to determine load resistances contributed by concrete and reinforcing steel bars by integrating compressive and tensile stresses over the whole cross-section of the column.

In this direct sectional analysis of the Eurocode-based approach, ultimate values of total strain $\varepsilon^{\theta}_{tot\text{-}u}$ and stress-induced strain ε^{θ}_{u} at point B (Figs. 3(c), (d)) are proposed as shown in Tab. 1.

Tab. 1 Strain failure criterion

Concrete temperature (°C)	$\varepsilon^{\theta}_{c1}\times10^{-3}$	$\varepsilon^{\theta}_{cu1}\times10^{-3}$	$\varepsilon^{\theta}_{u}\times10^{-3}$	Siliceous aggregates		Calcareous aggregates	
				$\varepsilon^{\theta}_{th}\times10^{-3}$	$\varepsilon^{\theta}_{tot\text{-}u}\times10^{-3}$	$\varepsilon^{\theta}_{th}\times10^{-3}$	$\varepsilon^{\theta}_{tot\text{-}u}\times10^{-3}$
20	2.5	20.0	3.5	-0.000	3.500	-0.000	3.500
100	4.0	22.5	5.0	-0.743	4.257	-0.494	4.506
200	5.5	25.0	6.5	-1.804	4.696	-1.192	5.308
300	7.0	27.5	8.0	-3.141	4.859	-2.058	5.942
400	10.0	30.0	11.0	-4.892	6.108	-3.176	7.824
500	15.0	32.5	16.0	-7.195	8.805	-4.630	11.370
600	25.0	35.0	26.0	-10.188	15.812	-6.504	19.496
700	25.0	37.5	26.0	-14.009	11.991	-8.882	17.118
800	25.0	40.0	26.0	-14.000	12.000	-11.848	14.152
900	25.0	42.5	26.0	-14.000	12.000	-12.000	14.000
1000	25.0	45.0	26.0	-14.000	12.000	-12.000	14.000
≥1100	25.0	47.5	26.0	-14.000	12.000	-12.000	14.000

In Tab. 1, the temperature-dependent terms $\varepsilon^{\theta}_{c1}$, $\varepsilon^{\theta}_{cu1}$ and $\varepsilon^{\theta}_{th}$ are respectively the strain corresponding to the compressive strength, ultimate strain, and thermal strain specified in EC2 Part 1-2 (Eurocode, 2004b). Yao (2003) proposed that neither $\varepsilon^{\theta}_{c1}$ nor $\varepsilon^{\theta}_{cu1}$ can be used as the strain failure criterion since the former marks the beginning of strain softening while the latter represents the end. Hence, the ultimate stress-induced strain ε^{θ}_{u} is determined by adding an amount of 1.0×10^{-3} to the respective yield strain $\varepsilon^{\theta}_{c1}$ (Fig. 3(i)). This additional value is adopted based on the ambient condition in which ε^{θ}_{u} is 3.5×10^{-3} and $\varepsilon^{\theta}_{c1}$ is 2.5×10^{-3}. It is also satisfied that ε^{θ}_{u} always lies in between $\varepsilon^{\theta}_{c1}$ and $\varepsilon^{\theta}_{cu1}$ in this proposed determination. In Tab.1, linear interpolation can be applied to calculate strain criterion at any temperature.

Once ε^{θ}_{u} is obtained, the direct sectional analysis can be conducted to obtain the temperature-dependent load resistance of the column:

$$N^{\theta}_{Rd} = \sum_{ij} \sigma^{\theta}_{cij} d_u^2 + \sum_{k_1} A_{sk_1} (f^{\theta}_{sck_1} - \sigma^{\theta}_{ck_1}) + \sum_{k_2} A_{sk_2} f^{\theta}_{sk_2} \quad (1)$$

$$M^{\theta}_{Rdy} = \sum_{ij} \sigma^{\theta}_{cij} d_u^2 z_i + \sum_{k_1} A_{sk_1} (f^{\theta}_{sck_1} - \sigma^{\theta}_{ck_1}) z_{k_1} + \sum_{k_2} A_{sk_2} f^{\theta}_{sk_2} z_{k_2} \quad (2)$$

$$M^{\theta}_{Rdz} = \sum_{ij} \sigma^{\theta}_{cij} d_u^2 y_j + \sum_{k_1} A_{sk_1} (f^{\theta}_{sck_1} - \sigma^{\theta}_{ck_1}) y_{k_1} + \sum_{k_2} A_{sk_2} f^{\theta}_{sk_2} y_{k_2} \quad (3)$$

where sub-indexes *i* and *j* represent concrete elements in compression zone; k_1 and k_2 denote steel bars located in compression and tension zones, respectively. The term d_u is dimension of the basic square concrete element E_{ij}; A_{ski} represents cross-sectional area of the reinforcing bar at position k_i; Stress σ^{θ}_{cij} of the concrete element E_{ij} at position (z_i, y_j) can be determined based on values of T_{ij}, $\varepsilon^{\theta}_{\sigma\text{-}ij}$, and the EC2 material model of concrete at elevated temperatures.

In the proposed model, since the inclined neutral axis can be directly determined, the convergence criteria of material failure would be simpler as they are expressed in a direct manner:

$$\text{If } N^{\theta}_{Ed} = N^{\theta}_{Rd} \text{ then } M^{\theta}_{Edy} = M^{\theta}_{Rdy} \text{ or } M^{\theta}_{Edz} = M^{\theta}_{Rdz} \quad (4)$$

The terms M^{θ}_{Rdy}, M^{θ}_{Rdz} in Eq. (4) are the real moment resistances about principal axes of the column cross-section. In Fig. 4, dashed curves AP'$_y$C'$_y$D'$_y$ and AP'$_z$C'$_z$D'$_z$, which are the intersections between the 3-D interaction surface and two vertical planes, represent the physical meanings of M^{θ}_{Rdy} and M^{θ}_{Rdz}, respectively.

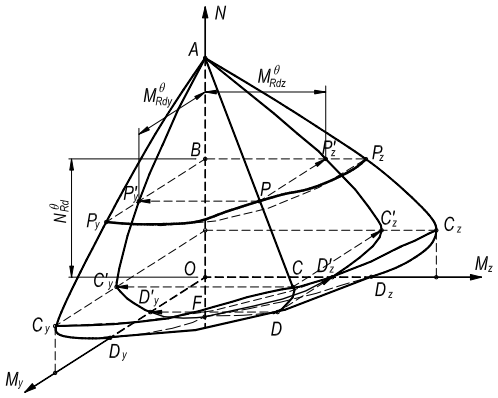

Fig. 4 Interaction surface at temperature θ

2.4 Proposed Computer Program

Based on the elevated-temperature direct sectional analysis introduced in Section 2.3, a computer program named FRRC was proposed. The basic principle applied in the program is to locate an inclined neutral axis throughout the cross-section by iterations. Three loops of iteration are involved: (1) Time steps; (2) Variation of angle β of the inclined neutral axis, and (3) Distance c_n from the neutral axis to the most-compressive corner of the cross-section.

As time progresses, nonlinear elevated-temperature mechanical properties can be determined through associated subroutines of the program. Sectional analysis can be conducted for any arbitrary neutral axis position. Potential failures can be checked following the convergence criteria shown in Section 2.3. The time step at which the program converges is identified as failure time.

3 CASE STUDIES

3.1 Case Study 1

Case study 1 was carried out based on test results of thirty-three RC columns subjected to fire conducted by Hass (1986). Details and test conditions of some typical specimens are shown in Tab. 2. The columns were subjected to either pure compression or uniaxial bending without any axial restraint. Standard fire curve ISO 834 was applied for all the fire tests.

Tab. 2 Case study 1 - Details of test specimens

No.	Ref.	b (mm)	H (mm)	Rebar (mm)	L (m)	f'_c (MPa)	f_y (MPa)	End Cond.	d' (mm)	e (mm)	N_{app} (kN)	t^{Test} (min)
1	1	300	300	6Φ20	3.76	24.1	487	p-p	38	30	710	86
2	2	300	300	6Φ20	3.76	24.1	487	p-p	38	0	930	84
33	41	300	300	6Φ20	4.70	31.5	526	p-p	38	150	465	50

Analysis results obtained from the proposed analytical approach and the associated computer program are shown in Tab. 3. The terms N_{Rd} and M_{Rd} are axial load and moment capacities of the columns at ambient condition, respectively. The term η_{fi} is the reduction factor, which is the ratio between the applied load N_{app} and the ambient resistance N_{Rd}. Failure time t^{FRRC} and other detailed descriptions of the column at failure including angle β of the inclined neutral axis, depth of neutral axis c_n, and contributions of concrete (N^{θ}_{Rdc}, M^{θ}_{Rdc}) and reinforcing steel bars (N^{θ}_{Rds}, M^{θ}_{Rds}) to the column load resistance, were determined by the FRRC program.

Tab. 3 Case study 1 – Analysis results of test specimens

No.	Ref.	N_{Rd} (kN)	M_{Rd} (kNm)	η_{fi}	N^{θ}_{Rdc} (kN)	N^{θ}_{Rds} (kN)	M^{θ}_{Rdc} (kNm)	M^{θ}_{Rds} (kNm)	β (rad)	c_n (mm)	t^{FRRC} (min)
1	1	1669.2	96.8	0.517	485.2	229.6	27.8	25.3	0	126	85
2	2	2132.6	62.5	0.436	666.0	348.6	21.1	18.8	0	150	82
33	41	690.6	150.5	0.673	658.2	-31.3	52.6	68.4	0	120	45

The strain and stress distributions in concrete given by the program are shown in Figs. 5(a) and 5(b), respectively. Comparison between the proposed analysis results and experimental data in terms of failure time is shown in Fig. 5(c). Statistical analysis shows a mean agreement of 0.947 and a COV of 0.220. It can be seen in this case study that when the Eurocode elevated-temperature material properties are incorporated, the proposed approach gives good agreement and conservative prediction of the fire resistance for axially- and uniaxially-loaded RC columns without axial restraint, compared to the test results.

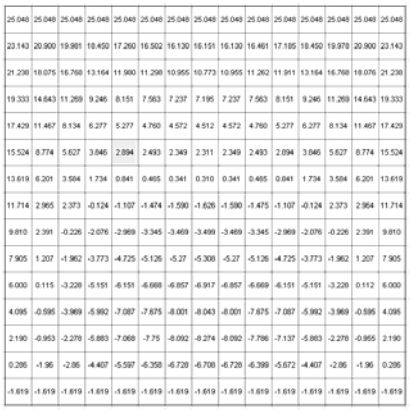

(a) Concrete stress-related strain

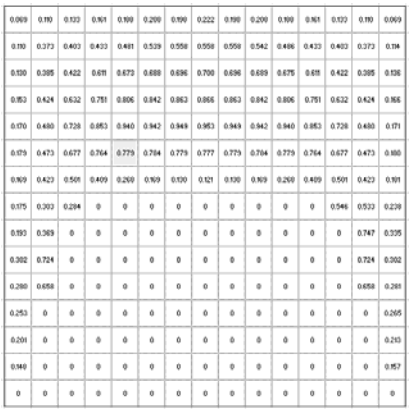

(b) Concrete stress

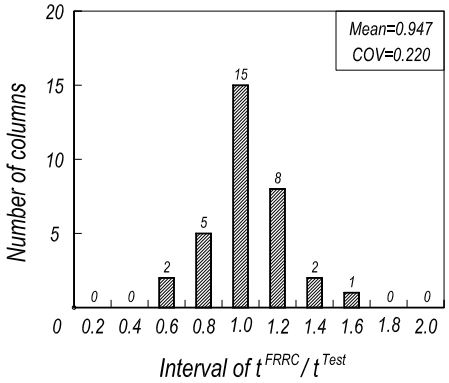

(c) Statistical analysis

Fig. 5 Case study 1

3.2 Case Study 2

In this case study, results of six axially-restrained column specimens tested at Nanyang Technological University in 2010 are used to validate the proposed approach. All the columns had identical 300 mm square cross-section and 3.3 m length. They were cast from the same batch of concrete with mean cylinder strength of 55 MPa. Reinforcing bars of 6T20 with 550 MPa yield strength were typically designed for the six specimens. In the tests, three specimens were uniaxially-loaded with eccentricities of 25, 40 and 60 mm and another three were loaded in biaxial bending with corresponding eccentricities of (25, 25), (40, 40) and (60, 60mm). As calculated from Tab. 4, the average ratio between the predicted and tested failure times (t^{FRRC}/t^{Test}) is 1.099. Hence, the proposed approach overestimates the fire resistance of axially-restrained columns.

Tab. 4 Case study 2 – Test and analysis results of failure time

Col.	C1-3		C1-4		C1-5		C2-1		C2-2		C2-3	
F. time	t^{Test}	t^{FRRC}	t^{Test}	t^{FRRC}	t^{Test}	t^{FRRC}	t^{Test}	t^{FRRC}	t^{Test}	t^{FRRC}	t^{Test}	t^{FRRC}
(min)	166	190	211	190	159	196	182	194	189	202	176	208
Ratio	1.145		0.900		1.232		1.065		1.069		1.182	

4 SUMMARY AND ACKNOWLEDGMENT

In the proposed rational analytical computer-based approach, effects of uniaxial and biaxial bending as well as axial restrained were considered in a direct sectional analysis. Good agreement in the failure time between the proposed approach and experimental data can be obtained for either axially-

restrained or unrestrained column subjected to eccentric load which is either uniaxial or biaxial bending. More conservative results were observed in the case of columns without axial restrain.

This research was funded by grant M47030016 A*STAR and supported by manpower research account MINDEF-NTU/JPP/FY05/14.

REFERENCES

Lie, T. T., Celikkol, B., Method to Calculate the Fire Resistance of Circular Reinforced Concrete Columns, Materials Journal, 88(1), 84-91, 1991.

Lie, T. T., Chabot, M., Evaluation of the Fire Resistance of Compression Members Using Mathematical Models, Fire Safety Journal, 20(2), 135-149, 1993.

Dotreppe, J. -C., Franssen, J. -M., Vanderzeypen, Y., Calculation Method for Design of Reinforced Concrete Columns under Fire Conditions, ACI Structural Journal, 96(1), 9-18, 1999.

Kodur, V. K. R., Wang, T. C., Cheng, F. P., Predicting the Fire Resistance Behaviour of High Strength Concrete Columns, Cement and Concrete Composites, 26(2), 141-153, 2004.

Bratina, S., Cas, B., Saje, M., Planinc, I., Numerical Modelling of Behaviour of Reinforced Concrete Columns in Fire and Comparison with Eurocode 2, International Journal of Solids and Structures, 42(21-22), 5715-5733, 2005.

Raut, N., Kodur, V. K. R., Modelling of Fire Response of Reinforced Concrete Columns under Biaxial Bending, Proceedings of the Sixth International Conference SiF, 206-215, USA, 2010.

Tang, C. Y., An Iterative Formula for Fire Resistance of Columns, Mater Thesis, Nanyang Technological University, Singapore, 2001.

Tan, K. H., Yao, Y., Fire Resistance of Four-Face Heated Reinforced Concrete Columns, Journal of Structural Engineering, 129(9), 1220-1229, 2003.

Tan, K. H., Yao, Y., Fire Resistance Reinforced Concrete Columns Subjected to 1-, 2-, and 3-Face Heating, Journal of Structural Engineering, 130(11), 1820-1828, 2004.

Hass, R., Practical Rules for the Design of Reinforced Concrete and Composite Columns Submitted to Fire, Institute fur Baustoffe, Massivbau und brandschutz der Technichen Universita Braunschweigo, 1986.

Frassen, J. M., SAFIR. A Thermal/Structural Program Modelling Structures under Fire, Engineering Journal, A.I.S.C., 42, 3: 143-158, 2005.

Eurocode EN 1991-1-1:2004, Design of Concrete Structures – Part 1-1: General Rules and Rules for Buildings, 2004a.

Eurocode EN 1991-1-2:2004, Design of Concrete Structures – Part 1-2: General Rules, Structural Fire Design, 2004b.

USING OPENSEES FOR AN RC FRAME IN FIRE

Jian Zhang[a], *Asif Usmani[b], Jian Jiang[b], Yaqiang Jiang[b], Panagiotis Kotsovinos[b] and Ian May[a]

[a] School of Built Environment, Heriot-Watt University, Edinburgh EH14 4AS, United Kingdom
[b] School of Engineering, The University of Edinburgh, Edinburgh EH9 3JF, United Kingdom

INTRODUCTION

With increasing urbanisation and industrialisation earthquakes represent an ever greater risk to life, livelihoods and to the sustainability of society's rapid development. In built-up areas, especially major cities with tall buildings and extensive gas mains, this risk is compounded by post earthquake fires. In fact, losses resulting from fires developing soon after the earthquake may be comparable to those resulting from the shaking (EQE International, 1995).The risk is certainly increased by the hampering of fire response due to the extreme traffic congestion, collapsed houses and buildings, rubble in the streets, the concomitance of multiple fires and the possible difficulties in water supply soon after the earthquake (Buchanan, 2001).

To develop a comprehensive earthquake and fire research programme based on exploiting the complementary strengths of the collaborating institutions, a project funded by UKIERI is currently underway. Objectives of this project may be stated as: a) Developing a detailed understanding of the mechanics of the response of earthquake damaged structures (primarily reinforced concrete frames) subjected to fire (through small and large scale testing and developing computational models); b) Developing mathematical models for determining the reliability of structural components and structures subjected to compound seismic and fire loading, which account for the uncertainties associated with the loading and damage estimation, to enable realistic quantification of performance.

To model the experiment, a software named OpenSees has been developed so that it could be used to perform thermo-mechanical analyses. OpenSees is an open source object oriented software framework developed at UC Berekeley and currently supported by PEER and Nees. OpenSees has so far been focussed on providing an advanced computational tool for analysing the non-linear response of structural frames subjected to seismic excitations (Usmani et al, 2010). A key feature of OpenSees is the interchangeability of components and the ability to integrate existing libraries and new components into the framework (not just new element classes) without the need to change the existing code (Mazzoni et al, 2007). However one of the limitations of OpenSees is that thermal analysis can not be carried out by it up to date. In order to overcome this flaw so that it can be used to model the experiment of UKIERI, some new classes have been added into OpenSees and the some thermal analysis has been performed. The compared results show an acceptable agreement between theory, OpenSees, Abaqus.

1 NEWLY ADDED OPENSEES CLASSES

As mentioned above, there is not much work to do to let the OpenSees "recognize" a new class, and this advantage can be shown by the progress of introducing thermal action to the elastic beam-column element. A new derived class of *ElementalLoad*, called *Beam2dThermalAction* or *Beam3dThermalAction*, and a new member function of elastic beam-column element were all required to add into OpenSees to perform the linear analysis of elastic element in thermal loading.

It is more complicated to perform a thermal analysis to the nonlinear beam-column element. *Material* and *SectionForceDeformation* classes' information has to be passed to the element class while carrying out the nonlinear analysis, and all of these classes must be temperature related. Fig. 1 above shows the new classes that have been implemented within the existing framework (the original OpenSees classed are identified by the greyed boxes).

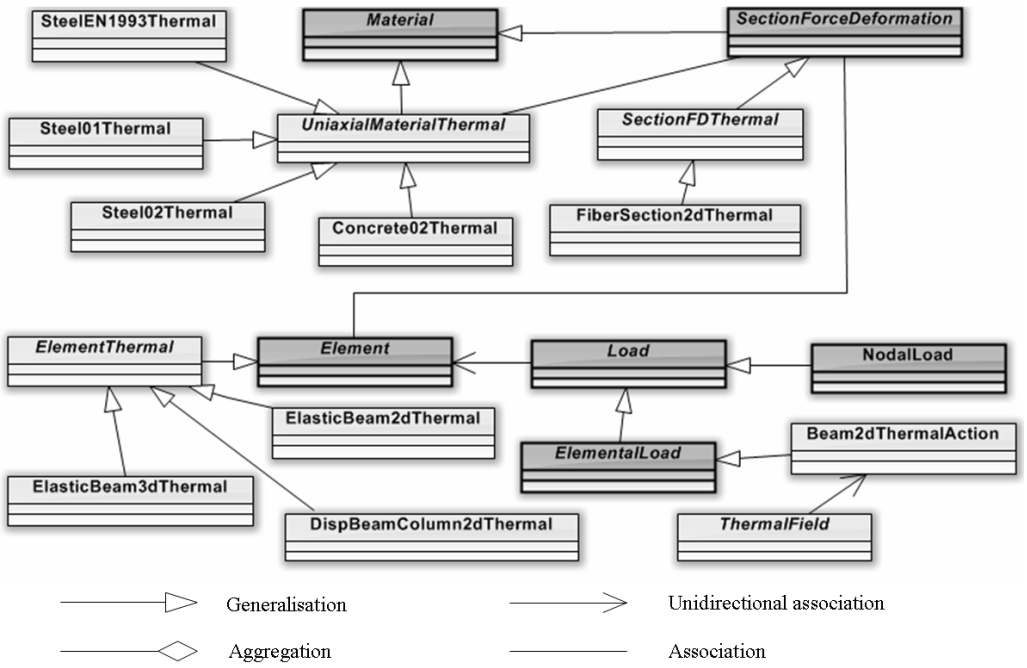

Fig. 1 New classes introduced to the current OpenSees framework for performing thermo-mechanical analyses

2 A BENCHMARK TEST FOR ELASTIC BEAM-COLUMN ELEMENT

A series of benchmark problems have been used to test the new thermo-mechanical code in OpenSees. For instance one was to predict the mid-span deflection, end rotation and axial force in an elastic beam (Young's Modulus E = 10GPa, area of cross section A = 9×10^{4}㎜^{2}) under udl and thermal loading (T_{top} = 20C, T_{bottom} = 800C, thermal expansion coefficient $\alpha = 12\times10^{6}$ /C) both ends of which are restrained in translation (Fig. 2), however the rotations are free. Analytical, OpenSees and ABAQUS solutions are shown in Table 1, all of which are in agreement.

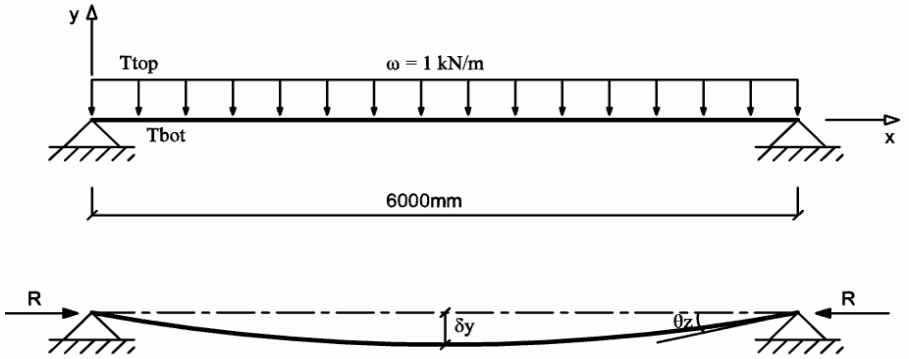

Fig. 2 An end-restrained elastic beam under udl and thermal loading

Table 1 compared results among analytical, OpenSees and ABAQUA

	udl			thermal			udl and thermal		
	analytical	**OpenSees**	**ABAQUS**	**analytical**	**OpenSees**	**ABAQUS**	**analytical**	**OpenSees**	**ABAQUS**
δy(mm)	2.5	2.5	2.51	140.678	140.4	140.4	143.178	142.9	142.91
θz(rad)	0.133	0.133	0.133	0.936	0.936	0.936	0.0949	0.0949	0.0949
R(kN)	0	0	0	4212	4212	4120	4212	4212	4120

3 MODELLING OF AN TEST FRAME

An RC frame is being tested in India under simulated earthquake damage and a subsequent fire. To predict the behaviour of the frame, a two dimension frame model has been analysed. The model was at first subjected to a gradually increased cycle of lateral displacements after loading the columns and the slab/beams with gravity loads. The complete analysis was carried out over a number of steps. In the first step the frame was subjected to increasing quasi-static cyclic displacements as shown in Figure 3. Displacement control was used for the analysis with node 1 (see Figure 4) regarded as the control point with a maximum displacement of approximately 200mm.

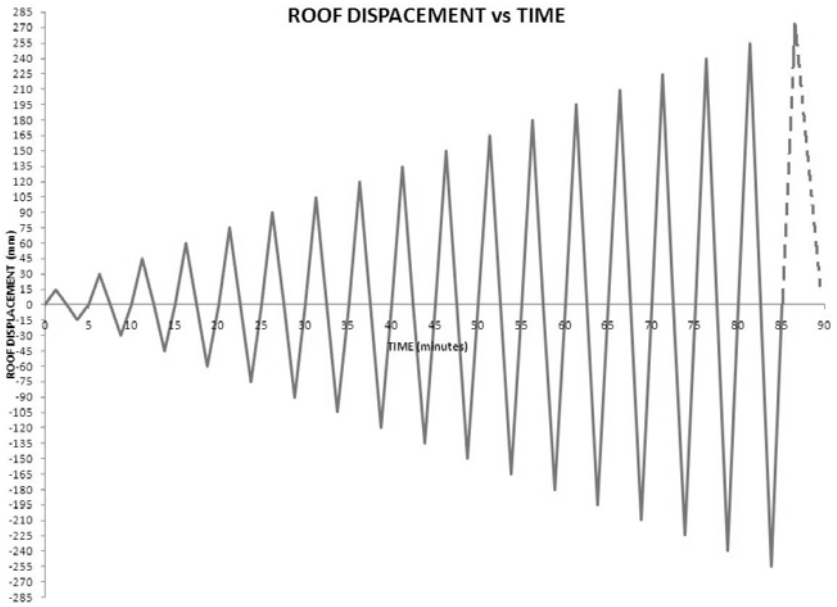

Fig.3. Frame model and the displacement – force curve of control node 1

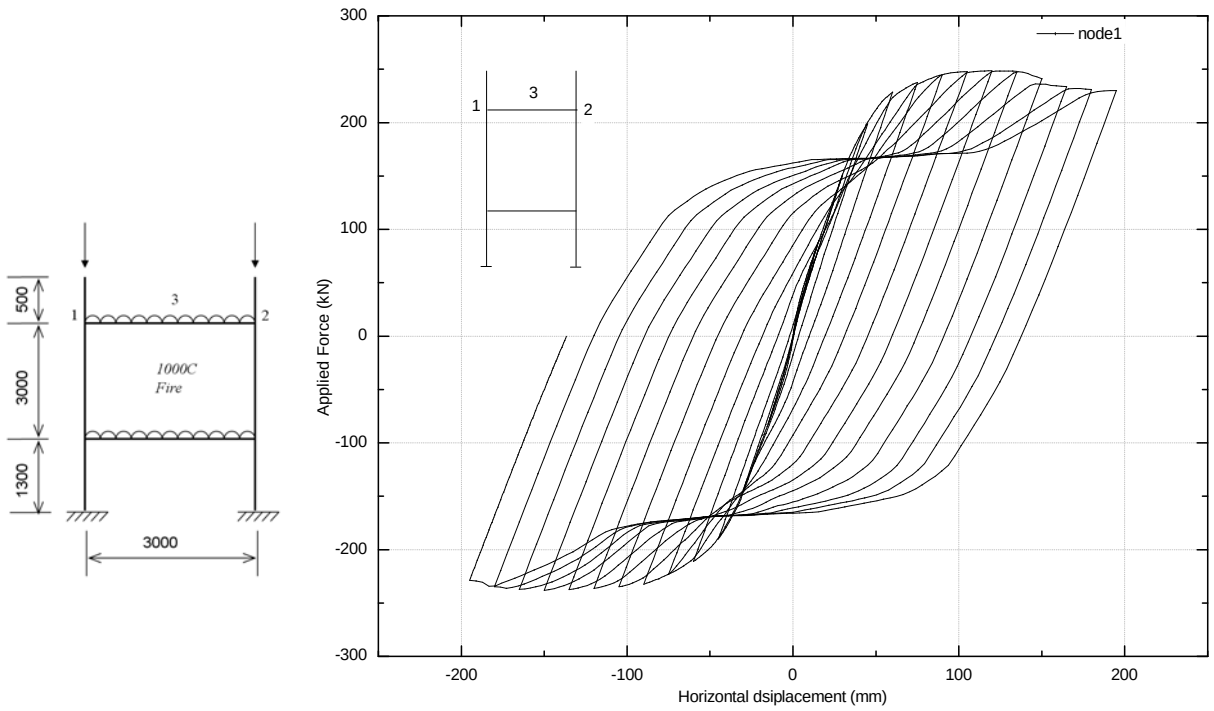

Fig.4. Frame model and the displacement – force curve of control node 1

The Figure 4 shows the complete force-displacement plot node 1. The plot shows that the analysis was carried until maximum displacements of just under 200mm were reached on both sides. The displacement was then reduced until the force at the control point become zero, leaving a permanent residual displacement of approximately 130mm. The displacement corresponding to zero force was obtained from an earlier analysis.

After the damage inducing cyclic displacement step, the frame was subjected to a 1000^{o}C constant fire lasting 3600 seconds. An interesting feature of the behaviour was that the frame seemed to "stiffen" because of the fire. The absolute displacement of node 1 decreased from around -140mm to -80mm under fire until the maximum (exposed face) temperature of the beam reached 450^{o}C, and then it dropped to around -130mm at the end of the heating (Fig. 5). The deflection at the midspan of the upper beam is also shown in Fig. 5 which shows relatively low values as the current model lumps the slab and beam sections together to form the beam. The test results are still awaited, however it is expected that the slab will produce greater deflections after the fire than possible with this 2D model

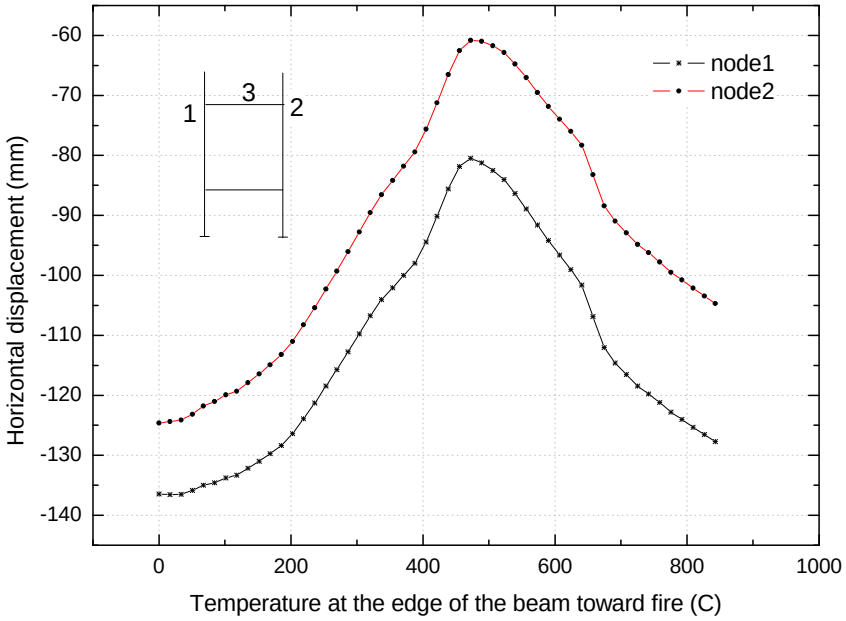

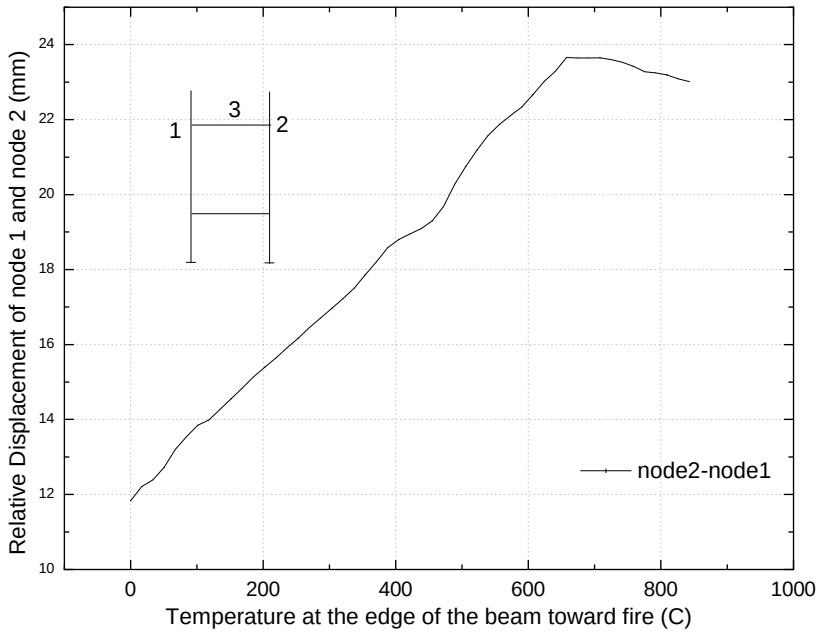

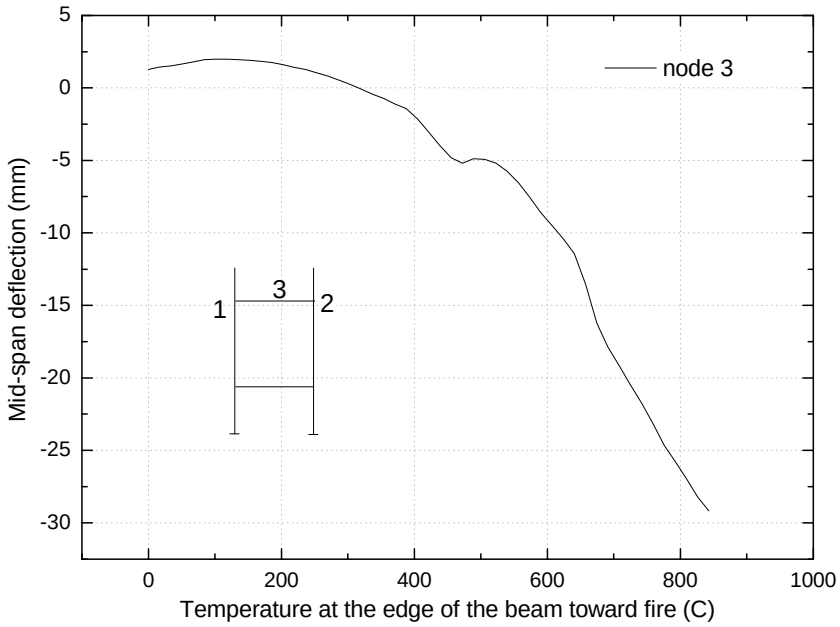

Fig.5. Displacements of node 1, 2 and 3

After the damage inducing cyclic displacement step, the frame was subjected to a 1000^{o}C constant fire lasting 3600 seconds. An interesting feature of the behaviour was that the frame seemed to "stiffen" because of the fire. The absolute displacement of node 1 decreased from around -140mm to -80mm under fire until the maximum (exposed face) temperature of the beam reached 450^{o}C, and then it dropped to around -130mm at the end of the heating. The relative displacement of node 1 and node increased steadily before the temperature reached 650^{o}C, following by a slight drop after that (Fig. 5). The possible reason is that the elongation of the upper beam was affected by two factors – axial thermal elongation and deflection of the beam. The relative displacement of the two nodes increased while axial thermal elongation dad a greater effect, otherwise it would decrease. The deflection at the midspan of the upper beam is also shown in Fig. 5 which shows relatively low values as the current model lumps the slab and beam sections together to form the beam. The test results are still awaited, however it is expected that the slab will produce greater deflections after the fire than possible with this 2D model

4 CONCLUSION

A fully nonlinear 2D thermo-mechanical frame analysis capability has been added to OpenSees and had been tested against a number of benchmark problems to ensure that it is working correctly. It has also been combined with the native nonlinear static analysis capability in OpenSees to model damaged frames subjected to fire. Open source codes offer an excellent opportunity for researchers to collaborate across geographical boundaries and build a truly international community to solve engineering problems that are of common concern. This work is a small contribution to the OpenSees movement and considerable further development is in train. Future developments will included full 3D thermo-mechanical analyses for frames by further developing OpenSees beam and shell elements.

REFERENCES

EQE International. The January 17, 1995 Kobe earthquake—an EQE summary report. April, 1995..

Buchanan AH. Structural design for fire safety. Chichester, England: Wiley; 2001.

A. Usmani, J. Zhang, J. Jiang, Y. Jiang, P. Kotsovinos, J. Zhang And I. May. Using OpenSees for structures in fire. 6th International Conference on Structures In Fire, 2010.

S. Mazzoni, F. Mckenna, et al, OpenSees Command Language Manual, 2007.

PROBABILISTIC ANALYSIS OF CONCRETE BEAMS DURING FIRE

Ruben Van Coile [a], Emmanuel Annerel [a], Robby Caspeele [a], Luc Taerwe [a]

[a] Ghent University, Department of Structural Engineering, Magnel Laboratory for Concrete Research, Ghent, Belgium

INTRODUCTION

In this paper a simple computational tool is presented, which provides insight in the time and temperature dependent reliability of concrete beams during fire. The uncertainty of basic variables is taken into account through Monte Carlo simulations, resulting in a quantification of the uncertainty regarding the bending moment capacity during fire and the corresponding evolution of the safety level. The results of these full-probabilistic simulations are compared with the semi-probabilistic calculation methods as specified in EN 1992-1-2 (CEN, 2004a).

1 MODEL CONCEPTS

The goal of this paper is to quantify the evolution of the structural safety of concrete beams subjected to bending during fire. Due to the changing temperature distribution over the concrete cross-section, the limit state function for bending during fire cannot be formulated analytically. Hence, a computational tool was developed in order to calculate the structural response of concrete members during fire iteratively and to enable a full-probabilistic analysis of this structural response.

1.1 Deterministic analysis

A basic deterministic model is developed in EXCEL, calculating the bending moment capacity for a concrete beam at t minutes of exposure to the ISO 834 fire curve. The beam is assumed to be exposed to fire from three sides (bottom and side faces). The temperature distribution in a cross-section is calculated by the finite element program DIANA and used as input for the EXCEL model.

The bending moment capacity ($M_{R,fi,t}$) is calculated in the ultimate limit state and by the assumptions of the classical linear-elastic structural analysis according to EN 1992-1-1 (CEN, 2004b). Stresses introduced by internal thermal restraint are not considered in this model.

The effects of fire on the material properties of both concrete and reinforcing steel are considered through a temperature dependent function. This kind of simplification corresponds to the methodology followed in EN 1992-1-2. The actual evaluation of the local temperatures θ_i in the concrete cross-section and the corresponding local material properties is performed in discrete square elements measuring 5 mm x 5mm. This type of discretization is visualized in Fig. 1, with ε_i the local strain in the ultimate bending limit state, equal for all i at the same vertical distance from the beam bottom. For each discrete concrete segment, the reduction factors of EN 1992-1-2 on the material properties are applied. The model allows to implement alternative definitions of the reduction factors.

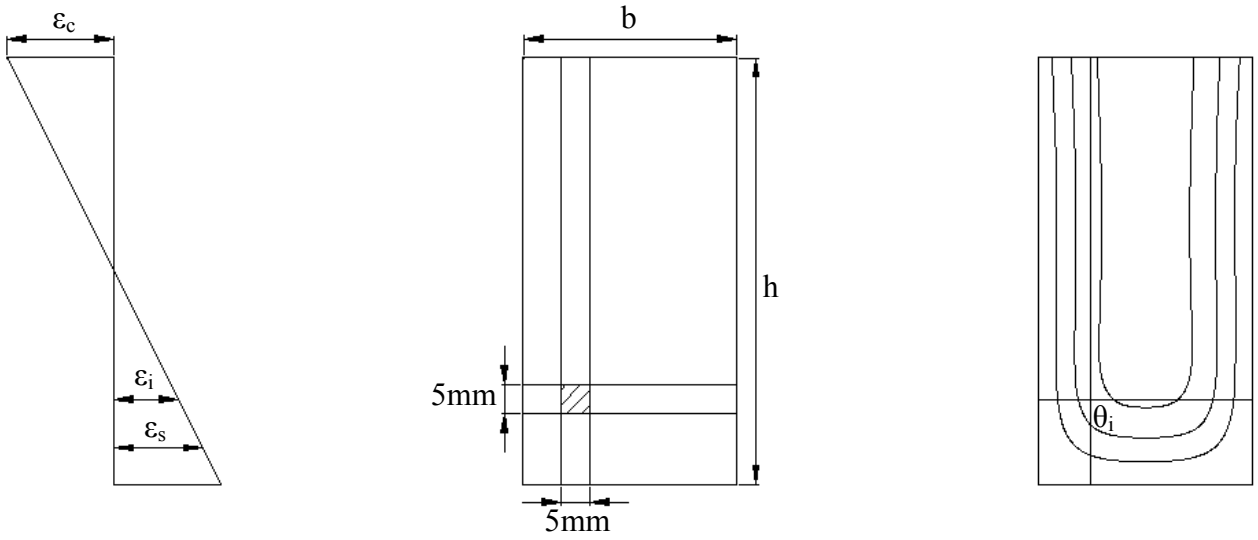

Fig. 1: Discretization of beam cross
(concrete beam (center), temperature distribution (right), distribution of strains (left))

1.2 Modelling of variables

In order to evaluate the uncertainty of the bending moment capacity during fire and to calculate the safety level, the uncertainties with respect to the basic variables must be incorporated in the model through their respective probability distribution functions. This modeling of uncertain variables is implemented independently from the deterministic analysis described above, and can therefore easily be modified. This procedure results in a high degree of flexibility and allows for the incorporation of updated information when this is available. The distributional characteristics considered in this paper are based on (Holický and Sýkora, 2010) and the applicable distribution types are presented in Tab. 1. All stochastic variables are considered independent. If more specific information is available with respect to the correlation between specific variables, the developed model can be further adjusted.

Tab. 1: Stochastic variables in full-probabilistic model

Symbol	Name	Distribution
h	beam height	Normal
b	beam width	Normal
$f_c(20°C)$	20°C concrete compressive strength	Lognormal
$f_y(20°C)$	20°C yield strength reinforcement	Lognormal
$E_c(20°C)$	20°C concrete modulus of elasticity	Lognormal
A_s	reinforcement section	Normal
c	concrete cover	bèta $[0;3c_{nominal}]$ (*)
χ	model uncertainty	Lognormal

(*) a bèta distribution with the same characteristics as described in (Holický and Sýkora, 2010), but defined over the range $[c_{nominal}-5;c_{nominal}+5]$ would be more suitable in the opinion of the authors of this paper

Additionally, in order to take the uncertainty regarding the reduction of the mechanical properties at high temperatures into account, a temperature-dependent normal distribution is proposed for the reduction factors for both the concrete compressive strength and the reinforcement yield strength. Both normal distributions are characterized by a mean value equal to the nominal reduction factor of EN 1992-1-2 and a standard deviation based on laboratory tests (Annerel, 2010). For the compressive concrete strength, the standard deviation of the reduction factor is assumed to be 0 at 20°C and 0.045 at 700°C. Linear interpolation is used for intermediate values. For the mechanical reinforcement properties, a similar assumption is made, with a standard deviation of 0.065 at

600°C. The concept is illustrated in Fig. 2 where the 5%, 50% and 95% fractiles of the reduction variable $f_c(\theta)/f_c(20°C)$ are visualized. It is important to note that this uncertainty in reduction factor is additional to the uncertainty on the material characteristics at ambient temperature (20°C). Similarly, Fig. 3 visualizes the 5%, 50% and 95% fractiles of the reduction variable $f_y(\theta)/f_y(20°C)$. No spalling is taken into account, although this could be implemented through a probabilistic degradation function for the concrete cover c.

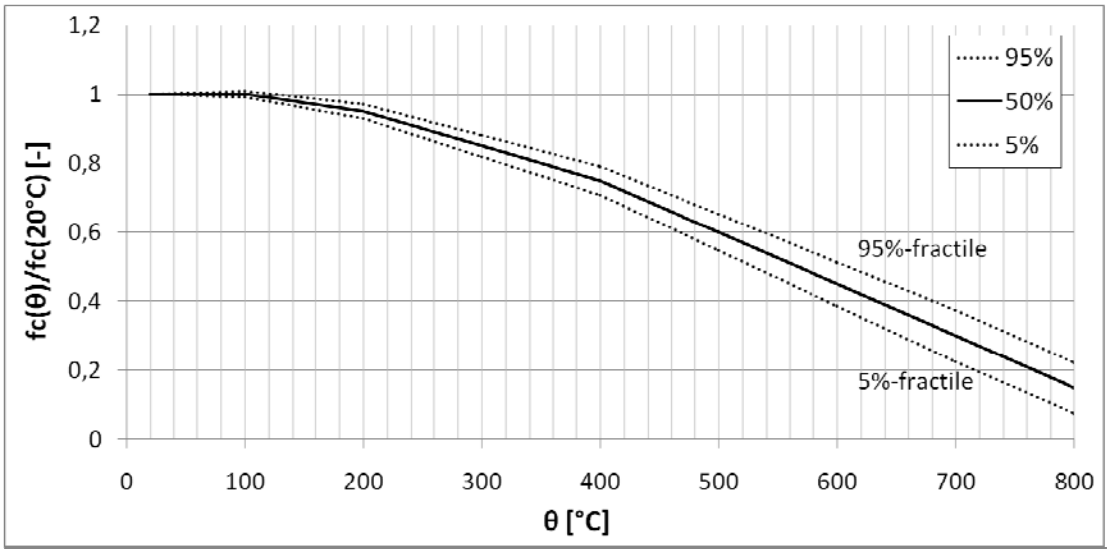

Fig. 2: 5%, 50% and 95% fractiles of reduction factor $f_y(\theta)/f_y(20°C)$

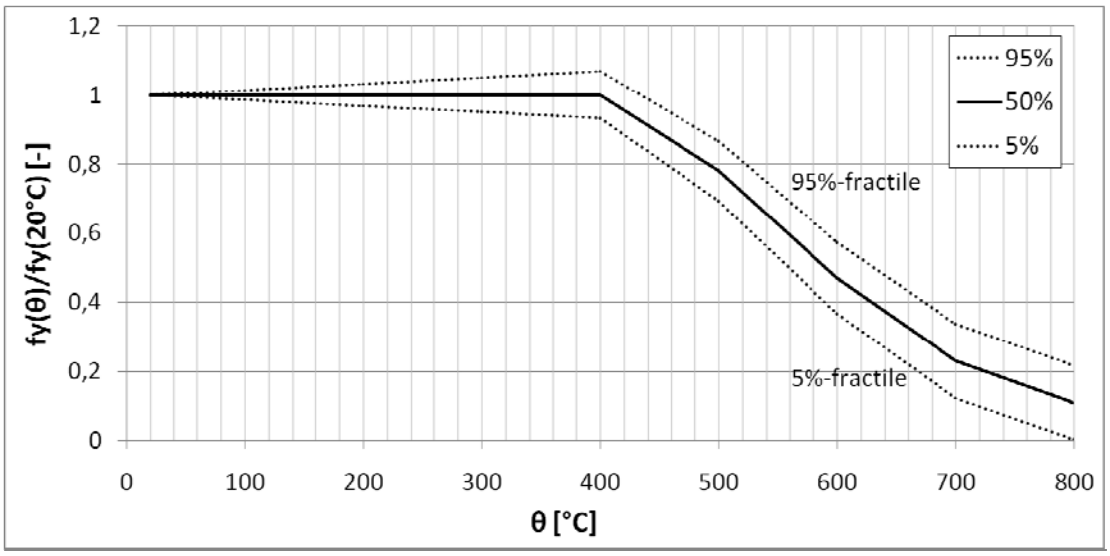

Fig. 3: 5%, 50% and 95% fractiles of reduction factor $f_c(\theta)/f_c(20°C)$

1.3 Uncertainty propagation: crude Monte Carlo simulations

The properties of each beam are characterized by a vector $\underline{X}_i$ of randomly generated values of the variables described above. 10000 vectors $\underline{X}_i$ are generated. For all of these realizations the bending moment capacity during fire is evaluated by the described deterministic analysis. The results of these calculations are analyzed statistically, resulting in an expected value and standard deviation of the bending moment capacity of the concrete beam exposed to fire. This type of analysis by repeated random sampling of the parameter space is generally referred to as Monte Carlo sampling.

2 INTERPRETATION OF MODEL RESULTS

Traditionally, EN 1992-1-2 defines the fire resistance time t_R through equation (2), with $M_{Rd,fi,t}$ the design value of the bending moment capacity and $M_{Ed,fi,t}$ the design value of the bending moment induced by the design loads.

$$M_{Rd,fi,t} \geq M_{Ed,fi,t} \qquad for\ t \leq t_R \tag{2}$$

$M_{Ed,fi}$ is considered to be constant, thus without consideration of indirect thermal actions, i.e. $M_{Ed,fi,t} \equiv M_{Ed,fi}$. A method for evaluating the safety level of a concrete beam during fire is proposed by equations (3) and (4).

$$P_{f,1} = P\left[M_{R,fi,t} < M_{Ed,fi}\right] = \Phi\left(-\beta_1\right) \tag{3}$$

$$P_{f,2} = P\left[M_{R,fi,t} < M_{Rd,fi,t}\right] = \Phi\left(-\alpha_R\beta_2\right) = \Phi\left(-\beta_2\right) \qquad \text{where } \alpha_R = 1 \text{ as } \sigma_E < 0.16\sigma_R \tag{4}$$

Both equations compare the results of the Monte Carlo simulations for the bending moment capacity with the design values of the semi-probabilistic calculation method of EN 1992-1-2. Equation (3) allows for an evaluation of the structural fire resistance, but is dependent on the variable load. On the other hand, as elaborated in (Gulvanessian et al, 2002), equation (4) allows to evaluate the intrinsic safety of the design value of the bending moment capacity of the beam configuration, i.e. β_2 indicates which fractile of the bending moment distribution corresponds to the design value given by the Eurocodes. According to Eurocode 0 (CEN, 2002), the sensitivity factor α_R can be assumed equal to 1 for this case since $\sigma_E/\sigma_R < 0.16$. This result is based on additional Monte Carlo simulations in which the standard deviation of the design value of the bending moment induced by the design loads was simulated and compared to the simulated standard deviation of the bending moment capacity. The stochastic characteristics for the design loads are based on (Holický and Sýkora, 2010).

Although β_1 and β_2 are not the conventional definitions of the safety index β and consider only the stochastic nature of the resistance effect, both equations allow to investigate the influence of the basic variables on the safety level. Since the main objective of this study is to compare the safety level of different configurations and to analyze the effect of basic stochastic assumptions on the evolution of the safety level, the deviation from the classical definition is acceptable. Furthermore, since α_R can be assumed equal to 1, at the fire resistance time t_R equations (3) and (4) are equal, as shown mathematically by equation (5). As such, the fire resistance time of the beam can be approximated by the intersection of the β_1 and β_2 curves.

$$\Phi\left(-\beta_{1,t_R}\right) = P\left[M_{R,fi,t_R} < M_{Ed,fi}\right] = P\left[M_{R,fi,t_R} < M_{Rd,fi,t_R}\right] = \Phi\left(-\alpha_R\beta_{2,t_R}\right) = \Phi\left(-\beta_{2,t_R}\right) \tag{5}$$

Finally, both equations (3) and (4) can be evaluated by using the frequentist interpretation of probability.

3 APPLICATION EXAMPLE

As an application example , simulation results are presented for the concrete beam presented in Table 2. The distribution parameters for the random variables considered are given in Tab. 3, based on (Holický and Sýkora, 2010). According to the 'table method' of (CEN, 2004a) the characteristics of the example beam correspond to a fire resistance of 90 min (a = 40 mm, a_{sd} = 50 mm, b_{min} = 300 mm) when the beam is simply supported. In accordance with the calculation methodology of EN 1992-1-1 (CEN, 2004b) the example beam has a design value of 358 kNm for the bending moment capacity at ambient temperature.

Table 2: Configuration example concrete beam

Symbol	Characteristic	Unit	Nominal Value
h	beam height	mm	600
b	beam width	mm	300
f_{ck}(20°C)	20°C characteristic compressive strength	MPa	40
f_{yk}(20°C)	20°C characteristic yield strength	MPa	500
E_c(20°C)	20°C concrete modulus of elasticity	GPa	34.5
E_s(20°C)	20°C steel modulus of elasticity	GPa	200
c_1	bottom concrete cover	mm	30
$Ø_1$	bottom reinforcement diameter	mm	20
$\#_1$	number of bottom reinforcement bars	-	5
s_1	spacing bottom reinforcement bars	mm	50
c_2	top concrete cover	mm	30
$Ø_2$	top reinforcement diameter	mm	20
$\#_2$	number of top reinforcement bars	-	5
s_2	spacing top reinforcement bars	mm	50
χ	model uncertainty	-	1.2

Tab. 3: Stochastic models for variables

Symbol	Variable	Distribution type	Mean μ	Standard deviation σ
h	beam height	normal	600 mm	5 mm
b	beam width	normal	300 mm	5 mm
f_c(20°C)	20°C concrete compressive strength	lognormal	45.4 MPa	2.7 MPa
f_y(20°C)	20°C steel yield strength	lognormal	581 MPa	41 MPa
E_c(20°C)	20°C concrete modulus of elasticity	lognormal	34.5 GPa	5.2 GPa
$c_{1,2}$	concrete cover	bèta [0;3$c_{nominal}$]	30 mm	2 mm
χ	model uncertainty	lognormal	1.2	0.15

Simulation results for the example beam are presented in Fig. 4. The curves in Fig. 4 are normalized according to the 50% fractile of the bending moment capacity ($M_{R,fi,t,50}$) at the start of the fire (i.e. at ambient temperature). The intersection of the design value of the bending moment capacity and the design value of the bending moment induced by the design loads is situated at approximately 83 minutes of exposure.

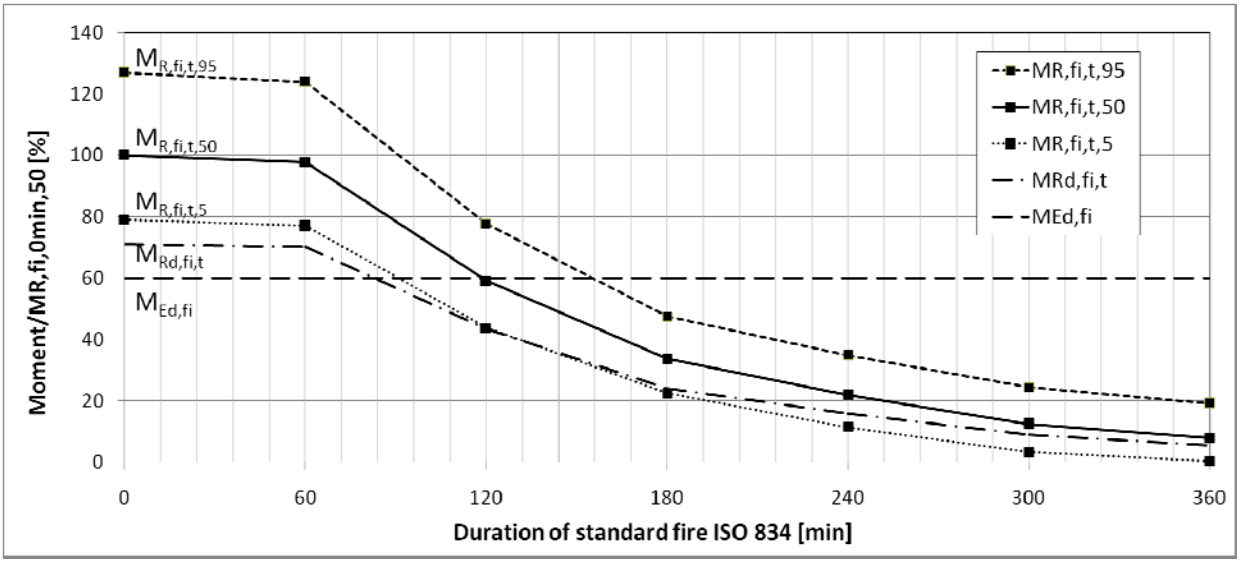

Fig. 4: Model results for example beam ($M_{R,fi,t,50}$ = 583 kNm)

The calculated safety indices β_1 and β_2 according to equation (3) and (4) are visualized in Fig. 5. The intersection of both curves corresponds to a fire resistance of 80 min. While the decrease of β_1 indicates the increasing probability of structural failure, the decrease of β_2 corresponds to an increasing probability that the design value of the bending moment capacity ($M_{Rd,fi,t}$) overestimates the actual bending moment capacity ($M_{R,fi,t}$) of the example beam. The latter can be explained by the uncertainty related to the reduction of material properties at elevated temperatures and the uncertainty of the reinforcement temperature (i.e. the concrete cover). These elements are not explicitly taken into account by the semi-probabilistic design methods in the Eurocode (CEN, 2004a).

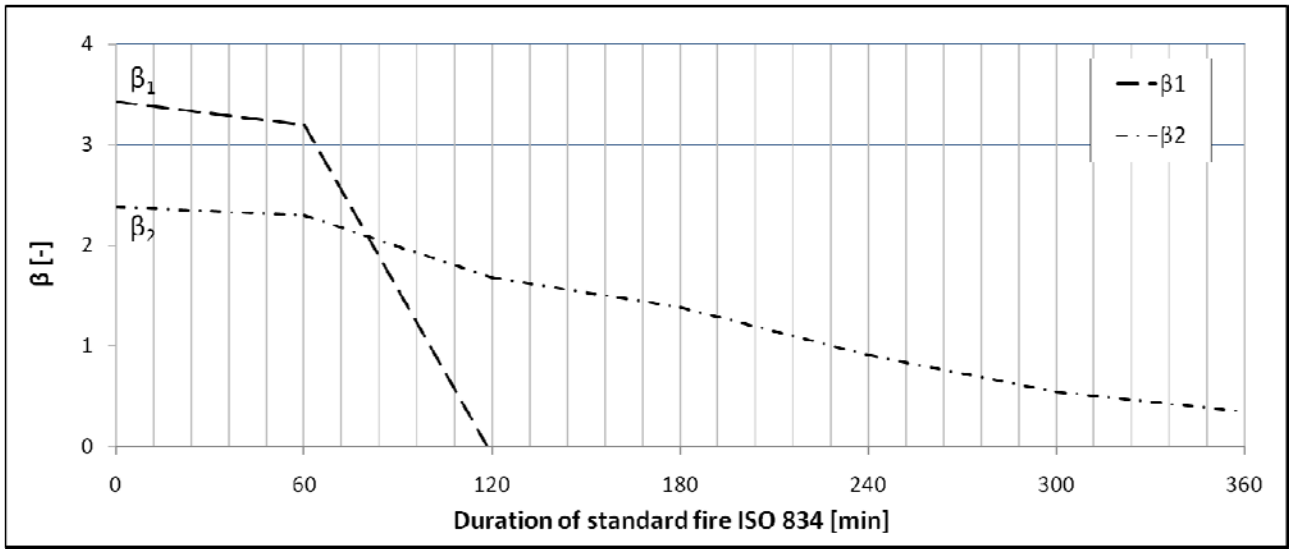

Fig. 5: β_1 and β_2 for example beam configuration

By altering the beam configuration the simulated fire resistance time can be increased. Simulations indicate that an increase of the concrete cover is particularly efficient, while increasing the concrete compressive strength has less impact.

4 CONCLUSIONS

- A full-probabilistic model is developed for analyzing the safety level of concrete beams
- Based on the probabilistic analysis of a beam the fire resistance time was found to be smaller than tabulated by EN 1992-1-2 (CEN, 2004a).
- The fire resistance of a beam can be increased by altering the beam configuration, or by decreasing the uncertainty on e.g. the concrete cover through sampling and testing.

REFERENCES

Gulvanessian H, Calgaro JA, Holický M. Designers' guide to EN 1990: Eurocode 0: basis of structural design. London: Thomas Telford; 2002

CEN. Eurocode 0: Basis of structural design. European Standard EN 1990; 2002

CEN. Eurocode 2: Design of concrete structures: Part 1-2: Structural fire design, European Standard EN 1992-1-2; 2004a

CEN. Eurocode 2: Design of concrete structures: Part 1-1: General rules and rules for buildings, European Standard EN 1992-1-1; 2004b

Annerel E, Taerwe L. Evolution of the strains of traditional and self-compacting concrete during and after fire. Mater. Struct. 2010; Online First

Holický M, Sýkora M. Stochastic models in analysis of structural reliability, Proceedings of the International Symposium on Stochastic Models in Reliability Engineering, Life Sciences and Operation Management, Beer Sheva, Israel; 2010

SHEAR STRENGTH OF CONCRETE AT ELEVATED TEMPERATURE

Holly K. M. Smith [a], Emma R. E. Reid [a], Andrew A. Beatty [a], Tim J. Stratford [a], Luke A. Bisby [a]

[a] BRE Centre for Fire Safety Engineering, The School of Engineering, The University of Edinburgh, Edinburgh, UK

INTRODUCTION

Performance based methods for designing concrete structures in fire have focused to date upon the flexural performance of beam and slab elements and large displacement mechanisms for sustained load capacity at high temperature. Shear failure has received little attention, but there is a growing awareness that shear can govern the failure of concrete structures in fire, for example in punching shear (Bamonte *et al.*, 2009) or as a consequence of restrained thermal expansion (Faria *et al.*, 2010).

Shear is carried in reinforced concrete through the interaction of (Regan, 1993)

- compressive force paths within the concrete;
- tensile crack bridging by the reinforcing steel (relying upon concrete-steel bond);
- dowel action in the reinforcing steel; and
- friction across cracked surfaces due to aggregate interlock.

Modelling the complex interplay of these shear-carrying mechanisms is notoriously difficult, even at ambient temperatures. Accurate finite element modelling requires a very detailed representation of the load carrying phenomena and their constitutive responses (Kotsovos & Pavlović, 1995). Whilst we have understanding of how (for example) the compressive strength of concrete and the tensile strength of steel are affected by elevated temperature (e.g. Khoury, 2000; Zhang *et al.*, 2000), there is currently insufficient elevated temperature understanding of the shear mechanisms and their interaction to allow reliable finite element modelling of concrete in shear in fire.

This paper describes an investigation of the effect of elevated temperature upon the shear performance of concrete. It is a first step in determining detailed constitutive information that can be used in modelling and design.

1 EXPERIMENTAL PROGRAMME

A series of shear blocks were constructed and tested, which are shown in Fig. 1. These were similar in concept to the shear blocks tested by Mattock (Mattock & Hawkins, 1972), but a modified geometry was adopted, based upon that used by Ali *et al.* (2008).

Shear blocks are designed to load a reinforced concrete section in pure shear, and hence fail along by cracking along the central shear plane (Fig. 1). The behaviour of this crack is characterised by aggregate interlock action and reinforcement bridging, and is particularly relevant to the shear failure of columns where aggregate interlock is mobilised due to the confinement provided by the axial force in the column.

The shear blocks were heated so as to expose the concrete to temperatures that are known to affect the properties of concrete. Residual strength tests were conducted on the specimens after cooling. (The second phase of these tests will involve strength tests whilst at elevated temperature).

1.1 Specimen Construction and Conditioning

Sixteen shear block specimens were cast. The specimens had dimensions 100×160×320mm, which was governed by the physical size and the thermal mass that could be effectively heated. The specimens were reinforced with 6 mm diameter smooth steel bars with an ambient yield strength of 415 MPa (Fig. 2). Four pieces of reinforcement crossed the shear failure plane, with additional reinforcement to provide anchorage and to prevent failure of the concrete away from the shear plane.

The concrete was provided by a local readymix supplier, with a maximum aggregate size of 10mm, an ambient compressive strength of f_c = 29 MPa (based upon cube tests), and an ambient tensile strength of f_t = 1.8 MPa (based upon split-cylinder tests).
After removal from the moulds, the specimens were cured in a water tank for one week, followed by seven weeks in a low humidity environment, controlled by a dehumidifier. To reduce the moisture content of the specimens and hence minimise the likelihood of spalling, the specimens were pre-dried at 90°C for seven days. Two standard 100mm cylinders specimens were cast for each shear block, and these were conditioned in the same way.

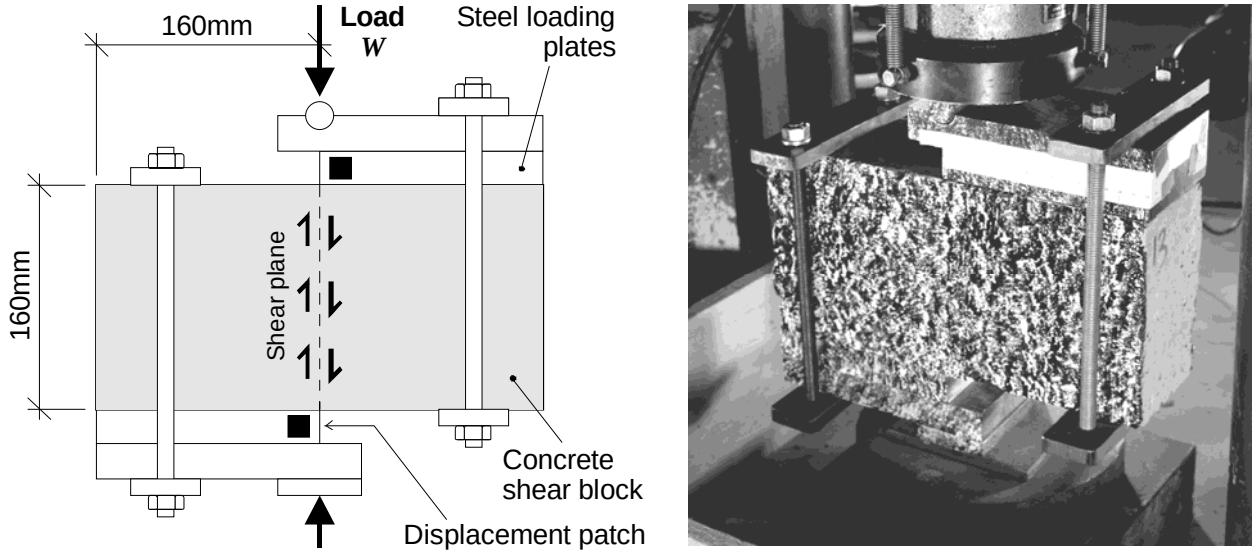

Fig.1 Overview of the shear block test arrangement

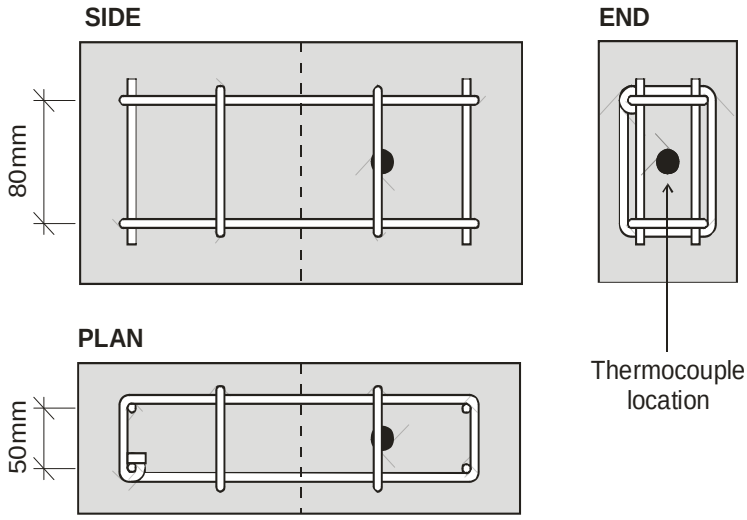

Fig.2 Details of the shear block reinforcement

1.2 Heating regime

The specimens were heated in an electric furnace, which could accommodate one shear block and two cylinders at a time. They were heated to temperatures of 112°C, 188°C, 390°C, 475°C and 622°C, as shown in Tab. 1. Another set of specimens was unheated (17°C).

Tab. 1 Specimen Test Programme and Key Results

Specimen ID	Heating duration [mins]	Target internal temperature [°C]	Achieved peak internal temperature [°C]	Compressive concrete strength [N/mm^2]	Tensile concrete strength [N/mm^2]	Shear failure load [kN]	Shear failure stress [N/mm^2]	Frictional shear stress [N/mm^2]
17-1	-	17	17.2	25.1	4.1	100.5	6.3	-
17-2			17.0			93.7	5.9	-
17-3			17.1			110.5	6.9	3.5
17-4			17.5			119.2	7.5	2.6
112-1	120	112	102.7	26.9	3.7	103.5	6.5	2.9
112-2			109.2			97.5	6.1	3.9
112-3			122.6			102.0	6.4	2.7
188-1	120	188	178.1	27.8	3.9	93.0	5.8	2.4
188-2			191.2			88.5	5.5	3.6
188-3			196.1			106.3	6.6	3.3
390-1	120	390	379.9	19.3	2.5	91.0	5.7	1.9
390-2			399.8			95.0	5.9	3.3
475-1	120	475	464.1	17.5	2.2	79.8	5.0	-
475-2			486.5			81.8	5.1	1.5
622-1	165	622	619.9	12.6	1.8	71.8	4.5	1.8
622-2			624.4			67.9	4.2	1.8

A thermocouple was placed at the centre of the shear block (Fig. 2) to record the internal temperature, and a second thermocouple was used to record the furnace temperature. The furnace was used to heat the specimens as quickly as possible, with an oven temperature increase rate in the range 5 and 15ºC/min. After the initial heating, the furnace was controlled manually to achieve the required temperature inside the concrete. All specimens were heated for 2 hours, except for those at the highest temperature, for which it was necessary to increase the heating duration to 2 ¾ hours.

After heating, the specimens were left in the furnace to cool, and then each specimen was left for seven days before its strength was determined.

1.3 Strength tests

Steel loading plates were added to the shear block to force shear failure, as shown in Fig. 1. The specimens were loaded using a hydraulic universal test machine at an initial rate of 20 kN/min, with the applied load recorded using a load cell.

Digital image correlation was used to obtain the specimen displacements from a sequence of 21 megapixel photographs taken at a frequency of 0.2 Hz. The specimens were painted with a high-contrast speckle pattern prior to testing, and a bespoke image-processing algorithm was used to track the motion of selected patches of the speckle pattern from image to image (Bisby & Take, 2009). Digital image correlation was chosen rather than a traditional displacement measurement technique because it allows the positions at which displacements are measured to be selected after the test; allows relative displacements to be measured within the concrete (hence avoiding the effects of local crushing at the supports); allows both the shear displacement and crack opening displacement to be measured across the cracked surface; and allows any variations in displacement along the crack surface to be observed. The resolution of digital image correlation for this application was in the order of 0.006 mm

A cylinder compression and split-cylinder tension test (conducted to EN 12390) accompanied each shear block test.

2 EXPERIMENTAL RESULTS

Tab.1 provides a summary of the key experimental results.

2.1 Heating regime

Fig. 3 shows the temperatures recorded within the concrete shear blocks and the corresponding temperatures in the furnace. The peak temperatures within each specimen are given in Tab. 1.

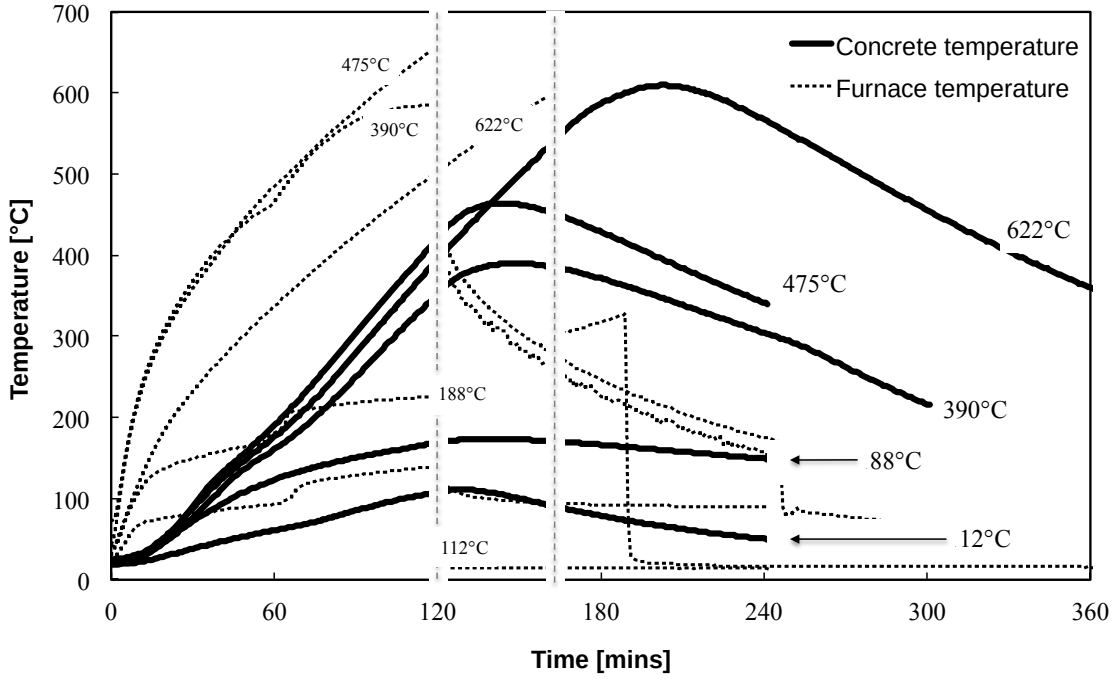

Fig. 3 Recorded temperatures in the furnace and within the concrete blocks

2.2 Strength variation with temperature

Fig. 4 plots the variation in compressive and tensile strengths of the concrete that were obtained from the cylinders that were heated at the same time as the shear blocks. For clarity, these have been normalised by the ambient temperature strength of the concrete, and the average strength variation with temperature is shown. The reduction in concrete strength with temperature is as expected, but it should be noted that some of the specimens suffered from poor compaction.

Fig. 4 also plots the variation in the shear strength of the shear blocks with temperature. The shear strength follows a similar trend to the concrete strength variation. However, the reduction in shear strength is less pronounced at high temperatures, because it is dependent upon the strengths of both the concrete and steel.

2.3 Load-displacement and crack opening width responses

Fig. 5 shows the load versus shear displacement measured across the crack. For clarity, one load-displacement response has been plotted for each temperature; these were chosen to be a good representation of the full set of results; other responses were similar.

The load-deflection response of the shear blocks has an initial peak load, at which point the shear crack fully forms and the shear capacity drops to a frictional value that is governed by aggregate interlock, confinement by the reinforcement, and reinforcement dowel action. The initial stiffness and the peak strength of the specimen reduced with temperature, whereas the displacement corresponding to the peak strength increased with temperature.

The post-peak frictional shear strength was also affected by temperature, with two clear groups apparent: the lowest three temperatures carried a frictional shear of 50 kN; the highest three temperatures carried a frictional shear of 25 kN. At the three lower temperatures, diagonal tension cracks initially formed at an angle to shear plane, which coalesced into a single shear crack. The reinforcement sheared across the crack, and caused some separation of the cover concrete.

At the three higher temperatures, the straight shear crack formed immediately. Cover concrete bursting was far more extensive, and this allowed the reinforcement to debond and reduced confinement of the shear crack. The aggregate could also be heard to "snap" during the higher temperature residual tests. Consequently, the performance of the shear blocks was governed by a combination of the residual strength of the concrete, the residual strength of the reinforcement and the complex interaction between the two.

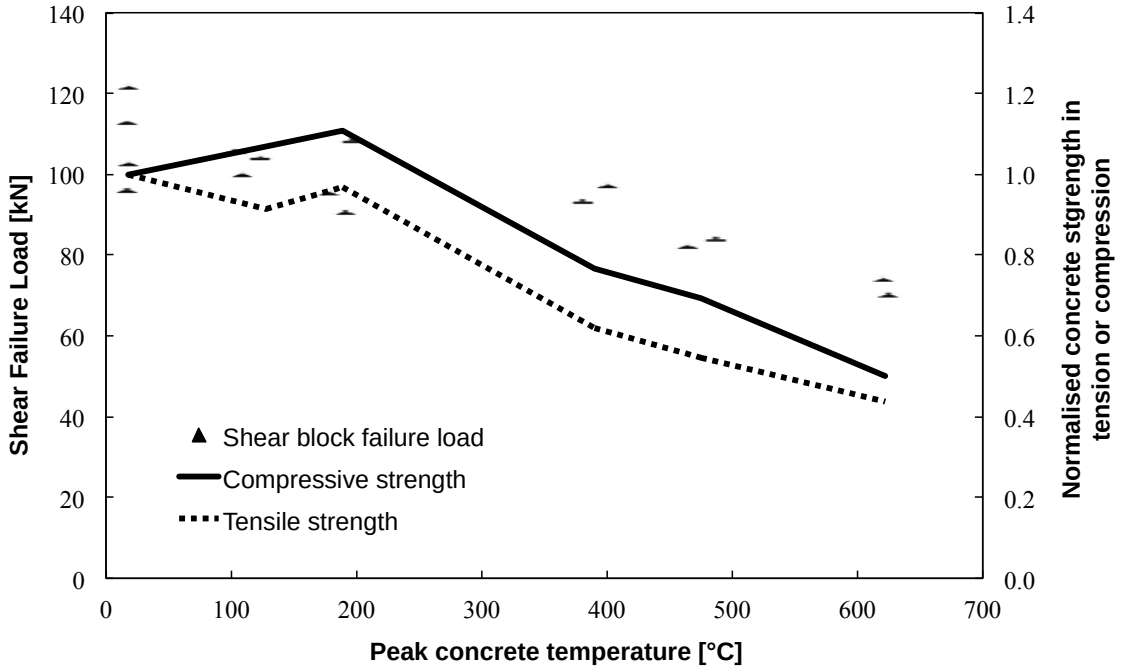

Fig. 4 The effect of temperature upon the residual strength of the shear block, and upon the residual compressive and tensile strengths of the concrete.

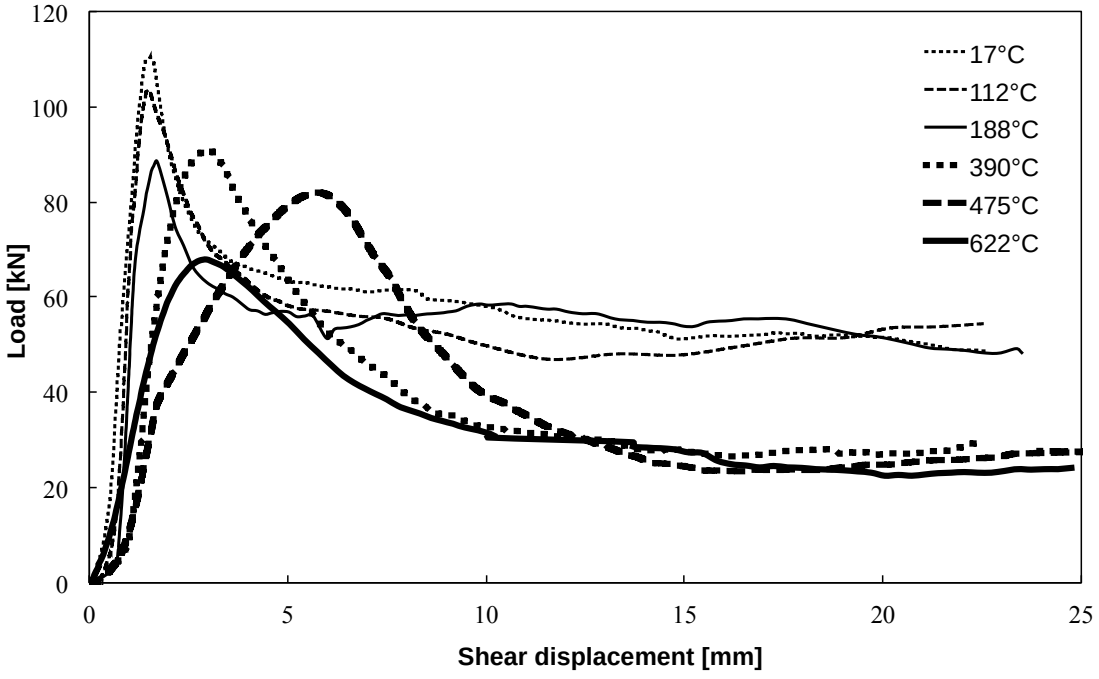

Fig. 5 The effect of temperature on the residual load-displacement response of the shear blocks

Digital image correlation was used to determine the crack opening widths that developed as the load was applied, and these are plotted in Fig. 6. Again, the response is split into two groups, with the three higher temperatures characterised by larger crack opening displacements, even prior to the peak load being reached.

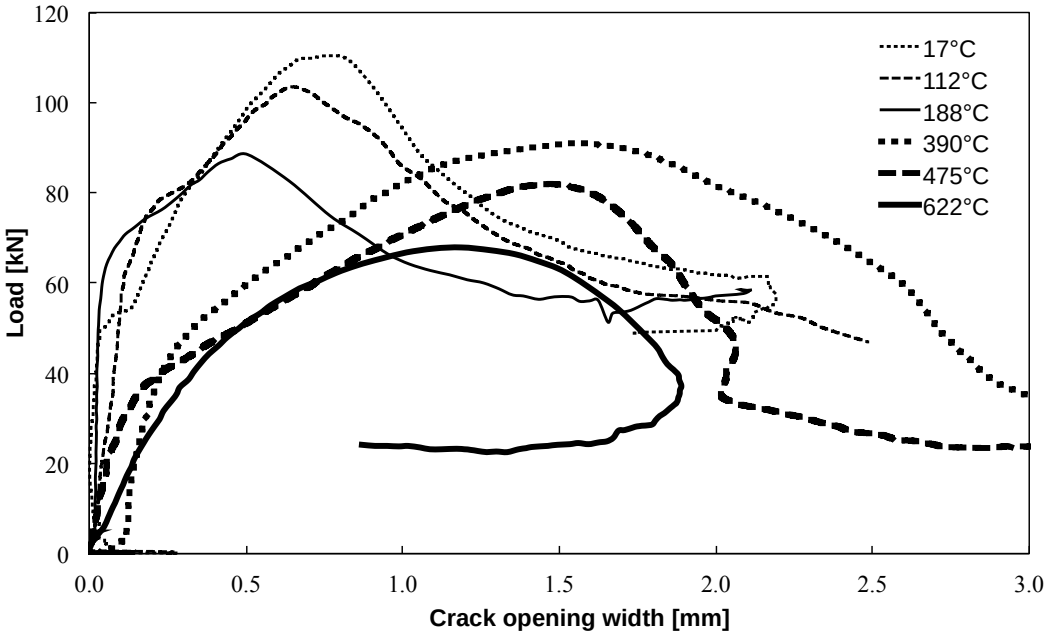

Fig. 6 The effect of temperature on crack opening width development.

3 SUMMARY

The results presented in this paper demonstrate that the residual shear strength of reinforced concrete is affected by the temperature to which is has been exposed. The reduction in shear performance depends upon the interaction of the concrete and the reinforcing steel. For example, the tests have shown that concrete exposed to high temperatures suffers from increased cover separation (due to the reduced tensile strength), which allows greater reinforcement debonding and hence less confinement, which in turn mobilise less aggregate interlock shear.

REFERENCES

Ali, M., Oehlers, D., & Griffith, M. (2008). Shear transfer across cracks in FRP strengthened RC members. Journal of Composites for Construction, 12(4):416-424.

Bamonte P., Felicetti R., Gambarova P.G. (2009). Punching shear in fire-damaged reinforced concrete slabs. American Concrete Institute, 265:345-366.

Bisby, L. A., Take, W. A. (2009). Strain Localizations in FRP Confined Concrete: New Insights. Proceedings of the ICE - Structures and Buildings, 162(5):301-309.

Faria R., Xavier H.F., Real P.V. (2010). Simplified procedure for shear failure assessment of RC framed structures exposed to fire. Structures in Fire – Proceedings of the 6th international conference, Michigan, 197-205.

Khoury, G. (2000). Effect of fire on concrete and concrete structures. Progress in Structural Engineering and Materials, 2(4):429-447.

Kotsovos M.D. & Pavlović M.N. (1995) Structural concrete – Finite-element analysis for limit-state design. Thomas Telford Ltd., London.

Mattock, A., & Hawkins, N. (1972). Shear Transfer in Reinforced Concrete - Recent Research. PCI Journal, (March-April):55-75.

Regan P.E. (1993). Research on shear: a benefit to humanity or a waste of time? The Structural Engineer, 71(19):337-347.

Zhang B., Bicanic N., Pearce C.J., Balabanic G. (2000), Assessment of toughness of concrete subject to elevated temperatures from complete load-displacement curve - part II: experimental investigations. ACI Materials Journal, 97(5):556-566.

FIRE DESIGN OF CONCRETE AND MASONRY STRUCTURES
Software Tools Developed at the Czech Technical University in Prague

Radek Štefan [a], Jaroslav Procházka [a], Michal Beneš [a]

[a] Czech Technical University in Prague, Faculty of Civil Engineering, Prague, Czech Republic

INTRODUCTION

During the last few years, scientific and professional community has focused on developing effective software tools to fire design of structures. In many cases, utilization of an appropriate software tool is the only way (except fire tests) to assess a real behaviour of a structure under fire conditions. On the other hand, when designing simple and commonly used structures or structural members, the usage of software tools is not necessary. However, in these cases, it also may lead to significant time saving.

In this paper, brief information about software tools to fire design of concrete and masonry structures developed at the Czech Technical University in Prague are summarised. Section 1 present computer program *TempAnalysis* (Štefan, Procházka, 2009), which is intended for thermal analysis of rectangular cross-sections exposed to fire. In Section 2, software *HygroThermAnalysis* (Štefan, Beneš, 2010) is briefly described. This software can be used to hygro-thermal analysis of concrete cross-sections under fire conditions. Moreover, using this software, it is also possible to predict concrete surface spalling. Section 3 describes software package *FiDeS* (Štefan, 2010), destined for fire design of concrete and masonry structures according to Eurocodes. The presented software tools have been developed in MATLAB (2008) environment. They are available for free on web site *http://concrete.fsv.cvut.cz/~stefan/research.htm*.

1 TempAnalysis SOFTWARE

1.1 Software description

TempAnalysis software (Štefan, Procházka, 2009) is intended for thermal analysis of rectangular cross-sections exposed to fire. Using this program, it is possible to solve one-dimensional (slabs, walls) and two-dimensional (beams, columns) heat transfer problem. The program consists of two parts: pre-processor for input data and post-processor for display of results. The pre-processor dialog window is shown in Fig. 1. Material properties (density, thermal conductivity and heat capacity) of an analysed cross-section can be assumed as linear (i.e. temperature independent) or non-linear (i.e. temperature dependent). For concrete, material model defined by EN 1992-1-2 (2004) is preset in the program. An analysed cross-section can be protected by insulation on the fire-exposed sides. In this case, the thickness of the protective layer and its material properties shall be defined. A design fire scenario is represented either by the standard temperature-time curve ISO 834 or, alternatively, by the parametric curve according to EN 1991-1-2 (2002). For a one-dimensional problem, one-sided or two-sided fire exposure can be set. For a two-dimensional problem, two-, three- or four-sided fire exposure can be chosen.

Heat transfer model included in the program is described in detail in (Štefan, Procházka, 2010c). The space discretization of the governing equations is carried out using a finite element method. The time discretization is performed using a semi-implicit difference scheme. In the previous version of the *TempAnalysis* software, a two-dimensional problem has been based on a simplified approach proposed by Hertz (2006), which consists in two separate one-dimensional solutions in x- and y-direction, see (Procházka, Štefan, 2009; Štefan, Procházka, 2010c). In the current version, a two-dimensional problem can be solved either using the simplified approach mentioned above or, alternatively, with the use of the two-dimensional finite element method with bilinear quadrilateral finite elements, for comparison see Fig. 4.

In the post-processor part of the program, it is possible to display a value of temperature of any point of the analysed cross-section and to plot a resulting temperature profile or temperature field, see Fig. 2–3.

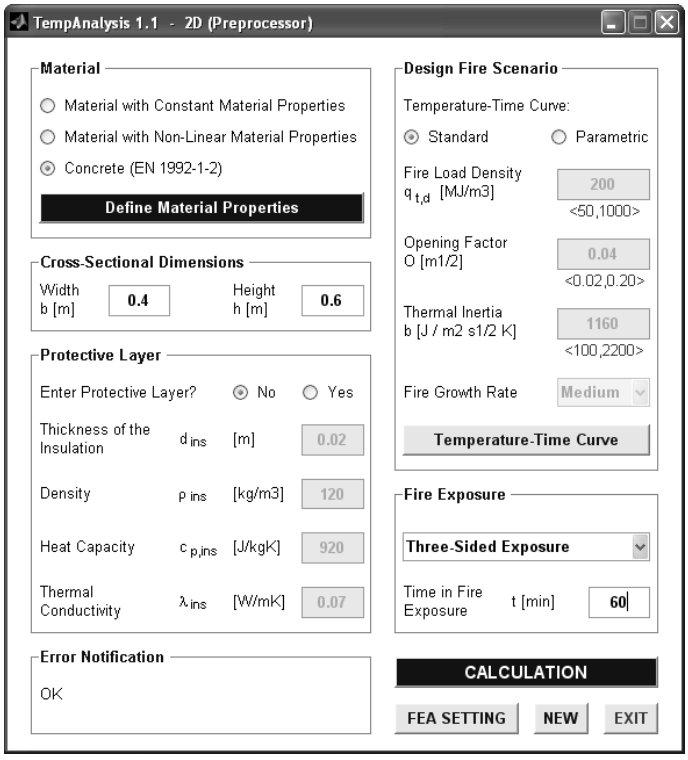

Fig. 1 Pre-processor dialog window

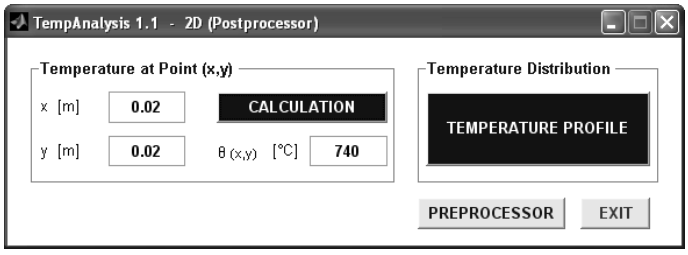

Fig. 2 Post-processor dialog window

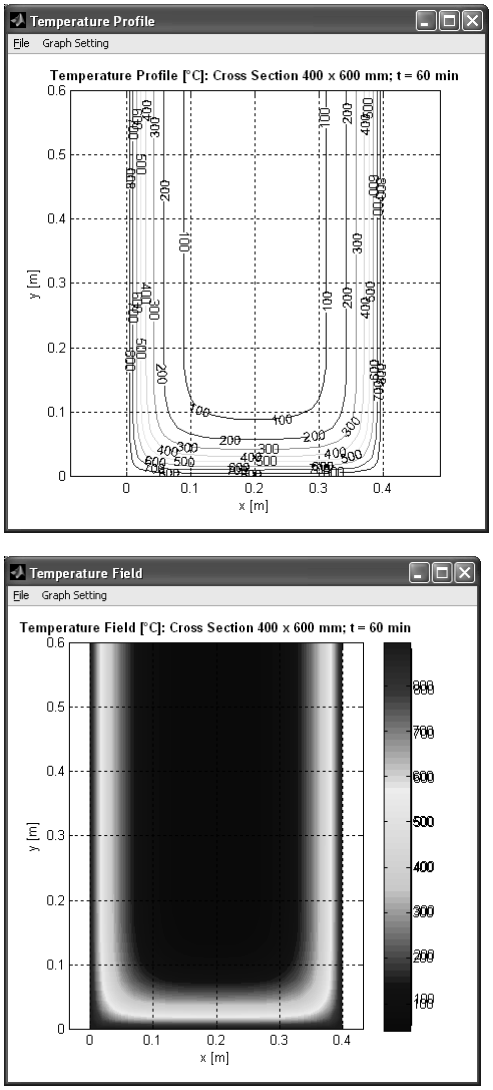

Fig. 3 Temperature profile/field

1.1 Software validation

A validity of the *TempAnalysis* software has been assessed by comparing the results obtained by the software with the corresponding data given by Eurocodes and by literature. Fig. 4 shows the temperature profiles of a concrete cross-section 400 × 400 mm^2 subjected to standard fire (ISO 834, four-sided exposure) for 60 minutes. It is obvious that when using the simplified procedure for the two-dimensional problem (two separate one-dimensional solutions), the results given by the *TempAnalysis* software are a little bit different from the standard profiles given by EN 1992-1-2 (2004). Nevertheless, for practical design, this accuracy seems to be sufficient. On the other hand, when using the two-dimensional finite element method, the results obtained by finite element analysis (FEA) are in accordance with the standard profiles.

For illustration, comparison of calculated temperatures with the measured data provided by (Haksever, Anderberg, 1981) appears in Fig. 5. A scheme of the analysed cross-section is shown in Fig 6. For the FEA, material properties of concrete have been taken from EN 1992-1-2 (2004) assuming the values listed in Table 1. Regarding the uncertainties in the input data, an accordance of the calculated temperatures with the measured data can be evaluated as fully sufficient.

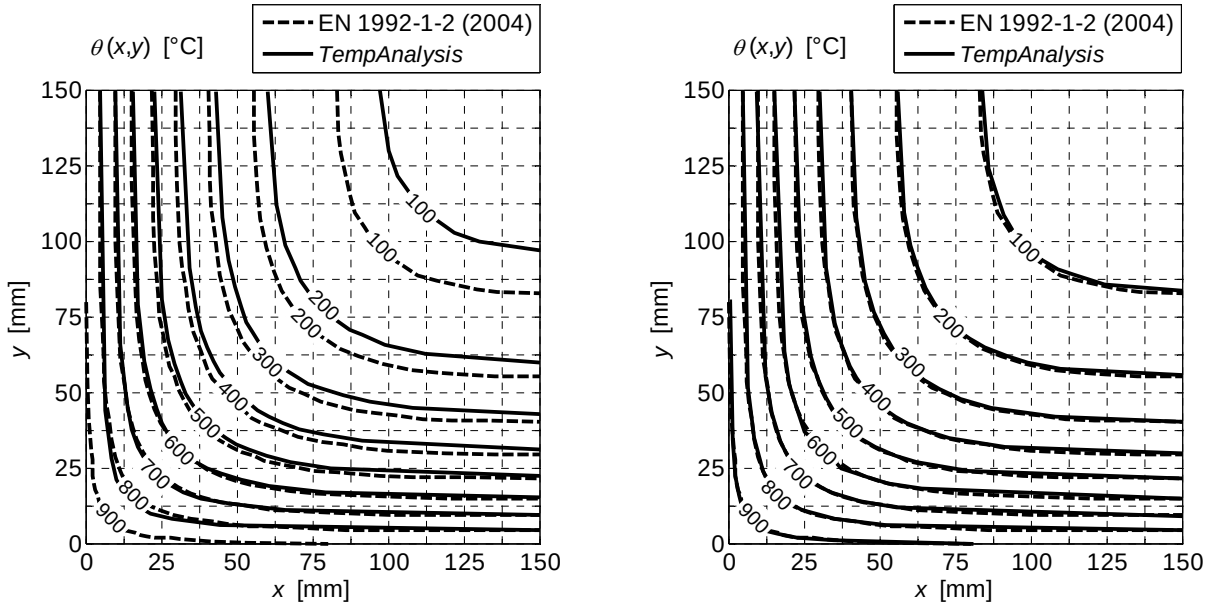

Fig. 4 Comparison of temperature profiles obtained by *TempAnalysis* software using a simplified algorithm (left) or using two-dimensional finite element method (right) with the temperature profiles given by EN 1992-1-2 (2004)

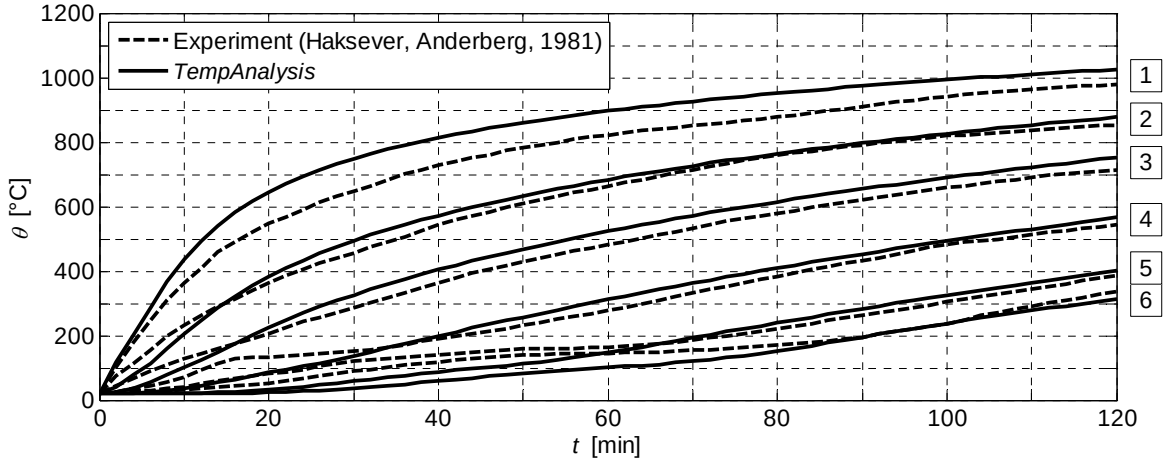

Fig. 5 Comparison of temperature profiles obtained by *TempAnalysis* software using two-dimensional finite element method with the measured data given by (Haksever, Anderberg, 1981)

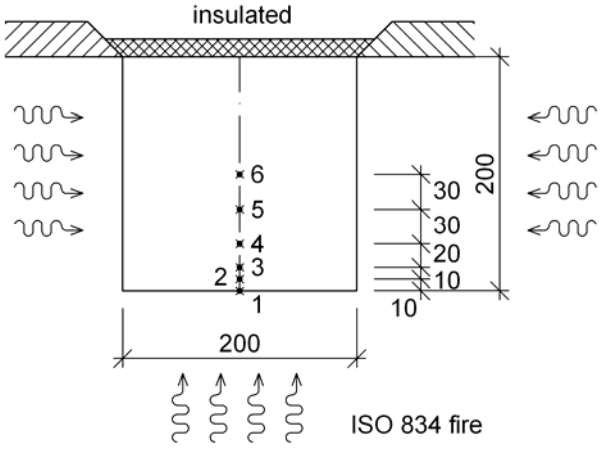

Fig. 6 Scheme of the analysed cross-section (Haksever, Anderberg, 1981)

Table 1 Parameters used in FEA

Parameter	Value	Unit
α_c	25	W m^{-2} K^{-1}
Φ	1	-
ε_s	0.7	-
ε_f	1	-
σ	$5.67 \cdot 10^{-8}$	W m^{-2} K^{-4}
$\rho(20)$	2400	kg m^{-3}
u	3	% of weight
λ	Lower limit	

2 HygroThermAnalysis SOFTWARE

HygroThermAnalysis software (Štefan, Beneš, 2010) is intended for hygro-thermal analysis of concrete rectangular cross-sections exposed to fire. Using this program, it is possible to solve one-dimensional (slabs, walls) and two-dimensional (beams, columns) heat and moisture transfer problem. The program consists of two parts: pre-processor for input data and post-processor for display of results. The pre-processor dialog window is shown in Fig. 7.

Heat and moisture transfer model included in the program is based on Bažant-Thonguthai (1978) model and it is described in (Beneš, Štefan, 2010; Beneš et al., 2011). The space discretization of the governing equations is carried out using a finite element method. The time discretization is performed using a semi-implicit difference scheme.

In the post-processor part of the program, it is possible to display values of temperature, water content and pore pressure at any point of the analysed cross-section and to plot resulting temperature, pore pressure and water content distributions, as shown in Fig. 8. Using a heuristic engineering criterion (see Beneš et al., 2011), spatial distribution of the spalling damage can be predicted by the program, see Fig. 9.

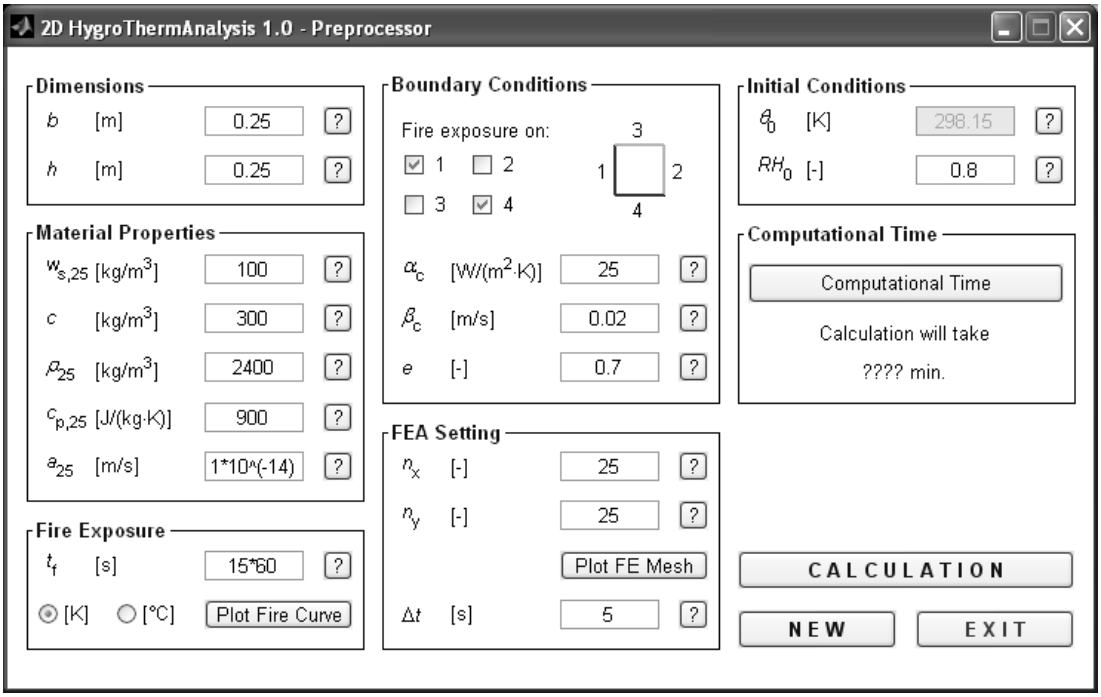

Fig. 7 *HygroThermAnalysis* – pre-processor dialog window

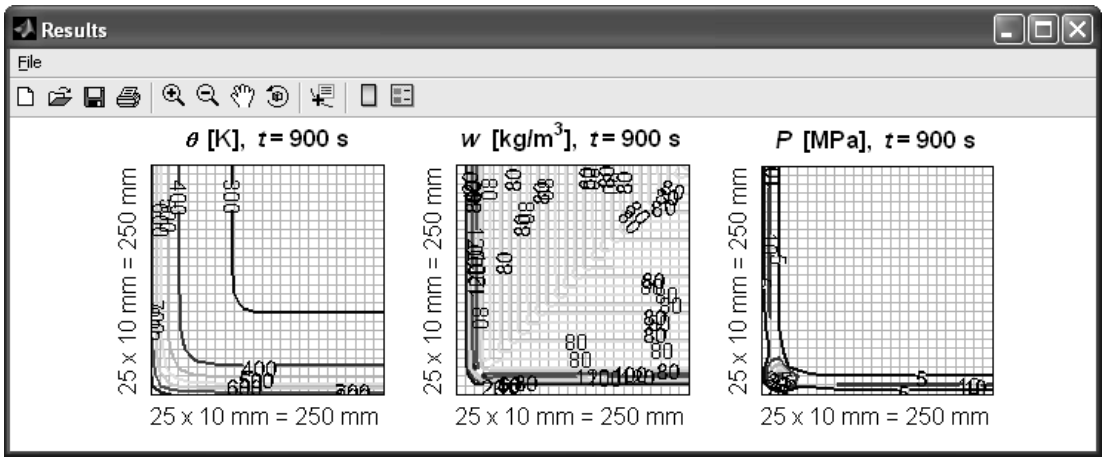

Fig. 8 *HygroThermAnalysis* – distribution of temperature, water content and pore pressure

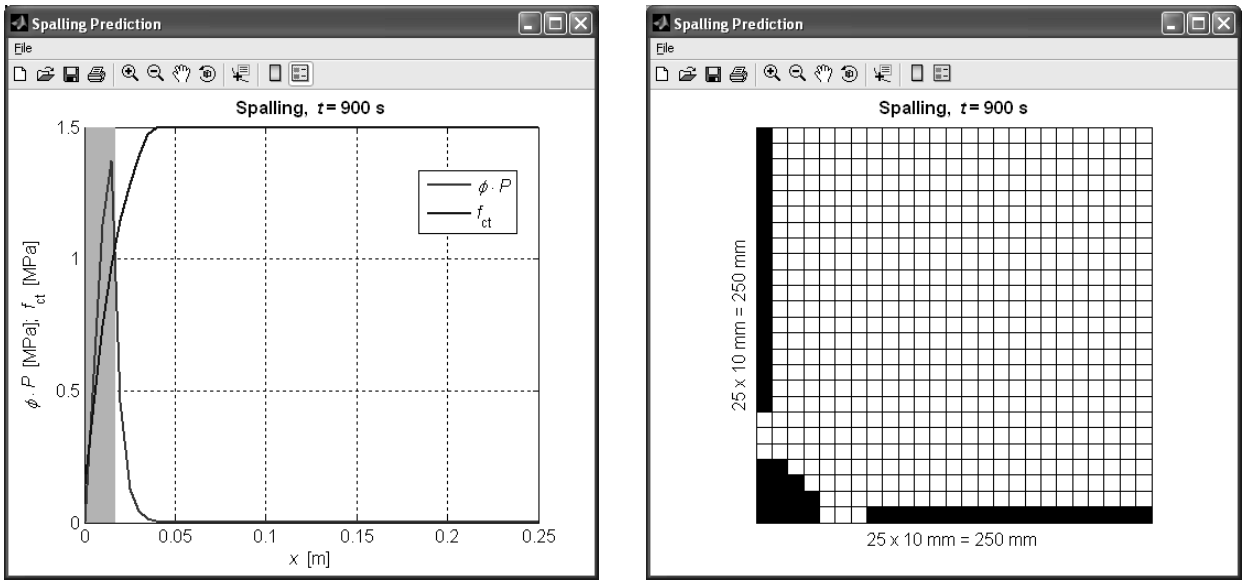

Fig. 9 *HygroThermAnalysis* – prediction of spalling of concrete wall (left) and column (right)

3 FiDeS SOFTWARE PACKAGE

FiDeS (Štefan, 2010) – ***Fi***re ***De***sign ***S***oftware is a software package to fire design of concrete and masonry structures according to Eurocodes. This package consists of five computer programs: (i) computer program to temperature analysis of a fire compartment according to EN 1991-1-2 (2002); (ii) computer program to temperature analysis of a cross-section exposed to fire; (iii) computer program to fire design of concrete structural members according the tabulated data given by EN 1992-1-2 (2004); (iv) computer program to fire design of concrete structural members using the simplified calculation methods given by EN 1992-1-2 (2004); and (v) computer program to fire design of masonry structural members according the tabulated data given by EN 1996-1-2 (2005).
In the actual version of the *FiDeS* software, the user interface is only in Czech. However, the English version is currently being prepared, see Fig. 10. More information about this software can be found in (Štefan, R., Procházka, J., 2010a, 2010b; Wald et al., 2011).

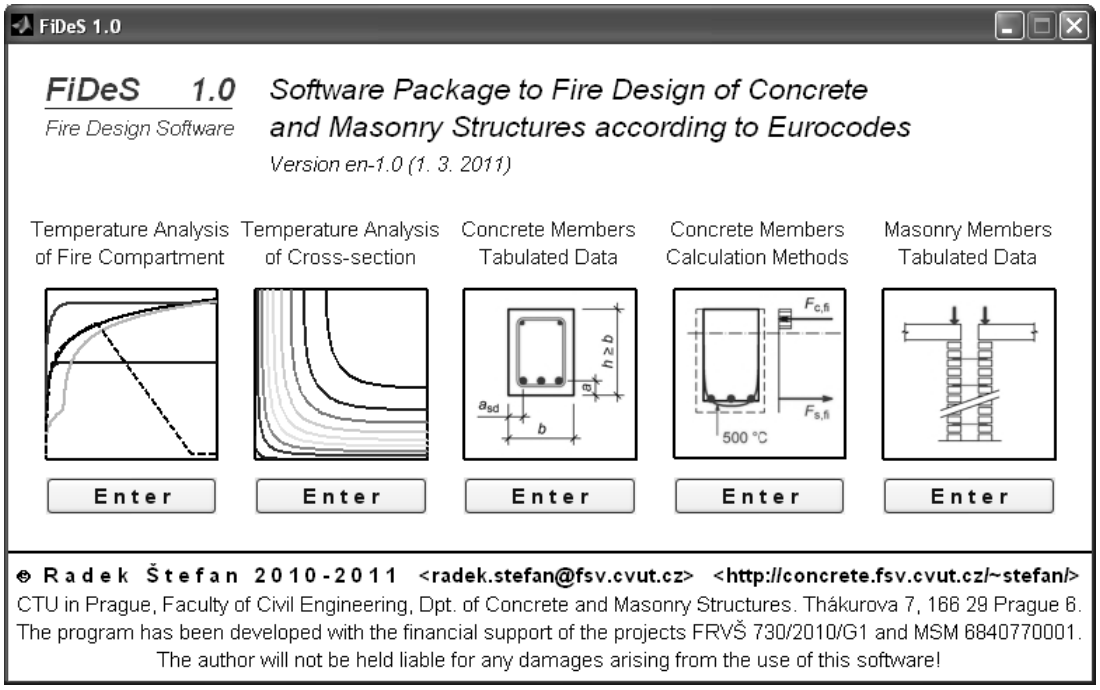

Fig. 10 *FiDeS* – main dialog window

4 SUMMARY AND ACKNOWLEDGMENT

In the present paper, software tools to fire design of concrete and masonry structures developed at the Czech Technical University in Prague have been briefly described.

This outcome has been achieved with the financial support of the Ministry of Education, Youth and Sports of the Czech Republic, project No. MSM6840770001 (the first and the second author) and project CIDEAS No. 1M0579 (the third author). Additional support from the grant Reg. No. OHK1-041/11 "Modelling of concrete structures during fire" (the first and the third author) provided by the Grant Agency of the CTU in Prague is greatly acknowledged.

REFERENCES

Bažant, Z. P., Thonguthai, W (1978), Pore Pressure and Drying of Concrete at High Temperature. J. Eng. Mech. Div. 104 (1978), 1059–1079.

Beneš, M., Štefan, R. (2010), Surface spalling of concrete structures during fire, Stavební obzor (submitted 2010). (in Czech).

Beneš, M. et al. (2011), Analysis of coupled transport phenomena in concrete at elevated temperatures, Appl. Math. Comput. (accepted 2011), DOI: 10.1016/j.amc.2011.02.064.

EN 1991-1-2 (2002), Eurocode 1: Actions on structures – Part 1-2: General actions – Actions on structures exposed to fire, CEN, Brussels.

EN 1992-1-2 (2004), Eurocode 2: Design of concrete structures – Part 1-2: General rules – Structural fire design, CEN, Brussels.

EN 1996-1-2 (2005), Eurocode 6: Design of masonry structures – Part 1-2: General rules – Structural fire design, CEN, Brussels.

Haksever, A., Anderberg, Y. (1981), Comparison between measured and computed structural response of some reinforced concrete columns in fire. Fire Saf J 4, 1981, pp. 293-297.

Hertz, K. (2006), Users Guide for the Program ConTemp.exe [online], Kgs. Lyngby: DTU, Institute of Building Structures, 2006. URL: http://www.byg.dtu.dk/English/Research/Software.aspx

MATLAB (2008) [computer program]. Version 7.6.0.324 (R2008a). USA, The MathWorks, 2008.

Procházka, J., Štefan, R. (2009), Temperature Distribution through a Cross-Section Exposed to Fire, In Concrete and Concrete Structures, Žilina: Žilinská univerzita, Stavebná fakulta, 2009, p. 277-284. ISBN 978-80-554-0100-3.

Štefan, R. (2010), FiDeS – Software Package for Fire Design of Concrete and Masonry Structures according to Eurocodes [software online]. Prague: CTU in Prague, Faculty of Civil Engineering, 2010. (in Czech) URL: http://concrete.fsv.cvut.cz/~stefan/

Štefan, R., Beneš, M. (2010), HygroThermAnalysis [software online]. Prague: CTU in Prague, Faculty of Civil Engineering, 2010. URL: http://concrete.fsv.cvut.cz/~stefan/

Štefan, R., Procházka, J. (2009), TempAnalysis – Computer Program for Temperature Analysis of Cross Sections Exposed to Fire [software online]. Prague: CTU in Prague, Faculty of Civil Engineering, 2009. URL: http://concrete.fsv.cvut.cz/~stefan/

Štefan, R., Procházka, J. (2010a), Computer Program for Assessment of Fire Resistance of Concrete Beams and Slabs Using Tabulated Data Given by EN 1992-1-2, In Betonárske dni 2010: Zborník prednášok, Bratislava: STU, 2010, s. 253-256. ISBN 978-80-8076-089-2. (in Czech).

Štefan, R., Procházka, J. (2010b), Computer Program for Assessment of Fire Resistance of Concrete Columns and Walls Using Tabulated Data Given by EN 1992-1-2, In Betonářské dny 2010, Praha: ČBS ČSSI, 2010, s. 461-463. ISBN 978-80-87158-28-9. (in Czech).

Štefan, R., Procházka, J. (2010c), Program for Determination of Temperatures in Concrete Rectangular Cross Sections Exposed to Fire, Stavební obzor, 2010, roč. 19, č. 9, s. 274-278. ISSN 1210-4027. (in Czech).

Wald F. et al. (2011), Software Tools to Structural Fire Design, Prague: CTU in Prague, Faculty of Civil Engineering, 2011. ISBN 978-80-01-04746-0.

STUDY OF SLAB FIRE RESISTANCE ACCORDING TO EUROCODE
Using different computational methods

Radim Čajka [a], Pavlína Matečková [a]

[a] VSB-TU Ostrava, Faculty of Civil Engineering, Ostrava, Czech Republic

INTRODUCTION

Eurocode 1992-1-2 includes the following alternative design methods: detailing according to tabulated data, simplified calculating method for specific types of members and general calculating method for simulating the behavior of structural members, parts of structure or the entire structure. For determining the fire resistance of reinforced concrete slab structure the tabulated data and the simplified calculating method are used. Temperature distribution in concrete cross-section is determined using FEM analysis (ANsys) and numerical solution (Nonstac) of differential equation of heat transfer. Calculated temperatures are compared with temperature profiles given in annex A. Structural response of slab cross-section is determined using "500°C" isotherm method.

1 HEAT EXPOSURE

1.1 Study example and input data

In the paper study example of slab cross-section with thickness 200 mm is analysed. The slab is reinforced with profile 10/100 mm, concrete cover is 25 mm, distance between the reinforcement centre of gravity and exposed side of the slab is 30 mm. Slab is made of concrete C20/25 and steel B420B.

Thermal properties of concrete are assumed as temperature dependant according to Eurocode 2 (2006). Heat conductivity is given with upper (1) and lower (2) limit value.

$$\lambda_c = 2.0 - 0.2451(\theta/100) + 0.0107(\theta/100)^2 \quad (1)$$

$$\lambda_c = 1.36 - 0.136(\theta/100) + 0.0057(\theta/100)^2 \quad (2)$$

Basic value of concrete specific heat is 900 (J/kgK). With increasing temperature concrete specific heat growths to the value 1100 (J/kgK).

According to P ENV version of Eurocode 2 (1998) it is recommended to use the value 2300 kg/m^3, without the temperature dependence. According to Eurocode 2 (2006) the density is given as a function of temperature, as the density is influenced with water evaporation, but without the recommended value for the initial density. The common concrete density is given also in Eurocode 1, part 1-1 (2004) with the value 2400 kg/m^3, reinforced concrete 2500 kg/m^3. Reinforcement in the concrete cross-section influences the final density but as the reinforcement is placed locally it could not influence significantly the result temperature distribution. Therefore in this study example the density is supposed with value 2300 kg/m^3 and 2400 kg/m^3.

Temperature in burning space is supposed according to standard time temperature curve, heat transfer goes on partly with convection and partly with radiation. Temperature on unexposed side is supposed constant. Appropriate parameters of heat transfer are given explicitly in Eurocode 1, part 1-2 (2004).

1.2 Temperature profiles

The easiest way to appoint the temperatures in cross-section exposed to standard fire is to use temperature profiles in Annex A of Eurocode 2. As for the slab structures, the temperature profile is given only for the thickness 200 mm. Particular temperatures in reinforcement are compared with calculated temperatures in the Fig. 1.

1.3 FEM analysis

The FEM analysis is provided using ANsys computer program. In the Table 1 there are sequenced temperatures in reinforcement for different input data. Temperature profiles in concrete slab respond well with the values calculated for time dependant material properties, with the initial density 2400 kg/m^3, and initial coefficient of heat conductivity 2.0 J/kg.K according to (2). Temperatures in reinforcement are compared in the Fig.1.

Tab. 1 Temperatures in reinforcement – Ansys

	temperature dependent			constant		
λ	2.0	1.36	2.0	2.0	1.36	2.0
density	2400	2400	2300	2400	2400	2300
Time	**Temp.**	**Temp.**	**Temp.**	**Temp.**	**Temp.**	**Temp.**
min	**°C**	**°C**	**°C**	**°C**	**°C**	**°C**
0	20	20	20	20	20	20
30	271	245	277	370	332	367
60	423	402	430	574	533	574
90	517	502	524	687	647	689
120	585	575	592	765	726	767

1.4 Numerical analysis - Nonstac

Numerical analysis is provided using Nonstac computer program, (Čajka, 2010). Though the temperature distribution in cross-section in case of fire is generally three dimensional in many cases one dimensional temperature distribution satisfies with sufficient accuracy. Nonstac computer program solves numerically Fourier differential equation of one dimensional heat transfer using Runge-Kutta method (Nevřiva, 1975) and it is possible to input time dependant thermal properties of material and heat transfer due to convection and radiation. Thermal material properties have to be input as linear or quadratic function and therefore the thermal properties have to be input as regression polynomial. In the Table 2 there are sequenced temperatures in reinforcement for different input data.

Tab. 2 Temperatures in reinforcement – Nonstac

	temperature dependent		constant		
λ	2.0	1.36	2.0	1.36	2.0
density	2400	2400	2400	2400	2300
Time	**Temp.**	**Temp.**	**Temp.**	**Temp.**	**Temp.**
min	**°C**	**°C**	**°C**	**°C**	**°C**
0	20	20	20	20	20
30	331	291	370	332	340
60	504	465	574	533	540
90	604	569	687	647	654
120	670	643	765	726	732

Considering the temperature independent values of thermal material properties the result temperatures in reinforcement calculated using ANsys and Nonstac software respond together. Considering the temperature dependant values of thermal material properties the temperatures calculated using Nonstac software are higher than temperatures calculated using ANsys software. One of the reasons could be the fact that thermal properties are input as regression polynomial. The temperatures are compared in the Figure 1.

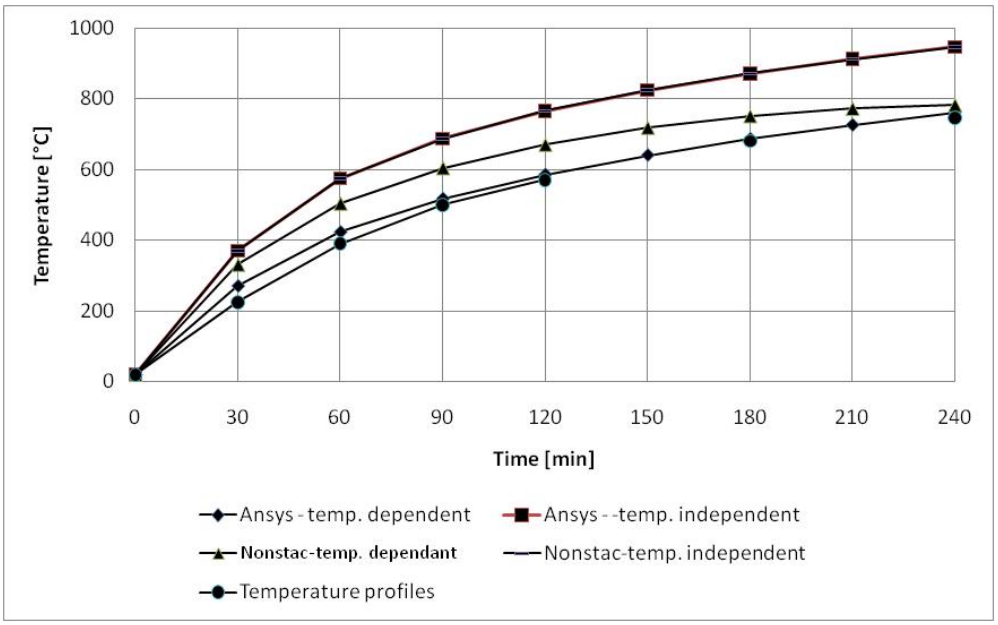

Fig. 1: Comparing the temperature in reinforcement

2 STRUCTURAL RESPONSE AND FIRERESISTANCE

2.1 Action effect

In this study example bending moment from action effect for permanent design situation is $m_{Ed} \cong m_{Rd} = 46$ kNm/m.

Reducing coefficient for accidental situation in case of fire is in the interim approximately 0.4 to 0.7. In the simplified analysis it is possible to use 0.7 on the safe side, then $m_{Ed,fi} = \eta_{fi}.m_{Ed} = 0.7 \times 46 = 32$ kNm/m.

2.2 Fireresistance

The simple way to appoint the fire resistance is to use the tables in the chapter 5 Eurocode 2 (2006). In the Table 5.8. in Eurocode 2 (2006) it is possible to settle the fireresistance 90 minutes.

In the Table 3 there are sequenced load bearing capacities in case of fire for the time 90 minutes, temperature in reinforcement is supposed according to temperature profiles and calculated using Nonstac and Ansys software, thermal material properties are considered as temperature dependant.

Tab. 3 Bending moment load bearing capacity – time 90 minutes

			Profiles	**Ansys**	**Ansys**	**Nonstac**
Heat conductivity - temp. dep.	λ	kJ/kg.K		2.0	2.0	2.0
Density - temperature dep.	ρ	kg/m^3		2400	2300	2400
Temperature in reinforcement	θ_R	°C	500	517	524	604
Steel strength	$f_{yd,fi}$	Mpa	328	305	232	193
Bending moment - capacity	$m_{Rd,fi}$	kNm/m	42	39	30	25
Bending moment - action effect	$m_{Ed,fi}$	kNm/m	32	32	32	32
Assessment			OK	OK	X	X

It is obvious that appointing the temperature in reinforcement according the temperature profiles and consequent fireresistance corresponds with the table fireresistance.

Temperature in reinforcement according to temperature profiles respond well with the temperatures calculated using ANsys software for the initial density 2400 kg/m^3, and initial coefficient of heat

conductivity 2.0 J/kg.K . Criterion R for bending moment load bearing capacity in fulfilled for time 90 minutes.
Considering the initial density 2300 kg/m^3 the temperatures in reinforcement are higher and criterion R for bending moment bearing capacity for time 90 minutes is not fulfilled.
Temperature in reinforcement calculated using Nonstac software are higher than using Ansys software and the fireresistance for time 90 minutes for criterion R-bearing capacity is not fulfilled.

3 SUMMARY

In the paper the study example of reinforced concrete slab is analyzed. Temperature in reinforcement is settled using temperature profiles and Ansys and Nonstac software. Input data for thermal analysis are not given strictly, in the paper there are compared temperatures in reinforcement for different input data using different computational methods and particular software. Numerical solution of differential equation of heat transfer is provided using FEM analysis and Ansys software and Runge-Kutta method and Nonstac software. Considering temperature independent thermal properties the result temperatures correspond together. Considering the temperature dependant thermal properties the result temperatures calculated using Nonstac software are higher than using ANsys software. One of the reasons could be the fact that thermal properties are input as regression polynomial.
Table fireresistance of analyzed slab is 90 minutes. In this time the bending moment load bearing capacity is settled for different calculated temperatures in reinforcement. As the simplified method is more advanced then detailing according to tabulated data, it is expected that resulting fire resistance of slab structure using simplified calculating methods gives more favorable values than detailing according to tabulated data. This study would like to point out that in some cases design according to tabulated data is more favorable than simplified method.

4 ACKNOWLEDGMENT

This outcome has been achieved with the financial support of the Ministry of Education, Youth and Sports of the Czech Republic, project No. 1M0579, within activities of the CIDEAS research centre.

REFERENCES

CSN EN 1991-1-1: Eurocode 1: Actions on structures - Part 1-1: General actions - Densities, self-weight, imposed loads for buildings, Prague 2004

CSN EN 1991-1-2: Eurocode 1: Actions on structures - Part 1-2: General actions - Actions on structures exposed to fire, Prague 2004

CSN EN 1992-1-2: Eurocode 2: Design of concrete structures - Part 1-2: General rules - Structural fire design, Prague 2006

CSN PENV 1992-1-2: Design of concrete structures - Part 1-2: General rules - Structural fire design, Prague 1998

Čajka, R.: Software Nonstac, registration number AR-SW-2010-02, output of project Rheological sliding joint with thermo-controlled viscoelastic properties No. FR-TI2/746. Ostrava 2010

Nevřiva, P.: Simulation of regulating systems on computer. SNTL Prague 1975. In Czech.

AXIAL RESTRAIN EFFECTS ON FIRE RESISTANCE OF STATICALLY INDETERMINATE RC BEAMS

Meri Cvetkovska [a], Koce Todorov [a], Ljupco Lazarov [a]

[a] University "Ss. Cyril and Methodius", Faculty of Civil Engineering, Skopje, Macedonia

INTRODUCTION

Fire resistance is a measure of the ability of a building element to resist a fire. It's determination in case of structural systems is a complex nonlinear problem in which the strength and the stiffness of the elements as well as the inner forces are continuously modified. Mainly, several groups of nonlinearity sources can be identified: nonlinear distribution of temperature through the element thickness, temperature-dependent material properties (thermal and mechanical), nonlinear boundary conditions and nonlinearity due to reaching strength capacity.

In reinforced concrete structures the connections between columns and beams are usually constructed as relatively rigid, which means that interaction between these elements exists when they are exposed to external influences of different nature. In case of fire loading, applied only to one part of the structure, the high thermal expansion may produce high axial forces in the heated elements by the surrounding unheated elements. In some cases these forces can have either positive or negative influence on the fire resistance of the considered elements.

In this paper three different support conditions, such as: pin-pin, pin-fixed and fully fixed are used to model beams with various level of axial restrain. The beams are exposed to the ISO-fire curve. The numerically obtained results are presented and on the basis of these results it can be observed that the augmented axial spring stiffness increases the induced axial forces, as well as the fire resistance of elements.

1 SUPPORT CONDITIONS OF STRUCTURAL BEAM ELEMENTS

Reinforced concrete beams as a part of space frame structural systems are axially restraint elements. The level of axial restrain depend on many factors, such as: type of structural system, dimensions of surrounding elements (beams and columns), their lengths, type of connections, characteristics of used structural materials, etc. At the beginning of fire loading, axial restrains are maximal. During the time, as a result of high temperatures and nonlinear temperature distribution in the cross sections of the heated elements, modulus of elasticity of steel and concrete decreases, internal forces are redistributed and additional cracks appear. These initiate decrease of columns and beams stiffness and reduction of axial restrain effects (Daniela, 2004 and Mostafaei et al., 2009).

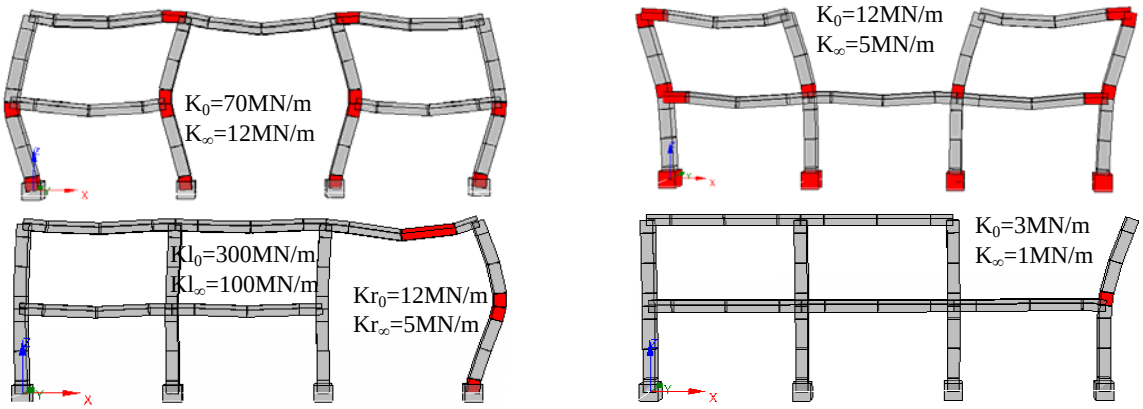

Fig. 1 Influence of structural system on the beam axial stiffness restrain

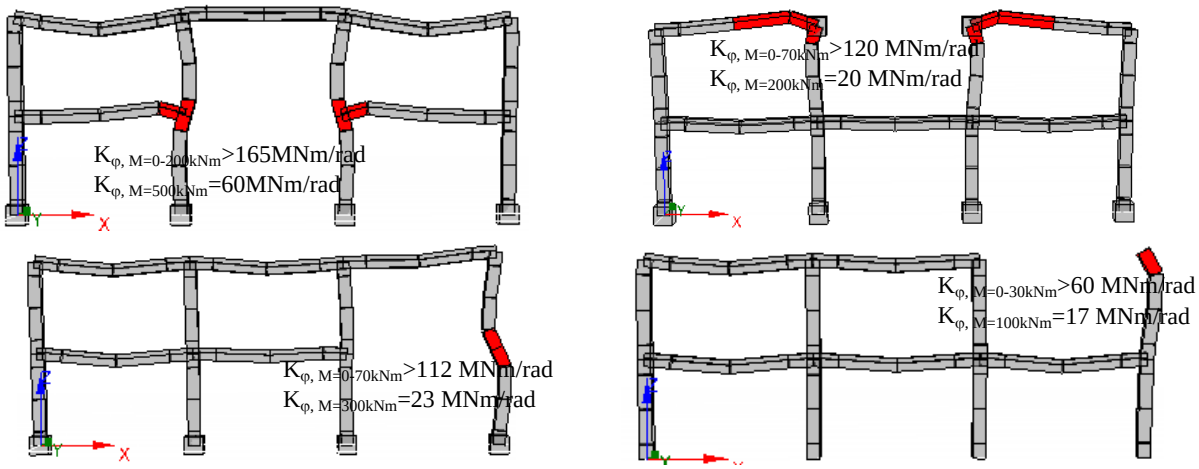

Fig. 2 Influence of structural system on the beam rotational stiffness restrain

If we want to analyse the beam behaviour as a separate unite, isolated from the structure, the appropriate time dependent boundary conditions should be applied to the beam ends. Selected results for the boundary conditions for different positions of the beam element as a part of a 3 bay, 2 story frame are presented on Fig.1 and Fig.2. The frame geometry is: 3.0m story height and 5.0m bay span. All columns and beams are of size 40/40cm. Axial and rotational stiffness dependence of the beam element position and the nodes displacements (axial translation and rotation) are presented on Fig.3.

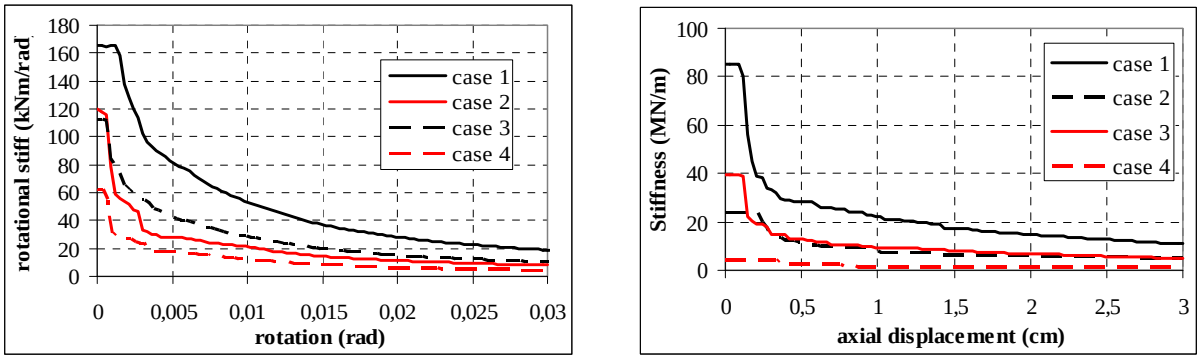

Fig.3 Rotational and axial stiffness dependence of node displacements

2 COUPLED THERMAL – STRESS ANALYSIS

Today, as a result of many years of investigations, there are three basic methods for determining the fire resistance of structural elements and their assemblies. The oldest method is the performance of a fire test of loaded elements, in compliance with the national regulations and standards, or comparison of the elements with the results from already performed tests on similar or identical elements. The second method implies the use of empirical formulae that are based on the results from performed fire tests and holds for a certain combination of: structure, material and protective coating. The third method, based on the principles of structural mechanics and theory of heat transfer, represents an analytically elaborated approach to design elements with a predefined fire resistance. Generally, numerical analysis of the whole structure in case of fire proofs that the structure, or its elements, loaded by a defined load and exposed to thermal effects, satisfies certain functional requirements, expressed through the ultimate state for bearing capacity and usability. Verification of the numerically achieved results usually is based on comparison with the experimental results from the fire tests preformed on the same or similar elements (Cvetkovska et al., 2009 and Ellingwood et al., 1991).

To define the fire resistance of structures as assemblies of structural elements, experimental investigations of models are almost impossible. Spreading the temperature field in time domain is

practically impossible to be simulated on a model of small proportions. Hence, model investigations can hardly be accepted due to the high cost. For the last twenty years, particular importance has therefore been given to the analytical definition of the problem.
The program FIRE (Cvetkovska, 2002) carries out the nonlinear transient heat flow analysis (modulus FIRE-T) and nonlinear stress-strain response associated with fire (modulus FIRE-S). The solution technique used in FIRE is a finite element method coupled with time step integration. The modulus FIRE-S takes in to accounts the dimensional changes caused by temperature differences, changes in mechanical properties of materials with changes in temperature, degradation of sections by cracking and/or crushing and acceleration of shrinkage and creep with an increase of temperature.
The effect of creep at elevated temperatures in the program FIRE is included by the temperature dependent stress-strain relationships for concrete and steel, recommended in EC2. The model proposed is capable of predicting the fire resistance of reinforced concrete structural elements with a satisfactory accuracy.

3 AXIAL RESTRAIN EFFECTS ON FIRE RESISTANCE OF BEAMS

In order to investigate the influence of axial stiffness restrain on the fire resistance of reinforced concrete beams, few numerical parametric analyses are performed. The beam and the cross section geometry, as well as reinforcement details are presented on Fig. 4 and Fig. 5. The beam is analysed as one span beam with different end boundary conditions (pin-pin, pin-fixed and fixed-fixed). In the first case the beam is fixed on the both sides and the uniform load is 45 KN/m'. For the second case fixed-pin boundary conditions are used and the uniform load is 28 KN/m'. For the third case pin-pin boundary conditions are used and the uniform load is 15 KN/m'. For all three cases the reinforcement is taken in such a way that the stresses in steel bars due to nominal load q are approximately 60% of the yield strength, for the negative moment reinforcement, and 45%, for the positive moment reinforcement. The variable stiffness in axial direction is achieved by spring element at one end of the beam. The spring stiffness is varied from K=0 MN/m to K=∞.

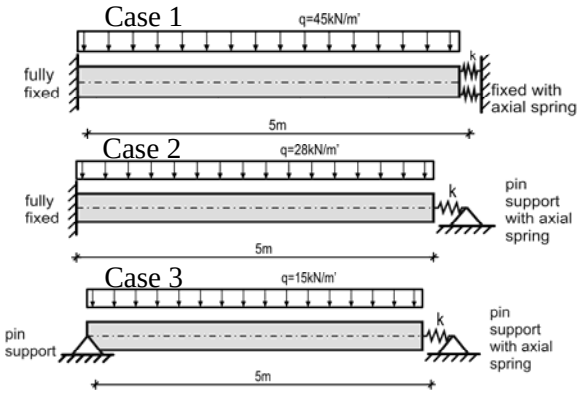

Fig. 4 Beam geometry and variable support conditions

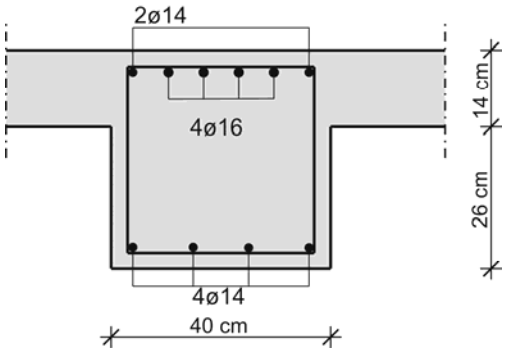

Fig. 5 Cross section geometry and reinforcing details at the fixed support, for Case 1

The fire induced axial forces in case of restrained axial displacements by springs with different stiffness are presented on Fig.6 and Fig. 7. The moment redistribution, caused by the non-uniform temperature field in the cross section of the beam exposed to fire from the bottom side, results in increase of negative moment at the supports and decrease of positive moment at the mid-span. In Case 1 the fixed boundary conditions enable redistribution of moments on both sides that results in lower values of the induced axial forces than in Case 2, where the redistribution is enabled only at the fixed support. For that reason in Case 3 the induced axial forces have highest values, but only if the axial spring stiffness is less than 7 MN/m (Fig. 9). The maximal values of the induced axial force as a function of the axial spring stiffness are presented on Fig.8 and Fig. 9.

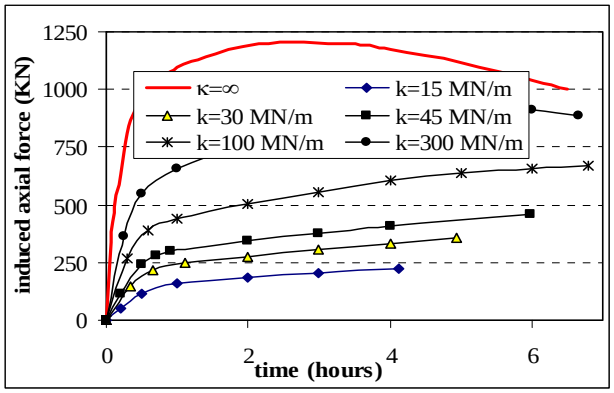

Fig. 6 Fire induced axial force for different spring stiffness in Case 1 (fixed-fixed ends)

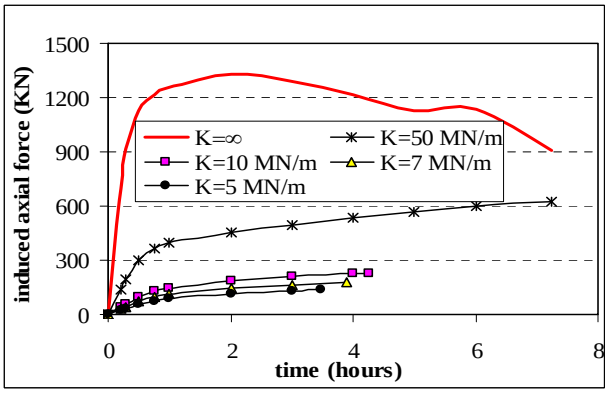

Fig. 7 Fire induced axial force for different spring stiffness in Case 2 (pin-fixed ends)

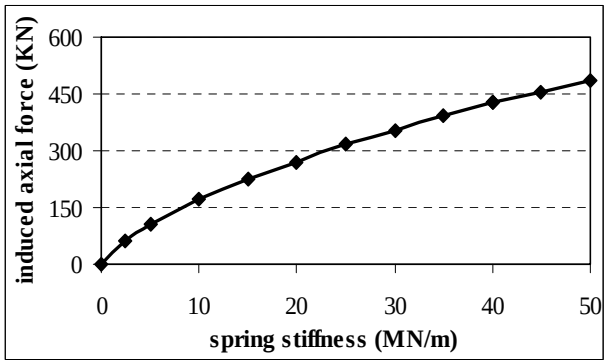

Fig. 8 Max. induced axial force dependence of spring stiffness for Case 1

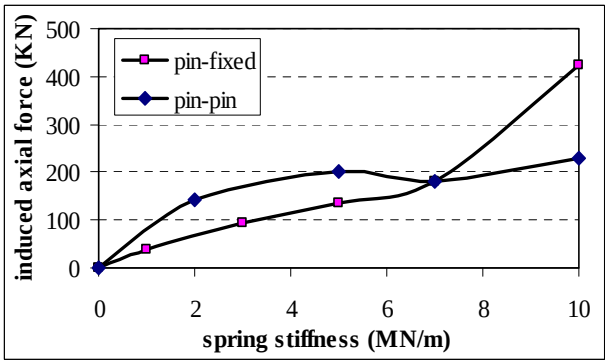

Fig. 9 Max. induced axial force dependence of spring stiffness for Case 2 and Case 3

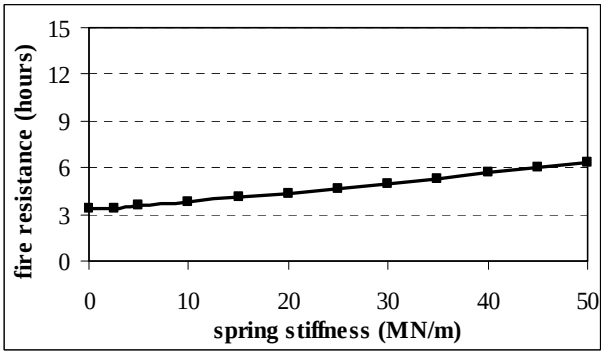

Fig. 10 Axial spring stiffness influence on the fire resistance of the beam in Case 1

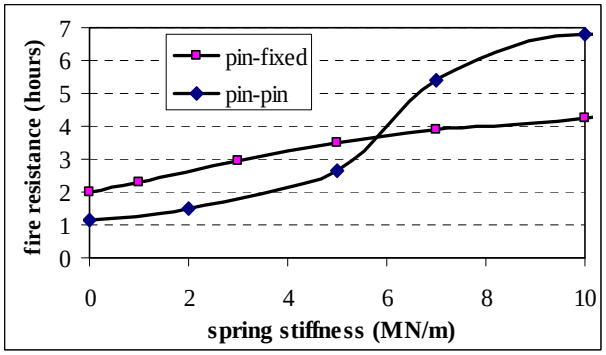

Fig. 11 Axial spring stiffness influence on the fire resistance of the beam in Case 2 and Case 3

The induced axial force acts as a prestressing force and delays the moment when yielding of the top reinforcement will occur, so it has a positive effect on the fire resistance of the beam. It has a positive effect on the bottom reinforcement, too. In the case without axial restrain, as a result of the moment redistribution, the positive moment at the mid-span decreases, but the stresses in the bottom reinforcement are still high and close to the yield strength for the current temperature. If the restrain exists the induced axial force decreases the stresses of the positive moment. The augmented axial spring stiffness increases the induced axial force, as well as the fire resistance of the beam (Fig. 10 and Fig.11) and in the same time decreases the longitudinal displacement at the end of the beam (Fig. 12 and Fig. 13). If, in Case 1, the spring stiffness was increased over 50 MN/m the positive effect on the fire resistance of the beam is negligible, therefore results are presented only for the lower values. In Case 2 and Case 3 the positive effect is negligible for spring stiffness higher than 10 MN/m.

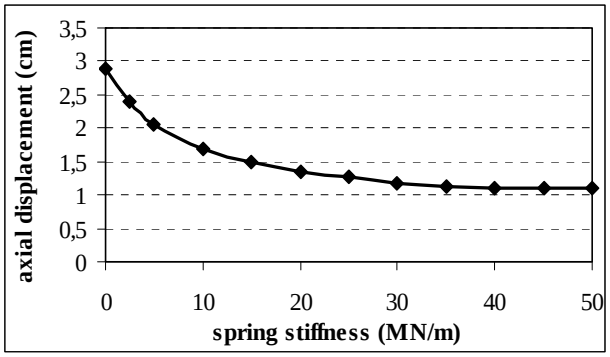

Fig. 12 Axial spring stiffness influence on the support displacement for Case 1

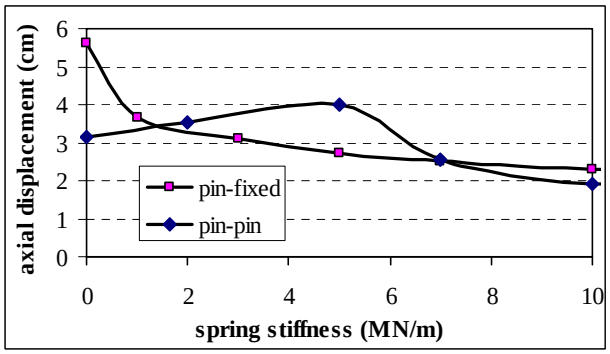

Fig. 13 Axial spring stiffness influence on the support displacement for Case 2 and Case 3

4 FIRE RESISTANCE OF A BEAM AS A PART OF A STRUCTURE

As it was priviously mentioned, to define the fire resistance of a beam as a separate unite, isolated from the structure, the appropriate time dependent boundary conditions should be applied to the beam ends.

For examle, if we want to analyse the fire scenario when the fire is in the first story middle span by separating the beam from the structure, the appropriate boundary conditions have to be defined according to the values presented on Fig. 1 and Fig.3 - case 1. For that purpose the expected values for the axial displacements of the nodes should be adeqately considered. According to the values presented on Fig. 2-case 1, the rotational stiffness should be defined. The axial stiffness restrain at each node varies from K1=40 MN/m (Fig. 3, case 1), in the moment when the structure is loaded only by uniform load q, to K1=20 MN/m (or K1=10 MN/m only on one side), after 1 hour fire action. Because the suraunding elements are not fire exposed, the rotational stiffness during the fire action is almost constant on both sides and shold be taken with the initial value of 850MNm/rad. The cross section geometry, as well as reinforcement details for the current beam are the same as for the beam presented on Fig. 4, case 1 and Fig. 5.

A satisfactory accuracy is achieved by comparing the results obtained by analysing the beam as a separate element (fire scenario FS1) with the results obtained by analysing the whole structure (fire scenario FS2). For both cases the results are presented in Tab. 1. The real behavior of the beam (as a part of the whole structure) is presented on Fig. 14.

According to the results presented on Fig. 10, the fire resistance of the same beam with the same loading conditions and the same final axial stiffness of the spring (K1=10 MN/m only on one side), but with a different rotational stiffnes (K3=∞ on both sides) is t=3.83 hours. In case when the beam is treated as a separate element (FS1, Tab. 1) the fire resistance is 3.75 hours. The real fire resistance of the whole structure is t-3.45 hours.

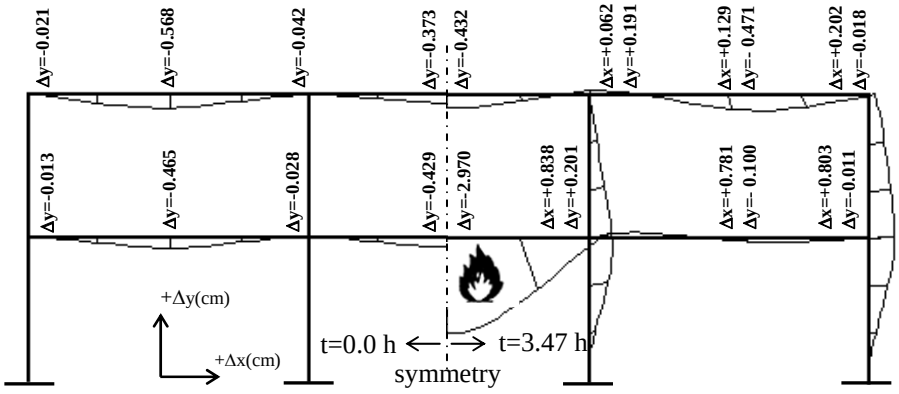

Fig.14 Deformation history of the frame exposed to fire in the first story middle bay

The final results for the displacements in axial direction (Fig. 12, Δx=1.69cm =2*0.845cm) and for the vertical displacement at mid-span (Δy=3.42cm) at the moment of failure are almost the same, but little higher than in fire scenario 1 (FS1). The reason is the assumed constant value for the axial spring stiffness and the difference in the assumed rotational stiffness. In this case the rotational stiffness has a small effect on the final results, but for an another fire scenario it should be considered adeqately.

Tab. 1 Fire resistance of a beam as a separate element and as a part of a structure

	fire scenario	axial displacement on one side Δx (cm)	vertical deflection in the middle Δy(cm)	negative moment M_1(KNm)	moment at the middle of spam, M_2(KNm)	induced axial force N (KN)
t=0.0	FS1	0	0.413	-100.57	39.16	0
	FS2	0	0.429	-101.55	38.17	0
t=1.0	FS1	-0.572	1.301	-164.6	-25.40	-114
	FS2	-0.584	1.344	-165.6	-26.27	-128
t=2.0	FS1	-0.700	2.087	-152.66	-14.00	-139
	FS2	-0.707	2.171	-152.40	-13.01	-140
t=3.47	FS1	-0.805	2.966	-136.36	1.90	161
	FS2	-0.838	2.970	-136.3	2.57	147
t=3.75	FS1	-0.827	3.213	-132.6	5.05	166

5 CONCLUSIONS

According to the results, complete or even partial restraints of end supports displacements in axial direction dramatically change, for better, the fire resistance of this type of structures. This is mainly attributed to the axial force induced due to the support restraints. Generally speaking, the axial compression force increases the fire resistance of the structure.

Since a physical testing program for investigating the response of a large variety of structural elements under differing restraint, loading, and fire conditions is impractical and expensive, analytical studies supported by the results of physical experiments could efficiently provide the data needed to resolve questions related to the design of structures for fire safety.

REFERENCES

Cvetkovska M., Nonlinear stress strain behaviour of RC elements and RC frames exposed to fire, PhD. Thesis, University Ss.Cyril and Methodius – Skopje, R. Macedonia, 2002.

Cvetkovska M., Trpevski S., Ivanisevic N, Nonlinear Finite Element Analysis of RC Beams Subjected to Fire, 33rd IABSE Symposium (International Association for Bridge and Structural Engineering), Bangkok, Thailand, 2009.

Daniela B., The Effect of Support Conditions on the Fire Resistance of a Reinforced Concrete Beam, Fire Engineering Research Report 04/5, 2004.

Ellingwood B., Lin T.D., Flexure and shear behavior of concrete beams during fires, Journal of the Structural Engineering, Vol.117 No.2, 1991.

Mostafaei H., Mannarino J., A Performance -based approach for fire-resistance test of reinforced concrete columns, IRC-RR-287, 2009.

NUMERICAL INVESTIGATIONS OF COMPOSITE SLAB-BEAM FLOOR SYSTEMS EXPOSED TO ISO FIRE

Tuan Trung Nguyen [a], Kang Hai Tan [a]

[a] Nanyang Technological University, School of Civil and Environmental Engineering, Singapore

INTRODUCTION

Due to Basingstoke and Broadgate fire incidents, composite slabs consisting of steel beams and lightly reinforced concrete slabs with steel decking showed remarkable resilience by mobilizing tensile membrane action (TMA) at large displacements. The conditions necessary for the mobilisation of TMA are two-way bending of the slab and vertical support along all four edges. Over past 20 years, a number of research works on TMA of composite slabs in fire have been conducted. Almost all the previous studies utilise the assumption of continuous vertical restraint at all times during a fire. However, at elevated temperatures the edge beams will deform, and will experience large deflections. Therefore, further research studies are necessary to consider the effects of slab-beam interactions on the development of TMA in slabs. Parameters such as perimeter beam deflections, effect of stiffness and strength of fire-protected boundary beams as well as different slab configurations will be studied.

This paper presents finite element (FE) investigations on the behaviour of composite slab-beam systems under fire conditions. A simplified FE model is developed using ABAQUS because of its capabilities for static loading, thermal analysis, and a robust concrete material model. The model is first validated against published test data. A parametric study is then undertaken using this validated model. The investigated parameters are: stiffness of perimeter beams and aspect ratios of slab panels.

1 VERIFICATION OF NUMERICAL MODELLING

1.1 Solution Strategy

Structures in fire are generally subjected to large deformations. An accurate simulation of this behaviour usually meets with numerical convergence difficulty. To overcome this, an explicit dynamic solver is adopted because it uses consistent large-deformation theory. Furthermore, compared to standard static analysis, the explicit dynamic solver allows pre-processing and provides an easy solution procedure (Hongxia et al. 2008).

To simulate accurately the behaviour of a structure in a fire, knowledge of the temperature distributions within heated structural members is essential. *Sequentially coupled thermal-stress analysis procedure* is used because the thermal fields are the driving forces for the stress analysis but the thermal solution does not depend on the stress solution. Therefore, the numerical models will consist of two different parts, one for heat transfer analysis and the other for structural analysis.

Concrete damaged plasticity model is adopted since it is a fairly robust concrete model which defines the biaxial and uniaxial material behaviour subjected to generally monotonic loading through a variety of input parameters. In the following simulations, reinforcement is modelled by using the rebar layer technique. In this approach, the effects associated with the rebar/concrete interface, such as bond slip and dowel action, are modelled approximately by introducing 'tension stiffening' into concrete modelling to simulate load transfer across cracks through rebar.

Thermal and mechanical properties of concrete and steel at elevated temperatures specified in Eurocode 4 are adopted in this study. However, it is necessary to convert material data from engineering stress-strain curves in Eurocode to true stress-strain relationships, especially for large deformation problems, where strain localisation in reinforcing bars plays a significant role in the behaviour of reinforced concrete structures. The following equation can be used (ABAQUS 2009):

$$\sigma = S(1+e) \quad ; \quad \varepsilon = \ln(1+e) \tag{1}$$

where *S and e* represent engineering stress and engineering strain, respectively.

1.2 Thermal Model

The temperature distribution within all heated members is determined from the thermal analysis of a 1-D model based on heated cross sections. It means that the analysis assumes that temperatures only vary across the thickness and do not vary in the horizontal direction. The recorded temperatures at different positions of the composite slab from the Fracof test (Zhao et al. 2008) are adopted for this validation. In this test, the total depth of the composite slab was 155 mm and it was exposed to the ISO fire condition from below. More details of the test are presented in Section 1.3. Material properties for thermal analysis, i.e. specific heat and conductivity, can be found in Palm (1994).

Thermal analysis is performed by discretizing the cross section with DC2D8 element (8-node quadratic heat transfer quadrilateral). Reinforcing bars are not included in the thermal analysis and are assumed not to affect the temperature distribution in the cross section. The temperatures of the reinforcing bars are assumed to be equal to those of the concrete at the same level in the cross section. The effect of concrete cracks on thermal distribution is also ignored.

Fig. 1 shows a typical temperature distribution across the slab thickness. The recorded temperature at the heated surface is used as input data. Comparisons of temperature distribution between FE simulation and experimental results are conducted for the mid-depth and unheated surfaces (Fig. 2). It can be observed that the simulation matches very closely the recorded temperatures.

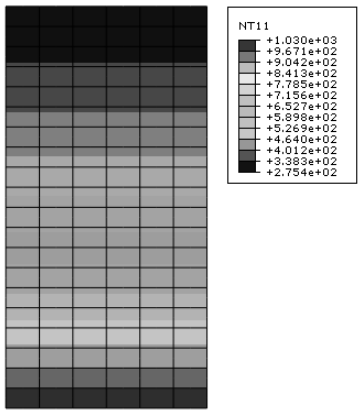

Fig. 1 Shell temperature distribution

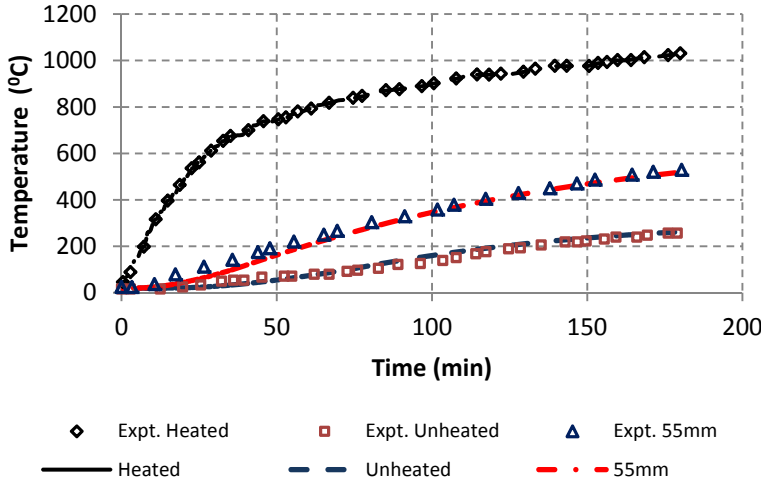

Fig. 2 Temperature comparison

1.3 Slab-Beam System Model

To verify the validity of the slab-beam model, the Fracof fire test conducted in France (Zhao et al. 2008) is adopted here for comparison purpose. In this test, a single slab panel with two unprotected intermediate beams was tested under exposure to a 120 minute ISO 834 Standard fire. The slab, representative of a corner compartment, had a long span of 8.74m and a short span of 6.66m. It consisted of four equally-spaced IPE 300 secondary beams spanning in the longer direction and two IPE 400 primary beams in the shorter direction. The slab/beam system was supported by four HEB 260 steel columns using simple connections. Total depth of the slab was 155mm with COFRAPLUS 60 decking. To simulate continuity across two adjacent edges of the slab, reinforcing steel mesh (7mm diameter bars at 1500mm centres, placed 50mm below the top of the slab) was welded to two additional steel beams. All perimeter beams and columns were fire-protected, while intermediate beams and the composite slab were left unprotected. The slab resisted a uniform load of 3.84kN/m^2, representative of imposed load at the fire limit state.

A simplified model is proposed, taking account of steel beams, concrete slab and reinforcing mesh. Assuming that the contribution of the steel decking on the load-carrying capacity of the slab is insignificant, the 150mm thick concrete slab is modelled as a flat slab, representative of the effective depth of the composite slab. The layers of reinforcing bars in the slab are treated as being smeared uniformly across the concrete shell element.

The model considers the slab as an isolated slab panel, vertically supported at the column positions. The vertical support along the slab edges is provided by the protected perimeter beams. Rotational restraints along two adjacent edges are used to simulate the slab continuity across these edges.

Shell element type S4R is used to discretize the beams and the slab. The top flange of the steel beams and parts of the slab above these beams are tied together using *surface-based contact interactions*. To avoid an overlap between the two reference surfaces, an offset between two tied surfaces is adopted.

To simulate transient heating, the FE simulation comprises two steps: (1) apply mechanical loading; (2) apply heating. The recorded temperatures are used as input data, based on which the mechanical behaviour is obtained.

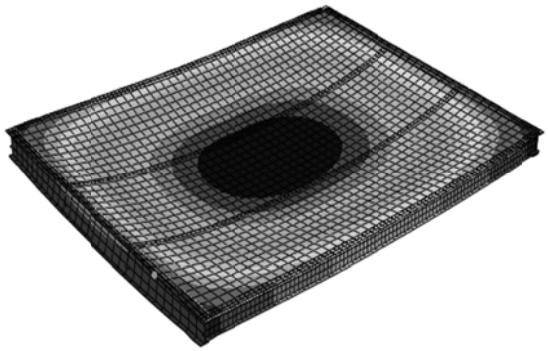

Fig. 3 Deformed shape

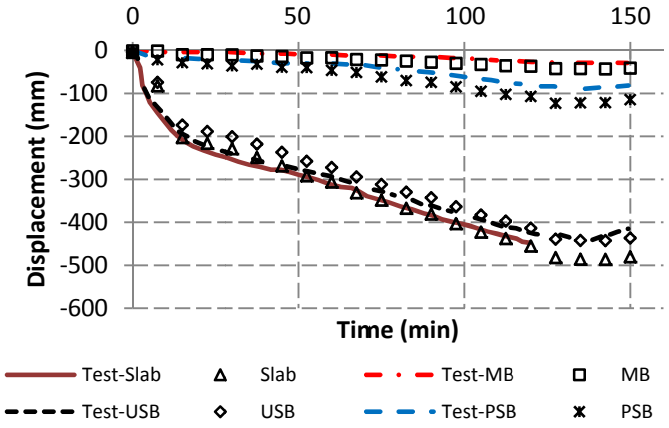

Fig. 4 Comparison of the results

A comparison of the central vertical displacements of the members between the numerical predictions and actual test results is shown in Fig. 4. It can be seen that the numerical results follow closely the experimental curves.

2 PARAMETRIC STUDY

2.1 Introduction

Given the reasonably good agreement between the numerical model and the experimental data for both structural and thermal responses, the above FE model shows the capability to simulate the behaviour of composite slab-beam systems in fire. Therefore, this model is adopted for parametric study.

Considering the size of the electrical furnace in the experimental programme, it is decided to test small-scale specimens. The investigated prototype slab panel is an interior 9m x 9m panel. In the parametric study, the slab obtained by scaling down to ¼ of the panel is chosen as the control specimen (Figs. 5 & 6). The control slab is uniformly loaded with a predefined load level of 0.6 with a value of 19.20kN/m^2. This load level is defined as the applied load divided by the yield-line load at ambient temperature (P_{test}/P_{yield}). After being loaded up to the desirable load level, the slab is heated from the bottom.

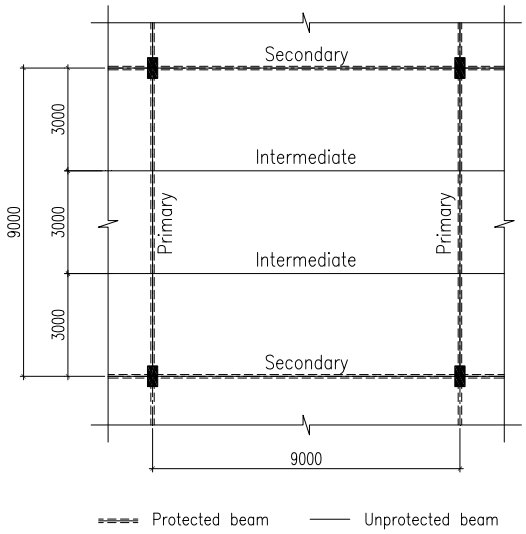

Fig. 5 Prototype interior slab panel

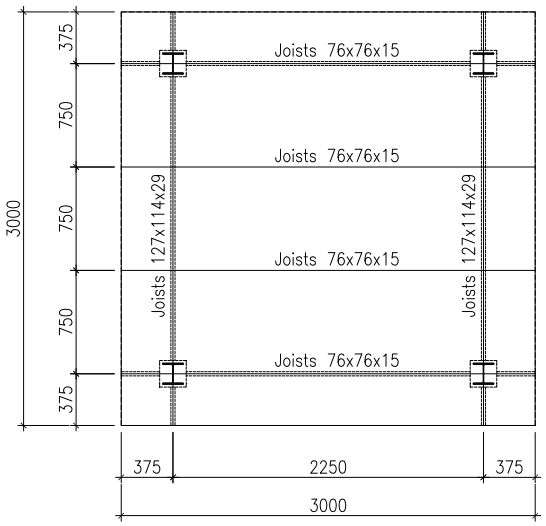

Fig. 6 Control slab

It is worth noting that the steel decking is not modelled in the simulations in recognition of de-bonding of steel decking under fire conditions, resulting in no contribution to the load-carrying capacity of the slab at the limit state.

2.2 Heat transfer analyses

Under fire conditions, the mechanical behaviour is adversely affected by temperatures. Therefore, a series of thermal analyses have to be conducted to ascertain the temperature distributions for the control model before embarking on structural analysis. Using the validated model in Section 1.2, thermal analyses are performed for the 50mm concrete slab, the 127x114x29-joists protected main beam (MB), the 76x76x15-joists protected secondary beam (PSB) and the 76x76x15-joists unprotected secondary beam (USB). It is assumed that the slab is exposed to the ISO 834 fire curve from the bottom, while the beams are exposed to the same fire curve from three sides.

In ABAQUS, to conduct thermal analysis for protected steel beams, the protective material is defined as one independent part attached to the beam section through a surface-based contact interaction. *Gap conductance* is adopted and specified as a function of clearance that is incorporated through contact property assignment. Thermal boundary conditions are simulated by defining prescribed temperatures at particular points.

Fig. 7 shows the variation of temperatures within the cross sections of the main and secondary beams and the slab. Based on these temperatures as input data, the mechanical behaviour of the model can be obtained.

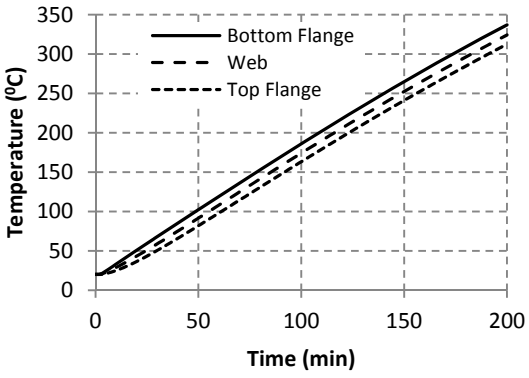

a) Protected main beam (MB)

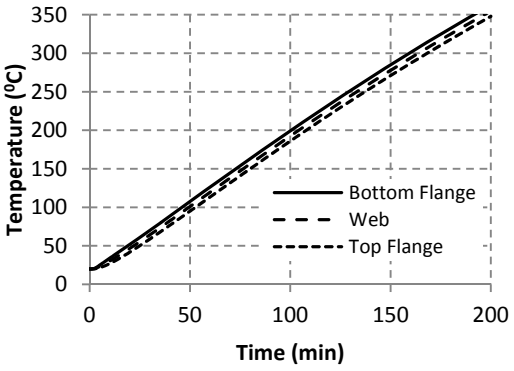

b) Protected secondary beam (PSB)

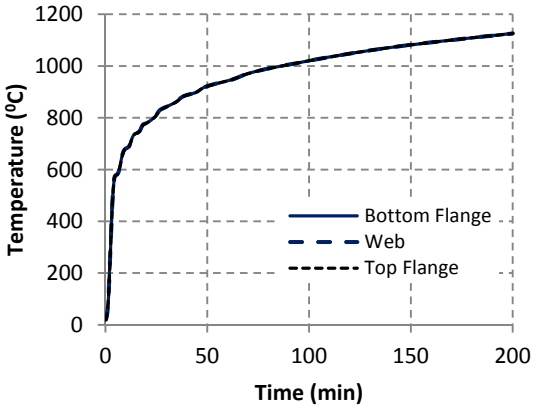

c) Unprotected intermidiate beam (USB)

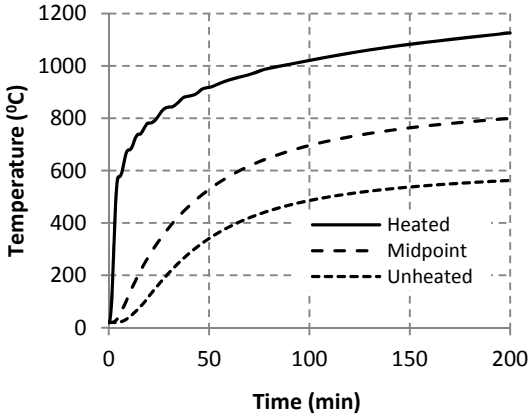

d) Slab

Fig. 7 Simulation of heat transfer analyses

2.3 Effect of stiffness of perimeter beams

To investigate the effect on stiffness of perimeter beams on the development of TMA in the slab, four cases are analysed with different sizes of beams for one slab configuration as shown in Tab. 1.

Tab. 1 Case studies for stiffness of perimeter beams

Case study	Denote	MB	SB	I_y - MB	I_y - SB	Note
4	ST0	Joists 127x114x29	Joists 76x76x15	$\boldsymbol{I_1}$	-	No intermediate beam
5	ST1	Joists 127x114x29	Joists 76x76x15	$\boldsymbol{I_1}$	$\boldsymbol{I_2}$	**Control model**
6	ST2	Joists 127x114x29	Joists 89x89x19	$\boldsymbol{I_1}$	$\boldsymbol{2I_2}$	
7	ST3	Joists 152x127x37	Joists 76x76x15	$\boldsymbol{2I_1}$	$\boldsymbol{I_2}$	

Fig. 8 compares the midspan vertical deflection of the slabs. It can be seen that slab ST0 without intermediate beams has a similar deflection trend to those models with intermediate beams, but with significantly greater deflection. It can also be observed that as stiffness of the edge beams increases, failure of the slab occurs later with a smaller deflection. Increasing the stiffness of protected secondary beams has a greater beneficial effect on the slab deflection than increasing the stiffness of primary beams. Increasing the stiffness of primary beams only has the effect on the slab deflection when it has undergone 2.9*d* (*d*: effective depth of slab).

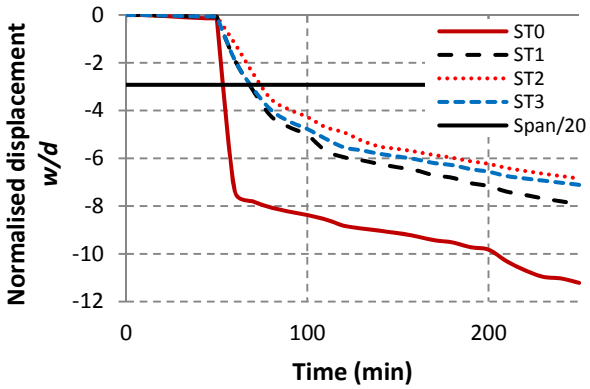

Fig. 8 Midspan vertical slab deflection with different stiffness of perimeter beams

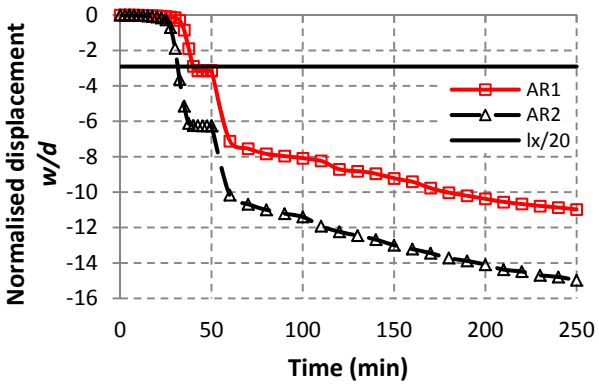

Fig. 11 Midspan vertical deflection of the slabs with different aspect ratios

A comparison of the distribution of membrane forces across the slab thickness at midspan at a slab deflection of 6.8*d* for three cases is shown in Fig. 9. In this figure, positive values indicate tensile forces and negative values compressive forces. As can be seen, in slab ST2, greater tensile

membrane forces are mobilized compared to slab ST1. However, at this deflection, slab ST3 provides less tensile membrane forces than slabs ST1 and ST2. Due to T-beam action, parts of the slab above the beams are still in compression. Therefore, estimating the enhancement of the slab load-carrying capacity due to TMA without considering the presence of the perimeter beams may not be accurate. It is obvious that the in-plane membrane mechanism comprises a compressive ring of concrete around the slab perimeter and tensile membrane action in the central region of the slab.
Based on the strains of both concrete and reinforcement, the predicted failure modes are given in Fig. 10. The slab may fail by fracture of reinforcing rebars over the unprotected secondary beams, or by failure of the compressive ring at the corners. If the intermediate beams are over-stiff, a different failure mode may occur. As can be seen in Fig. 9(b), in slab ST2, part of the slab is still in compression. This shows that as stiffness of secondary beams increases, it seems to be more difficult to mobilize TMA in both directions, resulting in possible formation of plastic hinges in the perimeter beams, i.e. folding mechanism (Abu et al. 2010).

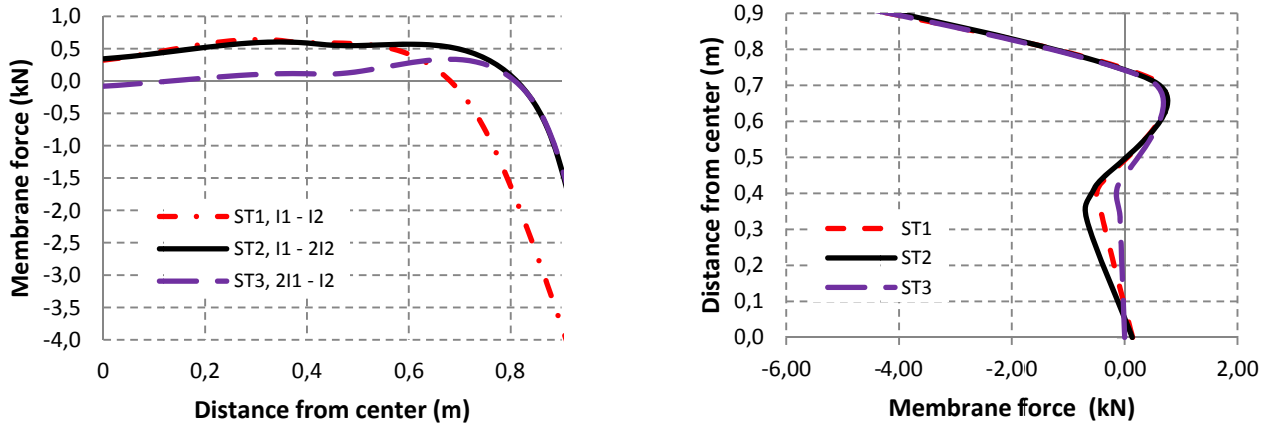

a) Along Y axis (parallel to secondary beam) b) Along X axis (parallel to main beam)

Fig. 9 Distribution of membrane forces at the slab deflection of 6.8*d*

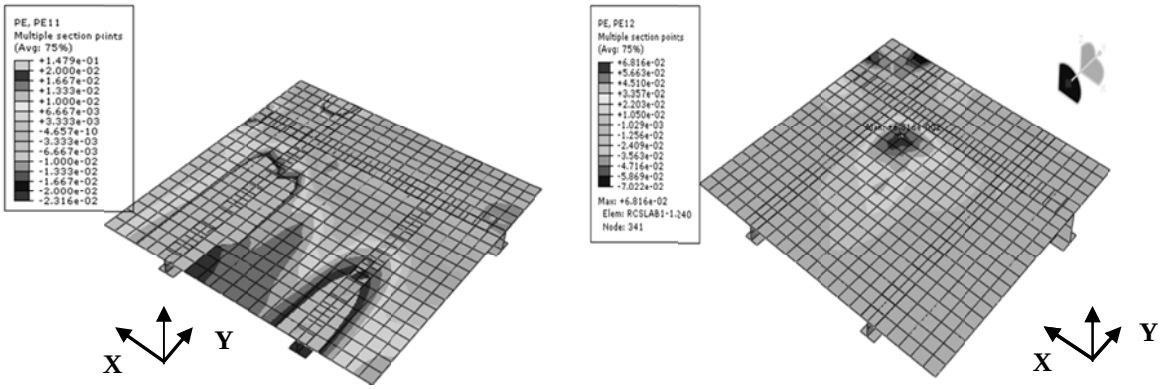

Fig. 10 Predicted failure modes

2.4 Effect of aspect ratios of slabs

In this section, two different slab geometries are analysed to investigate the effect of aspect ratio of slabs on the development of TMA. To clearly delineate this effect from the others, isolated panels without intermediate beams (IB) are adopted for analysis. For both cases, the slab is 50mm thick with the same size of perimeter beams.
Fig. 11 compares the midspan vertical deflection of the slabs. The span/20 criterion is also indicated. As can be seen, during the first 20 minutes, the slabs have a similar rate of deflection. After 20 minutes, the deflection of slab AR2 increases at a faster rate than that of slab AR1. Slab AR2 reaches the deflection limit of 112mm, just after 31 minutes at the loading phase.

Tab. 2 Case studies for aspect ratio of slabs

Case study	Denote	l_x (m)	l_y (m)	*Aspect ratio*	Note
8	AR1	2.25	2.25	1.0	No IB
9	AR2	2.25	3.375	1.5	No IB

The distribution of membrane forces across the midspan sections at the slab deflection of 10*d* is plotted in Fig. 12. It can be observed that as the aspect ratio increases, the behaviour of two-way spanning slabs approaches that of one-way slabs. Thus, less tensile membrane force is mobilised. It is worth noting that since the temperatures of the protected perimeter beams are still low, these beams can maintain strength and stiffness in fire. Therefore, in the vicinity of the perimeter beams, there is significant compressive membrane force.

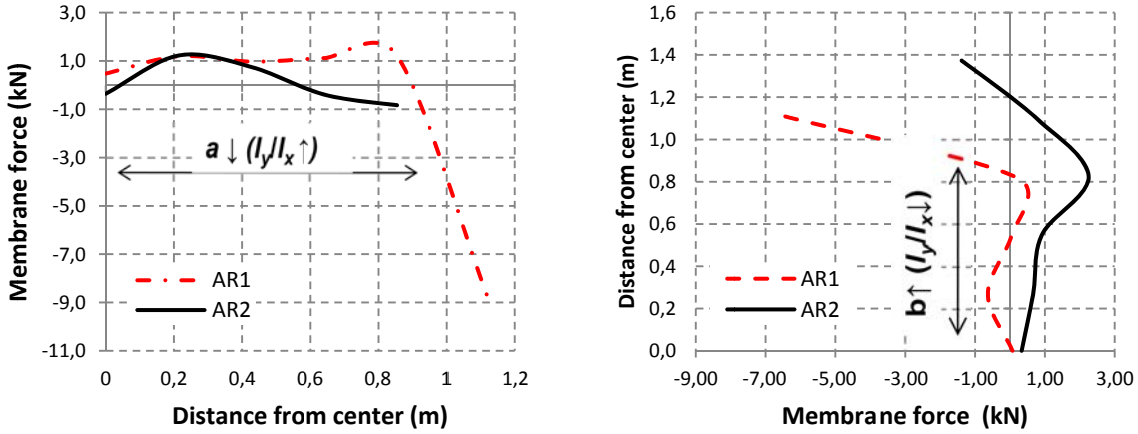

a) Along X axis (parallel to shorter span) b) Along Y axis (parallel to longer span)

Fig. 12 Distribution of membrane forces at the slab deflection of 10*d*

3 CONCLUSIONS

In this paper, numerical simulations were used to investigate the behaviour of composite slab-beam systems under fire conditions. It is demonstrated that the FE model gives reasonable accuracy compared to test results, providing an efficient, economical and yet accurate tool to study the membrane behaviour of composite slab-beam systems in fire. From the parametric study, it can be concluded that: (1) Unprotected intermediate beams can reduce slab deflection and increase the fire resistance of composite slab-beam systems; (2) At the same large deflection of the slab, if the secondary beams have greater stiffness the slab can generate greater tensile membrane force compared to the control model; (3) As the aspect ratio of two-way RC slabs increases, less tensile membrane force is mobilised; (4) Failure modes of composite slab-beam systems may be different from those of composite slabs.

Currently, an experimental programme conducted on ¼ scale models of composite slab-beam systems under fire conditions is being prepared in NTU to study the behaviour experimentally.

ACKNOWLEDGMENT

The work presented in this paper is supported by the research funding from Agency for Science, Technology and Research (A*STAR). Their financial support is gratefully acknowledged.

REFERENCES

Abu, A. K., V. Ramanitrarivo, et al. (2010). Collapse Mechanisms of Composite Slab Panels in Fire. Sixth International Conference on Structures in Fire (SiF'10).

Hongxia, Y., I. W. Burgess, et al. (2008). "Numerical simulation of bolted steel connections in fire using explicit dynamic analysis." Journal of Constructional Steel Research **64**: 515-525.

Palm, J. (1994). "Temperature analysis using ABAQUS." Fire Technology **30**(3): 291-303.

Zhao, B., M. Roosefid, et al. (2008). Full scale test of a steel and concrete composite floor exposed to ISO fire SiF'08, Singapore, NTU.